Scilight

Physics and the Cosmos
https://www.sciltp.com/journals/pac

Review

High-Energy Astrophysical Tests of Lorentz Symmetry

Rafael Alves Batista [1,2]

[1] Institut d'Astrophysique de Paris, Sorbonne Université, CNRS UMR 7095, 98 bis bd Arago, 75014 Paris, France; rafael.alves_batista@iap.fr
[2] Laboratoire de Physique Nucléaire et des Hautes Énergies, Sorbonne Université, 4 Place Jussieu, 75005 Paris, France

How To Cite: Alves Batista, R. High-Energy Astrophysical Tests of Lorentz Symmetry. *Physics and the Cosmos* **2026**, *1*(1), 4.

Received: 5 November 2025
Revised: 16 December 2025
Accepted: 7 January 2026
Published: 28 January 2026

Abstract: High-energy cosmic messengers, such as gamma rays, neutrinos, and cosmic rays, have become indispensable tools for probing fundamental physics, providing a natural laboratory that far exceeds the reach of terrestrial particle accelerators. Owing to their extreme energies and vast propagation baselines, which can amplify tiny Planck-scale effects, these messengers offer some of the most promising avenues for testing theories of quantum gravity and for exploring the nature of spacetime itself. In this review, I present a critical synthesis of current constraints on deviations from Lorentz invariance, with emphasis on propagation-based observables such as modified interaction thresholds and time-of-flight effects. Particular attention is devoted to astrophysical uncertainties that may affect the interpretation of these observations, and to what these constraints reveal about the viability of detecting quantum-gravity–induced modifications to spacetime symmetries.

Keywords: multi-messenger astrophysics; Lorentz symmetry; quantum gravity phenomenology; Lorentz invariance violation; astroparticle physics

1. Introduction

Lorentz symmetry lies at the heart of the modern conception of spacetime. It intertwines space and time into a unified four-dimensional entity–spacetime–ensuring that the form of the laws of physics remain invariant for all inertial observers, regardless of their relative motion. One might be tempted to ask "*relative with respect to what?*", a question that harkens back to the pre-relativistic notion of absolute space and the hypothetical pervasive luminiferous ether, once thought to be the medium through which electromagnetic waves propagated.

Lorentz symmetry is not merely a property of physical laws, but a manifestation of the structure of spacetime itself, with the invariant interval $\mathrm{d}s^2 = -c^2\mathrm{d}t^2 + \mathrm{d}x^2 + \mathrm{d}y^2 + \mathrm{d}z^2$ preserved under Lorentz transformations. This insight eliminated the need for an absolute space to serve as the arena wherein physical phenomena occur, and is at the core of special relativity (SR). General relativity (GR) extends this idea by incorporating local Lorentz invariance into a dynamical, curved spacetime framework. This four-dimensional relational ontology underlies both relativity and quantum field theory (QFT), where the symmetries of spacetime and of the dynamical laws are intimately connected. Spacetime, in this view, is a geometric structure whose symmetries define what we mean by *space*, *time*, and *motion*.

Relativity withstood a century of experimental tests [1, 2], proving itself to be an extraordinarily robust framework for understanding the physical world; but so has quantum mechanics. These two pillars of modern physics seem fundamentally incompatible.

For decades, there has been a theoretical effort to unify quantum mechanics and general relativity, the two fundamental theories of modern physics [3–5]. Quantum gravity (QG) is one of the paths explored in this direction, based on attempts to quantise gravity. This endeavour is motivated by the success of QFT in describing the fundamental interactions apart from gravity, which resists straightforward quantisation due to its unique geometric nature, and the non-renormalisability of perturbative approaches.

The pursuit of a QG theory raises deep questions about the very nature of spacetime itself. *Is spacetime a fundamental entity? Is it a smooth manifold upon which physics unfolds? Or is it an emergent phenomenon arising*

from some more fundamental theory? While GR treats spacetime as a continuous fabric whose curvature encodes the notion of gravitation, built into QFT is the idea of a fixed, smooth background on which quantum processes occur. Maybe these two descriptions, which excel in their respective domains of applicability, can point to a deeper theory that unifies them, whose effects become significant only at extremely high energies or small scales, commonly thought to be near the Planck energy scale, $E_{\rm Pl} = \sqrt{\hbar c^5/G} \approx 1.22 \times 10^{28}$ eV, or conversely the Planck length, $\ell_{\rm Pl} = \sqrt{\hbar G/c^3} \approx 1.62 \times 10^{-35}$ m. At such scales, spacetime might no longer be well described as a continuous arena but as a discrete, relational, or even algebraic entity. Instead, what is perceived as a continuum can actually contain substructures or be an emergent phenomenon, rather than a fundamental aspect of reality. These deep questions about the ontology of spacetime are discussed in detail in the philosophical literature [6–9].

Given the intrinsic link between Lorentz symmetry and the structure of spacetime, it is plausible that any modification to our understanding of spacetime at the quantum level could also impact Lorentz symmetry. Thus, questions about the fundamental nature of spacetime and Lorentz symmetry motivate the search for experimental signatures that could reveal deviations from exact Lorentz invariance, potentially shedding light on the underlying structure of spacetime at the quantum level. It is, however, important to emphasise that Lorentz invariance is *not* a prerequisite for a theory of QG, and that finding Lorentz invariance violation (LIV) would not necessarily imply the existence of QG effects. This path is, nevertheless, a promising avenue to explore the nature of spacetime and its symmetries.

The Large Hadron Collider (LHC) currently provides the highest energies achievable in terrestrial laboratories, reaching up to 100 PeV in the lab frame [10], which is still over ten orders of magnitude below the Planck energy. Fortunately, nature itself accelerates particles to far higher energies, exceeding 100 EeV (1 EeV $\equiv 10^{18}$ eV), which is much closer to the Planck scale. Moreover, these particles traverse cosmological distances, allowing tiny effects to accumulate over time and distance, which can potentially lead to measurable deviations from standard physics. Furthermore, small changes in particle interactions may yield observable secondary signatures due to collective amplification effects during propagation. In the golden age of multi-messenger astrophysics, high-energy cosmic messengers are, therefore, one of the best probes of fundamental physics, including QG phenomenology [11,12].

The messengers covered in this review are very-high energy (VHE) gamma rays with energies $E \gtrsim 100$ GeV, high-energy neutrinos with $E \gtrsim 100$ TeV, and ultra-high energy cosmic rays (UHECRs) with $E \gtrsim 1$ EeV (1 EeV $\equiv 10^{18}$ eV). These messengers are of particular interest for QG phenomenology because they represent the most energetic particles routinely observed with present-day technology. To date, the most energetic neutrino detected has an energy exceeding 100 PeV [13], while the highest-energy gamma ray observed has an energy of order 1 PeV [14]. Even more extreme are the highest-energy cosmic rays (CRs) ever detected, with energies exceeding 0.1 ZeV (1 ZeV $\equiv 10^{21}$ eV) [15,16]. Although these energies remain many orders of magnitude below the Planck scale, $E_{\rm Pl} = \sqrt{\hbar c^5/G} \approx 1.22 \times 10^{28}$ eV, where quantum-gravitational effects are commonly expected to become significant, they far exceed those achievable in terrestrial accelerators. For comparison, the LHC reaches centre-of-mass energies of order 10^{13} eV. High-energy cosmic messengers therefore provide a unique window onto physical regimes that are otherwise experimentally inaccessible.

This review is intended for two communities: astrophysicists interested in fundamental physics, and QG researchers interested in the real-world implications of their theories. For the former, I try to introduce the central ideas of QG phenomenology in a concise yet pedagogical way, using familiar notation and keeping the mathematics as transparent as possible. For the latter, I give a brief overview of some astrophysical concepts I deem important, focusing on how astrophysical and instrumental uncertainties can influence the interpretation of observations. Inevitably, several arguments are simplified. My intention is to give a general overview of the topic, and to make the connections between theory and observation clear without overwhelming the reader with technicalities, which can be found in some of the references cited.

Here I concisely summarise the state of the art in QG searches with high-energy cosmic messengers. Section 2 covers the main aspects of the propagation of these messengers through cosmic distances. From Section 3, I start connecting the discussion to QG phenomenology, presenting some frameworks and observables. Section 4 is devoted to reviewing the main constraints on QG obtained with high-energy cosmic messengers, followed by a critical discussion of the state of the art and limitations of these studies in Section 5. Finally, in Section 6, I will pragmatically discuss where we stand, and the prospects for actually identifying signatures of QG with high-energy cosmic messengers in the near future.

2. Canonical Propagation of High-Energy Messengers

The power of high-energy particles to probe fundamental physics stems, to a large extent, from the cumulative effects that tiny deviations from standard physics can have over the vast distances they travel, from their sources to

Earth. Therefore, it is crucial to understand the main processes affecting their propagation.

This section is not meant to be an exhaustive review of all propagation effects, but rather a brief summary of the main phenomena relevant for interpreting the observations and for probing new physics with cosmic messengers. I first provide a concise overview of cosmological effects relevant for understanding propagation in Section 2.1. Then in Sections 2.2 and 2.3, I discuss phenomena such as scatterings, decays, and oscillations. Sections 2.4 and 2.5 focus on the effects of magnetic and gravitational fields on the propagation of these messengers. Finally, in Section 2.6, I briefly present some numerical tools commonly used to model the propagation of high-energy messengers.

2.1. Cosmological Effects

In an expanding universe, the rate of expansion at a given redshift z is described by the Hubble parameter $H(z)$, which, in the standard Λ cold dark matter (ΛCDM) cosmological model, is given by

$$H^2(z) = H_0^2 \left[\Omega_{\rm r}(1+z)^4 + \Omega_{\rm m}(1+z)^3 + \Omega_{\rm k}(1+z)^2 + \Omega_\Lambda\right] , \tag{1}$$

where H_0 is the present-day Hubble constant, and Ω_i are the fractional energy densities of radiation ($\Omega_{\rm r}$), matter ($\Omega_{\rm m}$), spatial curvature ($\Omega_{\rm k}$), and dark energy (Ω_Λ). These components satisfy the relation $\sum_i \Omega_i = 1$. In the concordance ΛCDM model, the curvature contribution vanishes ($\Omega_k = 0$).

Equation (1) determines how the expansion rate evolves with redshift, linking cosmic time and redshift, as follows:

$$\frac{{\rm d}t}{{\rm d}z} = -\frac{1}{1+z}\,\frac{1}{H(z)} . \tag{2}$$

2.2. Scatterings and Decays

High-energy cosmic messengers may decay or scatter off ambient background fields during their propagation. This alters the information they carry and leaves observable signatures that encode the interactions they underwent. Two main classes of processes govern these effects: decays and scatterings.

A *decay* process of the form

$$X_0^{(\rm i)} \to X_1^{(\rm f)} + \cdots + X_n^{(\rm f)}$$

is characterised by its intrinsic decay time, τ. A decay channel is kinematically allowed if its decay width is non-zero and if the centre-of-mass energy squared exceeds

$$s_{\rm min} = \left[\sum_{j=1}^{n} m_j^{(\rm f)} c^2\right]^2 , \tag{3}$$

where $m_j^{(\rm f)}$ denotes the mass of the j-th final-state particle. Here, s is the Mandelstam variable representing the square of the total energy in the centre-of-mass frame.

Consider an interaction process involving two particles in the initial state, labelled '$X_j^{(\rm i)}$', resulting in a final state composed of n particles, labelled '$X_j^{(\rm f)}$'. A generic reaction of this type can be written as:

$$X_1^{(\rm i)} + X_2^{(\rm i)} \to X_1^{(\rm f)} + \cdots + X_n^{(\rm f)} .$$

Its rate of occurrence depends on the type of target particle ($X_2^{(\rm i)}$) and the specific astrophysical environment where the messenger ($X_1^{(\rm i)}$) is propagating.

Over cosmological scales, the most relevant targets for interactions are photons, which pervade the whole universe. For instance, the cosmic microwave background (CMB) [17] is omnipresent and affects the propagation of high energy (HE) messengers at specific energy ranges. The integrated radiation field resulting from structure formation processes—the extragalactic background light (EBL) [18–20]—also plays a central role in the propagation, together with the cosmic radio background (CRB) [21,22]. On Galactic scales, the interstellar radiation field (ISRF) [23,24] can be important.

Hadronic backgrounds are overall negligible on cosmological scales, especially in the intergalactic medium, but they do matter within structures. For instance, in the Milky Way the existence of pervasive interstellar gas has been known since the last century [25–27]. In galaxy clusters, this can also be relevant for the propagation of high-energy messengers [28–31]. There is also a pervasive neutrino background, the cosmic neutrino background (CνB) [32], which may be important for the propagation of extremely energetic neutrinos and photons [33–35].

In what follows, I will concentrate on the case of target photons, i.e., on processes of the type:

$$X^{(\mathrm{i})} + \gamma_{\mathrm{bg}} \to X_1^{(\mathrm{f})} + \cdots + X_n^{(\mathrm{f})} \,.$$

The characteristic length (λ) for the interaction of a particle of energy E and speed βc, with a background distribution of isotropic photons with spectral number density $\frac{\mathrm{d}n(\varepsilon)}{\mathrm{d}\varepsilon}$, for an energy ε, is given by [11]

$$\lambda(E) = 8\beta E^2 \left[\int\limits_{\varepsilon_{\mathrm{min}}(E)}^{\varepsilon_{\mathrm{max}}} \int\limits_{s_{\mathrm{min}}}^{s_{\mathrm{max}}(E,\varepsilon)} \mathrm{d}\varepsilon \, \mathrm{d}s \, \frac{1}{\varepsilon^2} \frac{\mathrm{d}n(\varepsilon)}{\mathrm{d}\varepsilon} (s - m^2c^4) \, \sigma(s) \right]^{-1} , \tag{4}$$

wherein $\sigma(s)$ is the cross section, m is the mass of the particle, and s is the Mandelstam variable representing the square of the total energy in the centre-of-mass frame,

$$s(E, \varepsilon, \theta) = m^2c^4 + 2\varepsilon E(1 - \beta \cos\theta) \,. \tag{5}$$

Note that Equation (4) is usually calculated at specific redshifts (z), such that the time evolution of the background photon fields ought to be written as $\frac{\mathrm{d}n(\varepsilon)}{\mathrm{d}\varepsilon} = \frac{\mathrm{d}n(\varepsilon,z)}{\mathrm{d}\varepsilon}$, for generality, thus implying $\lambda(E) = \lambda(E, z)$.

The limits of the integral over s depend on the specific interaction considered. The lower limit, s_{min}, is determined by kinematics. Under Lorentz symmetry, the threshold corresponds to the configuration in which the outgoing particles are parallel to each other. In this case, the invariant satisfies $s^{(\mathrm{i})} = s_{\mathrm{min}}$, following the definition of Equation (3). Naturally, the initial state must allow for this configuration. For fixed incoming energies, this occurs when the initial particles are anti-parallel to each other, i.e., for head-on collisions ($\theta = 180°$). This gives the upper limit of integration of the inner integral of Equation (4), s_{max}:

$$s_{\mathrm{max}}(E, \varepsilon) = m^2c^4 + 2\varepsilon E(1 + \beta) \,. \tag{6}$$

2.2.1. Photons

High-energy photons can interact with background photon fields producing electron-positron pairs:

$$\gamma + \gamma_{\mathrm{bg}} \to e^+ + e^- \,, \tag{7}$$

where γ_{bg} represents a background photon. This process is kinematically allowed if the centre-of-mass energy exceeds the threshold $s_{\mathrm{min}} = 4m_e^2c^4$, where m_e is the electron mass. It is by far the most relevant interaction channel for high-energy photons propagating over cosmological distances, due to its relatively low energy threshold and high cross section, which enables efficient interactions with the CMB and extragalactic background light (EBL) [36–38].

Other possible channels include the production of muon or tau pairs of charged leptons [39–42], hadronic pairs [41–43] (e.g., $\pi^+ + \pi^-$), or other particles (e.g., $q + \bar{q}$). A higher-order quantum electrodynamics (QED) process is double pair production [44,45], $\gamma + \gamma_{\mathrm{bg}} \to e^+ + e^- + e^+ + e^-$, which becomes relevant at ultra-high energies, although generally subdominant with respect to the Breit-Wheeler channel.

The propagation of photons over cosmological distances is affected by their interactions with background photons, as described in Section 2.2, being Breit-Wheeler pair production the dominant process. For an object located at a distance L_{src}, corresponding to a redshift z_{src}, emitting photons with energy E_{src}, the observed flux at Earth, $\Phi_{\mathrm{obs}}(E)$, relates to the emitted flux, $\Phi_{\mathrm{src}}(E_{\mathrm{src}})$, through an exponential attenuation factor:

$$\Phi_{\mathrm{obs}}(E) = \Phi_{\mathrm{src}}(E_{\mathrm{src}}) \, \exp\left[-\tau_{\mathrm{PP}}(E_{\mathrm{src}}, z_{\mathrm{src}})\right] \,, \tag{8}$$

wherein $\tau_{\mathrm{PP}}(E_{\mathrm{src}}, z_{\mathrm{src}})$ denotes the *optical depth* for pair production, labelled by the subscript 'PP', defined as the distance-integrated inverse mean free path ($\lambda_{\mathrm{PP}}^{-1}$; see Equation (4)):

$$\tau_{\mathrm{PP}}(E_{\mathrm{src}}, z_{\mathrm{src}}) = \int\limits_0^{z_{\mathrm{src}}} \mathrm{d}z \, \frac{c}{\lambda_{\mathrm{PP}}(E(z), z)} \left| \frac{\mathrm{d}t}{\mathrm{d}z} \right| \,, \tag{9}$$

where $\mathrm{d}t/\mathrm{d}z$ is given by Equation (2). Note that the energy at emission (E_{src}) and at observation (E) are related as: $E(z) = E_{\mathrm{obs}}(1 + z)$. In this notation $\Phi_{\mathrm{src}}(E_{\mathrm{src}})$ shall be interpreted as the flux that would be observed at Earth in the absence of absorption, evaluated at the emitted energy E_{src}.

2.2.2. Electrons

An important process in astrophysical environments involving high-energy electrons is inverse Compton scattering [46,47],

$$e^{\pm} + \gamma_{\rm bg} \to e^{\pm} + \gamma \,. \tag{10}$$

This process efficiently transfers energy from high-energy electrons to low-energy background photons predominantly from the CMB at sub-EeV energies, and the CRB above.

Higher-order processes that can at times provide small but non-negligible contributions include triplet pair production [48,49] ($e^{\pm} + \gamma_{\rm bg} \to e^{\pm} + e^{+} + e^{-}$), which is relevant for ultra-high energy (UHE) particle propagation [50,51], and electroproduction of muon pairs, $e^{\pm} + \gamma_{\rm bg} \to e^{\pm} + \mu^{+} + \mu^{-}$.

2.2.3. Cosmic-Ray Nuclei

High-energy cosmic-ray nuclei can interact with background photon fields through various processes. This process can be generally represented as ${}^{A}_{Z}{\rm X} + \gamma_{\rm bg} \to \ldots$, where A is the atomic mass of the CR nucleus, and Z its atomic number. The most relevant interactions for the propagation of UHECRs are listed below.

Bethe-Heitler pair production.In this process, high-energy nuclei interact with background photons to produce electron-positron pairs [52]:

$${}^{A}_{Z}{\rm X} + \gamma_{\rm bg} \to {}^{A}_{Z}{\rm X} + e^{+} + e^{-} \,. \tag{11}$$

Although this process has a lower energy threshold compared to photoproduction of mesons and photodisintegration, its energy loss per interaction is relatively small. Nevertheless, it can contribute significantly to the overall energy loss of UHECRs over cosmological distances [53,54].

Photoproduction of mesons. This process occurs at the level of individual nucleons within the nucleus, leading to the production of mesons, primarily pions:

$$p + \gamma_{\rm bg} \to \begin{cases} p + \pi^{0} \,, \\ n + \pi^{+} \,, \end{cases} \qquad \text{and} \qquad n + \gamma_{\rm bg} \to \begin{cases} p + \pi^{-} \,, \\ n + \pi^{0} \,. \end{cases} \tag{12}$$

For UHE protons interacting with CMB photons, this process gives rise to a significant suppression in the cosmic-ray spectrum at the highest energies, above ~ 50 EeV — the so-called Greisen-Zatsepin-Kuzmin (GZK) cut-off [55,56]. In the case of nuclei, screening effects lead to a reduction in the effective cross section compared to free nucleons, which can be important for modelling the propagation of nuclei, as discussed in refs. [57,58].

The threshold energy for this process can be derived from Equation (5), yielding:

$$E_{\rm thr} = \frac{(m_n + m_\pi)^2 c^4 - m_p^2 c^4}{4\varepsilon} \,, \tag{13}$$

wherein ε denotes the energy of the CMB photon in the lab frame, and m_p, m_n and m_π are the proton, neutron, and pion masses, respectively. For the channel with neutral pion production, the mass of the neutron must be replaced by that of the proton. For typical CMB photons with energies $1\ \mu{\rm eV} \lesssim \varepsilon \lesssim 1$ meV, the threshold energy is $E_{\rm thr} \approx 50$–100 EeV, consistent with the observed suppression in the UHECR spectrum [59,60].

Photodisintegration. This process involves the interaction of high-energy nuclei with background photons, leading to the ejection of one or more nucleons from the nucleus [61]:

$${}^{A}_{Z}{\rm X} + \gamma_{\rm bg} \to \begin{cases} {}^{A-1}_{Z-1}{\rm X} + p \,, \\ {}^{A-1}_{Z}{\rm X} + n \,, \\ {}^{A-4}_{Z-2}{\rm X} + {}^{4}_{2}{\rm He} \,, \\ {}^{A'}_{Z'}{\rm X} + \ldots \,. \end{cases} \tag{14}$$

This process is particularly relevant for heavy nuclei, such as iron, and leads to a gradual reduction of the mass number of the cosmic-ray nucleus as it propagates through space [61,62].

In the ultra-high-energy regime, the cross section is dominated by the giant dipole resonance at $\varepsilon' \lesssim 50$ MeV and by quasi-deuteron processes for $50 \lesssim \varepsilon'/{\rm MeV} \lesssim 150$, while baryon resonances appear at $\varepsilon' \gtrsim 150$ MeV. Note that here ε' refers to the photon energy in the rest frame of the nucleus. The threshold for photodisintegration depends on the binding energy required to remove nucleons, and nuclear recoil is usually neglected, as ε' is much smaller than the nuclear mass. The uncertainties in cross sections are significant, affecting the interpretation of

UHECR data [63–65] and the production of secondary messengers [66].

2.2.4. Neutrinos

Neutrino interactions with photons are extremely suppressed within the Standard Model (SM). Direct neutrino–photon scattering like

$$\nu_\ell + \gamma \to \nu_\ell + \gamma\,, \tag{15}$$

where $\ell = \{e, \mu, \tau\}$, virtually vanishes at tree level, and proceeds only through higher-order loop diagrams involving charged leptons and $W^\pm$ bosons. Another possibility is the production of a charged lepton and a W boson,

$$\nu_\ell + \gamma \to \ell + W\,, \tag{16}$$

which becomes kinematically allowed only above an extraordinarily high threshold in the centre-of-mass frame:

$$E_{\rm thr} \simeq \frac{(m_W + m_\ell)^2 c^4}{4\varepsilon}\,. \tag{17}$$

This is the case of extremely energetic neutrinos interacting with the CMB [33,67–69].

Neutrino–neutrino interactions can lead to the attenuation of extremely energetic neutrinos propagating through the CνB. The most important processes of this kind include

$$\begin{aligned}
&\nu_\ell + \nu_\ell \to \nu_\ell + \nu_\ell,\\
&\nu_\ell + \nu_{\ell'} \to \nu_\ell + \nu_{\ell'},\\
&\nu_\ell + \bar{\nu}_{\ell'} \to \nu_\ell + \bar{\nu}_{\ell'},\\
&\nu_\ell + \bar{\nu}_\ell \to \ell^+ + \ell^-,\\
&\nu_\ell + \bar{\nu}_\ell \to f + \bar{f},\\
&\nu_\ell + \bar{\nu}_\ell \to W^+ + W^-,\\
&\nu_\ell + \bar{\nu}_\ell \to Z + Z.
\end{aligned} \tag{18}$$

These processes have very low cross sections [70], but they can become important for the propagation of neutrinos from high-redshift sources [71].

2.3. Oscillations

The phenomenon of oscillations arises when particles can exist in different 'flavours' that are superpositions of propagation eigenstates. The most important example is neutrino flavour oscillations, which occur because flavour eigenstates are superpositions of mass eigenstates.

Over cosmological baselines, flavour change in the universe is governed by the usual three-flavour framework, but with the additional consideration that the oscillation phase changes with redshift due to the adiabatic expansion of the universe. Let $|\nu_\alpha\rangle = \sum_i U_{\alpha i}\,|\nu_i\rangle$ be a flavour eigenstate, wherein U is oscillation matrix — the Pontecorvo-Maki-Nakagawa-Sakata (PMNS) matrix [72,73] for neutrinos. The vacuum transition probability from a flavour eigenstate α to a flavour eigenstate β is:

$$P_{\alpha\beta} = \delta_{\alpha\beta} - 4\sum_{i>j} \mathrm{Re}\left[U_{\alpha i} U^*_{\beta i} U^*_{\alpha j} U_{\beta j}\right] \sin^2\left(\frac{\phi_{ij}}{2}\right) + 2\sum_{i>j} \mathrm{Im}\left[U_{\alpha i} U^*_{\beta i} U^*_{\alpha j} U_{\beta j}\right] \sin\left(\phi_{ij}\right)\,. \tag{19}$$

In a spatially-flat non-expanding universe, the phase ϕ_{ij} is given by

$$\phi_{ij} = \frac{1}{2\hbar c}\frac{\Delta m^2_{ij} c^4}{E} L \approx 7.8\times 10^{13} \left(\frac{\Delta m^2_{ij}}{\mathrm{eV}^2}\right)\left(\frac{L}{\mathrm{Mpc}}\right)\left(\frac{E}{\mathrm{PeV}}\right)^{-1}\,, \tag{20}$$

where $\Delta m^2_{ij} = m^2_i - m^2_j$ represents the mass-squared difference between mass eigenstates i and j, and L is the propagation distance, for a neutrino with energy E, as measured today. However, the universe is expanding, such that the neutrino energy redshifts as $E \propto (1+z)$. This modifies the flavour transition probability, in particular the oscillation phase. To leading order in m^2c^4/E^2, for a neutrino emitted at redshift z and observed today with energy E, the phase becomes:

$$\phi_{ij}(z) \simeq \frac{1}{2\hbar c}\frac{\Delta m_{ij}^2 c^4}{E}\int_0^z \frac{1}{(1+z')^2\,H(z')}\,\mathrm{d}z'\,, \tag{21}$$

where $H(z)$ is given by Equation (1). At small redshifts ($z \ll 1$), this integral reduces to L/c, recovering the flat-spacetime phase given by Equation (20).

Equation (21) points to the fact that the oscillation probability is redshift-dependent. Each mass eigenstate ($|\nu_i\rangle$) propagates with a slightly different group velocity ($\frac{v_i}{c} \simeq 1 - \frac{m_i^2 c^4}{2E^2}$), leading to a gradual spatial separation of their respective wave packets. Coherence is lost once this separation exceeds the intrinsic spatial width (σ_x) determined by production or detection. This corresponds to a coherence length of [74,75]

$$L_{\mathrm{coh},ij} \simeq 4\sqrt{2}\,\sigma_x\,\frac{E^2}{|\Delta m_{ij}^2 c^4|}\,, \tag{22}$$

beyond which the interference terms in the transition probability (see Equation (19)) are exponentially suppressed. Note that this relation assumes Gaussian wave packets [74,75]; more sophisticated quantum field theory treatments yield similar scalings with additional process-dependent factors (see, e.g., refs. [76,77]).

After cosmological propagation and complete decoherence, the flavour composition of the neutrino flux detected at Earth depends linearly on the source composition through the averaged transition matrix,

$$\overline{P}_{\alpha\beta} = \sum_i |U_{\alpha i}|^2 |U_{\beta i}|^2\,, \tag{23}$$

which follows from the unitarity of the PMNS matrix. The flavour fractions measured at Earth are thus given by

$$f_\alpha^\oplus = \sum_\beta \overline{P}_{\alpha\beta}\, f_\beta^{\mathrm{src}}\,, \tag{24}$$

where f_β^{src} represents the fractional contribution of each flavour at production. For typical astrophysical sources, neutrinos are produced primarily via the mechanisms shown in Table 1.

Table 1. Neutrino flavour compositions at the source for different production mechanisms. Note that these values are only approximate, considering standard neutrino oscillations parameters [78].

mechanism	$\boldsymbol{f}^{\mathrm{src}}$	$\boldsymbol{f}^{\oplus}$
pion decay	$1:2:0$	$0.33:0.33:0.33$
muon damping	$0:1:0$	$0.25:0.37:0.38$
neutron β-decay	$1:0:0$	$0.55:0.23:0.22$

2.4. Effects of Magnetic Fields

High-energy charged particles are deflected by magnetic fields during their propagation. For an ultrarelativistic particle of charge q, which can be a CR, for example, the typical angular deflection ($\Delta\theta_B$) after travelling a distance L_{src} is [79]:

$$\Delta\theta_{B,\mathrm{CR}} \simeq \begin{cases} qc\dfrac{B\sqrt{L_{\mathrm{src}}L_B}}{E} = 0.5^\circ\, Z \left(\dfrac{B}{10^{-15}\ \mathrm{T}}\right)\left(\dfrac{E}{100\ \mathrm{EeV}}\right)^{-1}\left(\dfrac{L_{\mathrm{src}}}{100\ \mathrm{Mpc}}\right)^{\frac{1}{2}}\left(\dfrac{L_B}{1\ \mathrm{Mpc}}\right)^{\frac{1}{2}} & \text{if } L_{\mathrm{src}} \gg L_B\,, \\ qc\dfrac{BL_{\mathrm{src}}}{E} = 5.3^\circ\, Z \left(\dfrac{B}{10^{-15}\ \mathrm{T}}\right)\left(\dfrac{E}{100\ \mathrm{EeV}}\right)^{-1}\left(\dfrac{L_{\mathrm{src}}}{100\ \mathrm{Mpc}}\right) & \text{if } L_{\mathrm{src}} \ll L_B\,, \end{cases} \tag{25}$$

where B is the strength of the magnetic field perpendicular to the particle's trajectory, and L_B is its characteristic coherence length. Here Z is the atomic number of the charged particle, such that the charge is $q = Ze$, with e being the elementary charge. Equation (25) implies that the magnetically-induced time delays (Δt_B) are [79]

$$\Delta t_{B,\mathrm{CR}} \approx \begin{cases} q^2 c\,\dfrac{B^2\,L_{\mathrm{src}}^2 L_B}{18E^2} = 10^6\, Z^2 \left(\dfrac{B}{10^{-15}\ \mathrm{T}}\right)^2\left(\dfrac{E}{100\ \mathrm{EeV}}\right)^{-2}\left(\dfrac{L_{\mathrm{src}}}{100\ \mathrm{Mpc}}\right)^2\left(\dfrac{L_B}{1\ \mathrm{Mpc}}\right)\ \mathrm{yr} & \text{if } L_{\mathrm{src}} \gg L_B\,, \\ q^2 c\,\dfrac{B^2\,L_{\mathrm{src}}^3}{24E^2} = 4200\, Z^2 \left(\dfrac{B}{10^{-15}\ \mathrm{T}}\right)^2\left(\dfrac{E}{100\ \mathrm{EeV}}\right)^{-2}\left(\dfrac{L_{\mathrm{src}}}{100\ \mathrm{Mpc}}\right)^3\ \mathrm{yr} & \text{if } L_{\mathrm{src}} \ll L_B\,. \end{cases} \tag{26}$$

The propagation of CRs in magnetised environments is actually much more complex than what is captured by Equations (25) and (26), due to interactions and the inhomogeneous nature of magnetic fields within distances probed by UHECRs.

In the case of gamma rays, which are electrically neutral, $\Delta\theta_B$ is relevant only if the photons produce electromagnetic cascades during propagation (see Sections 2.2.1 and 2.2.2), with the subsequent regeneration of photons due to inverse Compton scattering. In this case, the magnetic field affects the charged components of the cascade (electrons and positrons), which in turn affect the subsequent propagation of the photons produced. At energies between roughly 10 GeV and 100 TeV, where gamma rays interact primarily with the EBL and electrons with the CMB, if $z_{\rm src}$ denotes the redshift corresponding to the source distance $L_{\rm src}$, the typical angular signature expected to be observed at Earth is [80]:

$$\Delta\theta_{B,\gamma} \simeq \begin{cases} \dfrac{0.01^\circ}{(1+z_{\rm src})^{\frac{1}{2}}} \left(\dfrac{\tau_\theta}{10}\right)^{-1} \left(\dfrac{E}{1\ {\rm TeV}}\right)^{-\frac{3}{4}} \left(\dfrac{B}{10^{-18}\ {\rm T}}\right) \left(\dfrac{L_B}{1\ {\rm kpc}}\right)^{\frac{1}{2}} & \text{if } \dfrac{L_B}{1+z_{\rm src}} \ll \lambda_{\rm IC}\,, \\ \dfrac{0.05^\circ}{(1+z_{\rm src})^{2}} \left(\dfrac{\tau_\theta}{10}\right)^{-1} \left(\dfrac{E}{1\ {\rm TeV}}\right)^{-1} \left(\dfrac{B}{10^{-18}\ {\rm T}}\right) & \text{if } \dfrac{L_B}{1+z_{\rm src}} \gg \lambda_{\rm IC}\,, \end{cases} \tag{27}$$

wherein E refers to the energy of the observed gamma ray, and τ_θ is the ratio between the angular diameter distance and the source to the mean free path for pair production. Two regimes are identified, depending on the relation between the coherence length of the magnetic field (L_B) and the mean free path for inverse Compton scattering at the redshift of interest ($\lambda_{\rm IC}$). The corresponding time delays are [80]:

$$\Delta t_{B,\gamma} \simeq \begin{cases} 1.0\times10^{4}\, \dfrac{\kappa\left(1-\tau_\theta^{-1}\right)}{(1+z_{\rm src})^{2}} \left(\dfrac{E}{1\ {\rm TeV}}\right)^{-2} \left(\dfrac{B}{10^{-21}\ {\rm T}}\right)^{2} \left(\dfrac{L_B}{1\ {\rm kpc}}\right)\ {\rm s} & \text{if } \dfrac{L_B}{1+z_{\rm src}} \ll \lambda_{\rm IC}\,, \\ 2.2\times10^{5}\, \dfrac{\kappa\left(1-\tau_\theta^{-1}\right)}{(1+z_{\rm src})^{5}} \left(\dfrac{E}{1\ {\rm TeV}}\right)^{-\frac{5}{2}} \left(\dfrac{B}{10^{-21}\ {\rm T}}\right)^{2}\ {\rm s} & \text{if } \dfrac{L_B}{1+z_{\rm src}} \gg \lambda_{\rm IC}\,, \end{cases} \tag{28}$$

where κ is a factor of order unity that captures uncertainties in the EBL model. Here the energy E refers to the energy of the observed gamma ray, which may or may not be the primary gamma ray that left the source. Note that B and L_B in these equations are the corresponding values at present time ($z = 0$).

On Galactic scales, these very same cascade processes happen to PeV gamma rays, which interact with the CMB, as well as with the ISRF [81,82], ultimately leading to time delays.

Equations (27) and (28) assume that pair production occurs much closer to the source than to the observer, which is valid for sources at cosmological distances. Moreover, these equations were derived (see ref. [80] for details) presuming only one generation of cascade photons, which is not an adequate simplification if the sources have very hard spectra, and if their emission spectrum extends to very high energies (above 100 TeV). Nevertheless, the equations do capture the main dependencies of the angular deflections and time delays on the relevant parameters, and provide adequate estimates for analysing observational data of gamma-ray observatories like Fermi-LAT and imaging atmospheric Cherenkov telescopes (IACTs).

Within the SM, neutrinos are not affected by magnetic fields. However, magnetically-induced time delays can also affect neutrinos if they are the by-product of processes involving charged particles, which is usually the case.

2.5. Effects of Gravitational Fields

The gravitational time delay (Δt_G) is caused by the presence of massive objects along the line of sight between the source and the observer. Suppose that in the observer's frame, the source of the particles is located at a distance $L_{\rm src}$ from Earth, and the object of mass M is at a distance $R_{\rm obj}$. If an ultrarelativistic particle passes at a distance r from this object, the gravitational time delay can be approximated as [83]:

$$\Delta t_G \approx \frac{2GM}{c^3} \ln\left(\frac{4L_{\rm src}R_{\rm obj}}{r^2}\right)\,. \tag{29}$$

Note that this equation is the leading-order post-newtonian result. It is valid only in the weak-field limit, and assumes a static, spherically symmetric mass distribution and a Schwarzschild metric. It does not hold if the massive object is too close to either the source or the Earth. This result is very different in the case of strong gravitational fields, where strong lensing can occur.

2.6. Simulating the Propagation

Equations (25)–(28) have a limited domain of validity. They provide only approximate descriptions that neglect the stochastic nature of particle transport and the inherent non-linearity of some relevant processes. To obtain accurate predictions for the propagation of high-energy cosmic messengers—particularly when searching for subtle signatures of new physics—one must resort to Monte Carlo simulations. These allow for a self-consistent treatment of relevant interactions, magnetic deflections, and gravitational effects. This type of approach is essential when modelling complex astrophysical environments or when studying the joint behaviour of multiple messengers simultaneously.

For the transport of gamma rays in the GeV–PeV range, where electromagnetic cascades and magnetic fields play a significant role, several dedicated Monte Carlo codes are available. CRPropa [84,85], ELMAG [86,87], and CRbeam [88] are among the most widely used, each implementing distinct treatments of pair production, inverse Compton scattering, and photon absorption on cosmological background fields. At energies beyond a few PeV, in addition to CRPropa, the EleCa code [89] provides an alternative for simulating UHE photon propagation.

For UHECRs, CRPropa [84,85,90,91] and SimProp [92,93] remain arguably the most popular tools. Both include the key energy-loss processes. However, only CRPropa performs fully three-dimensional simulations that incorporate both magnetic deflections and particle interactions. At lower CR energies, the GALPROP [94,95] and DRAGON [96,97] frameworks offer realistic descriptions of Galactic cosmic-ray transport, accounting for injection, reacceleration, and interactions with interstellar gas and radiation fields.

A particularly appealing feature of CRPropa 3 [84,85] is its unified treatment of ultrarelativistic messengers (CRs, gamma rays, and neutrinos) within a single computational framework. This consistency enables detailed multi-messenger studies, revealing correlations between different particle species, spectral connections across energy bands, and the cosmological evolution of their sources.

Note that while (semi-)analytical treatments provide useful insights into propagation phenomena, they often assume idealised conditions, including simplified fields, continuous energy losses, or rudimentary geometries. They therefore tend to overlook critical aspects of the problem, such as the complex interplay between different messengers and the environments they traverse. Monte Carlo simulations excel in capturing these complexities, offering a more faithful representation of the underlying physics that captures, to some extent, the stochasticity inherent to propagation phenomena. Monte Carlo techniques, by tracking individual particles through these random processes, naturally reproduce the fluctuations, correlations, and secondary cascades that define observables such as spectrum, arrival directions, and arrival times. This rigorous realism is what makes them indispensable for high-precision, multi-messenger studies, and ultimately for tests of Lorentz symmetry.

3. Lorentz Symmetry and Quantum Gravity Theories

One of the most remarkable aspects of high-energy cosmic messengers is their potential to probe the fundamental nature of spacetime and gravity. The quest for a consistent theory of QG that unifies GR and QFT has been a longstanding challenge in theoretical physics. In this section, I briefly describe some of the main fundamental and phenomenological (Section 3.1) frameworks that attempt to address this challenge, focusing on their implications for Lorentz symmetry and their potential manifestations in high-energy cosmic messengers (Section 3.2).

3.1. Theoretical and Phenomenological Frameworks

In coupling the SM to GR, one must keep in mind that GR is not a renormalisable theory, in the perturbative sense. As a consequence, effective phenomenological approaches such as the Standard Model extension (SME) [98] should not be seen as a complete description of nature, but rather as a template of possible manifestations of QG at accessible energies, akin to a phenomenological bridge between observations and a more fundamental quantum theory of spacetime. Therefore, despite its significant epistemological value, only genuinely ontological theories of QG can ultimately inform on the true nature of spacetime and gravity. Several such approaches indeed predict explicit or deformed violations of Lorentz symmetry.

Historically, Lorentz symmetry emerged as the natural explanation for the failure to detect a preferred frame (the ether) in Maxwell's electrodynamics and the rather revolutionary postulate of the constancy of the speed of light for all inertial observers (see, e.g., refs. [2,99,100] for historical accounts). This symmetry can be seen as less about the invariance of physical laws under frame transformations, and more about how the very architecture of spacetime encodes the principles of causality and the finite speed of information transfer. In fact, it is arguably the most deeply rooted symmetry in modern physics, being directly linked to both GR and the SM; it is no surprise that many approaches to quantise gravity lead to its modification or complete breakdown.

String theory [101–104] is arguably the most popular candidate for a theory of QG. It is based on the idea

that different vibrational modes of one-dimensional fundamental entities or strings (as opposed to point-like particles) correspond to different particles [103–105]. This includes the mediator of gravitational interactions, the graviton [106]. Consistency of the theory requires extra spacetime dimensions, adding up to a total of 10 dimensions in superstring theories and 11 in M-theory [107].

A major development within this framework is the discovery of a relation between anti–de-Sitter (AdS) and conformal field theory (CFT), known as the AdS/CFT correspondence [108], which conjectures an exact duality between a gravitational theory defined in a $(d+1)$-dimensional AdS spacetime and a d-dimensional boundary described by CFT [109], suggesting that gravitational dynamics emerge from the entanglement structure of the boundary theory.

In many formulations of string theory, Lorentz symmetry can be spontaneously broken due to non-zero tensor vacuum expectation values, thereby violating Lorentz symmetry (e.g., refs. [110–117])—this provides one route to observational constraints[1] with the astrophysical methods discussed in this review. This can sometimes be accompanied by charge, parity, and time reversal (CPT) violation and LIV [127]. Phenomenologically, this can be captured by a modified dispersion relation as in Equation (31) [128]. Moreover, non-local / non-commutative effects can arise in certain backgrounds, leading to further deviations from standard Lorentz-invariant QFT [129].

Non-commutative geometry [130,131] can be seen either as a starting point for QG or as a structural feature of full-fledged QG theories. It postulates that spacetime coordinates become non-commuting operators at very small scales, typically near the Planck length, leading to a "fuzzy" or quantised structure of spacetime [132]. It is characterised by coordinate operators that fail to commute:

$$[x^\mu, x^\nu] \;=\; i\ell_{\rm QG}^2\theta^{\mu\nu} + i\rho_\alpha^{\mu\nu}x^\alpha\ell_{\rm QG} \;=\; i\frac{\hbar^2c^2}{E_{\rm QG}^2}\theta^{\mu\nu} + i\frac{\hbar c}{E_{\rm QG}}\rho_\alpha^{\mu\nu}x^\alpha\,, \tag{30}$$

where $\theta^{\mu\nu}$ is a dimensionless antisymmetric tensor which encodes the smoothness of spacetime considering two directions μ and ν, fixing a spacetime area element, and explicitly breaking Lorentz symmetry, while $\rho_\alpha^{\mu\nu}$ is a position-dependent dimensionless tensor [133]. In this case, a preferred direction given by $\theta^{\mu\nu}$ leads to direction-dependent modified dispersion relations (MDRs) or birefringence, easily mapping onto effective field theories (EFTs) [134], like the SME [135]. Non-commutativity appears in various QG approaches, including string theory, where it arises naturally in the presence of background fields [129], as well as in loop quantum gravity (LQG) [136] and group field theory [137].

Loop quantum gravity (LQG) [138,139] is the umbrella term encompassing a plethora of closely-related background-independent approaches [138,139]. Within LQG, areas and volumes are fundamentally discrete, with a granular structure at some phenomenologically-relevant energy scale $E_{\rm QG}$, often described by polymer-like quantised states [136,140], semi-classical weave states [141], or spin networks [142]. The scale of this discreteness, which can be viewed as a fundamental length scale, $\ell_{\rm QG}$, reflects the "resolution" of spacetime. Loop phenomenology impacts not only high-energy particles, but also cosmology, including the treatment of the Big Bang singularity [143,144], as well as energy-dependent birefringence [145,146], among others [11].

LQG provides a background-independent quantisation of GR, avoiding perturbative non-renormalisability and all the troubles that come with it. Works from the past decade [147] show that quantum deformations of spacetime symmetries naturally emerge from LQG corrections, producing a deformed Poincaré algebra characteristic of deformed special relativity (DSR). This framework generates modified dispersion relations from first principles while maintaining background independence.

Group field theory [148] is a closely related framework, often seen as a sort of second quantisation of LQG, in particular its covariant spin foam formulation [149]. It defines a QFT on a group manifold rather than on spacetime, whose quanta are the nodes of spin networks [142]. Spacetime then emerges as a collective or condensate phase thereof. At a fundamental level, spacetime Lorentz invariance is not manifest, due to the absence of an underlying geometric structure; but at higher levels it reappears, being recovered in some appropriate continuum/semiclassical limit, but not below, owing to the discreteness of the emergent spacetime. Some formulations display deformed Poincaré or DSR-like symmetries, suggesting that spacetime symmetry itself may arise from the quantum dynamics of geometry [150,151].

Causal set theory [152] shares with LQG the notion of a fundamentally discrete spacetime, composed of a set of points with only order relations (causality) defining the structure of spacetime [153]. The ordering of the causal set relates to the ordering of events in spacetime, which could give rise to stochastic effects, thereby affecting

[1] There is a rather common misconception that string theory is neither testable nor falsifiable [118,119]. While these worries are well founded considering the framework of string theory as a whole, this ultra-positivist view tends to overlook the fact that certain string-motivated constructions combined with consistency conditions can yield empirically testable predictions [120–123], though not fully falsifiable [124–126].

Equations (31) and (49). A related but technically distinct approach is *causal dynamical triangulations* [154,155], which constructs a discrete spacetime geometrically, preserving causal ordering. Within both of these frameworks, Lorentz symmetry arises as a large-scale statistical feature of an underlying discrete causal structure which can be locally Lorentz-violating.

The *generalised uncertainty principle* [156,157] extends the standard Heisenberg relation by incorporating quantum-gravitational corrections that imply the existence of a minimal measurable length [158–162]. This deformation alters the phase-space structure, leading to MDRs and an energy-dependent notion of momentum, naturally connecting with deformed kinematical frameworks such as DSR.

Asymptotic safety [163, 164] is an approach to quantum gravity that posits the existence of a non-trivial ultraviolet fixed point in the renormalisation group flow [165] of gravitational couplings, which would imply gravity can be consistently quantised at high energies without any new degree of freedom [166–169]. In this framework, Lorentz symmetry is typically preserved, but some studies have tapped into one of the aspects of asymptotic safety—the renormalisation group flow—to explore the possibility of Lorentz-violating operators arising at higher energies [170,171].

GR can be understood within the framework of an effective field theory valid at energies much lower than the Planck scale [172,173]. This pragmatic approach regards the Einstein-Hilbert action as the leading term in a low-energy expansion of a more fundamental quantum theory of gravity, even if its microscopic completion is not known. Quantum corrections to classical GR can then be computed systematically by including all higher-dimension operators compatible with diffeomorphism invariance, suppressed by powers of the Planck energy scale ($E_{\rm Pl}$). In this case, general relativity emerges as the infrared limit of a more general quantum field theory of gravity, with new operators or degrees of freedom becoming relevant at higher energies. As a consequence, this approach can potentially connect gravitational EFT with renormalisable scenarios such as asymptotic safety or string theory [174]. In this case, Lorentz symmetry is preserved at all scales, by construction. Nevertheless, the theory can be extended to include Lorentz-violating operators, thereby connecting it with the SME framework [98].

The *Standard Model extension (SME)* is an EFT that extends the SM to accommodate a description for gravity [98,175]. It is generally described by higher-dimension operators that are suppressed by some high-energy scale ($E_{\rm QG}$), usually taken to be the Planck scale. In doing so, some tensor fields acquire non-zero vacuum expectation values, leading to changes in Lorentz symmetry, in particular its breaking, as in the case of LIV. Therefore, within this framework, deviations from Lorentz invariance follow naturally from the structure of a QG theory, rather than being imposed ad hoc. While this is a phenomenological consequence of *some* QG theories, Lorentz violation does not necessarily imply that gravity can be quantised.

The SME incorporates all possible Lorentz-violating terms that can be constructed from the fields present in the SM and gravitational sectors, while preserving gauge invariance and certain fundamental symmetries. It is, therefore, a tool to systematically study potential violations of Lorentz invariance in a model-independent way, regardless of the underlying QG theory.

The widely-used minimal Standard Model extension (mSME) is the minimal version of the SME that contains all Lorentz-violating operators of mass dimension $d = 3$ or $d = 4$ built from SM fields, whilst maintaining the usual gauge symmetries, $SU(3) \times SU(2) \times U(1)$. Operators of dimension $d = 4$ are CPT-even, while those with $d = 3$ are CPT-odd. Therefore, Lorentz violation associated with the latter is a natural consequence of CPT violation; but the reverse is not necessarily true [127,176].

Within the mSME, Lorentz symmetry can be broken spontaneously, through non-zero vacuum expectation values of tensor fields that permeate spacetime. These background tensors couple to the standard fields, leading to modifications in their dynamics and interactions. However, Lorentz symmetry is not broken at the level of observers, who still see the same physics regardless of their inertial frame of reference. Instead, it is the particles themselves that experience Lorentz violation due to their interactions with these background fields.

The non-minimal SME generalises the framework to include operators of arbitrary dimension, i.e., $d > 4$, which are not necessarily renormalisable, but which are expected to be suppressed by the QG energy scale, $E_{\rm QG}$. These higher-dimension operators can lead to a variety of phenomenological effects, including modified dispersion relations and anomalous interactions, which change the propagation of particles over long distances.

In LIV scenarios, Lorentz symmetry is *explicitly broken*, which directly modifies the usual energy-momentum dispersion relation. This reflects the existence of a preferred frame, commonly associated with the cosmic microwave background or some abstract notion of vacuum rest frame. The conventional energy-momentum conservation laws remain intact, which allows for novel kinematic effects such as shifted reaction thresholds and anisotropies in propagation [177]. For further details see, for example, refs. [11,178–180].

In contrast, DSR aims to preserve the relativity principle while *deforming* the symmetry structure. Here,

the underlying Poincaré algebra is modified in such a way that another invariant scale appears in addition to the speed of light (c), being associated with the QG energy scale ($E_{\rm QG}$) or, equivalently, a minimal length ($\ell_{\rm QG}$). The deformation affects both the dispersion relation and the law of composition of momenta, which become correlated and non-linear [181–185]. This non-linearity gives rise to the notion of *relative locality*, wherein the localisation of events depends on the observer's state of motion [186,187]. Unlike LIV, no preferred frame exists in DSR as invariance is preserved under a deformed set of transformations. Reviews can be found in refs. [11,188–191].

When searching for quantum-gravitational effects using astrophysical observations of high-energy cosmic messengers, one typically looks for tiny deviations from standard physics that accumulate over large distances or timescales, ultimately impacting some observable measured at Earth. The main observables in this case are those influenced by changes in particle propagation, such as modified interaction thresholds, energy-dependent time delays, and oscillations. Other observables include changes in particle decays, oscillations, and polarisation, among others [11,12,190].

3.2. Phenomenological Consequences

3.2.1. Modified Dispersion Relations (MDRs)

QG-induced modifications of particle dispersion relations affect the kinematics of interactions, as described in Section 3.1. The phenomenology depends on whether MDRs are universal (same coefficients for all particles) or particle-dependent, and whether they are combined with modified conservation laws. Non-universality introduces complexity, as different correction coefficients in the dispersion relations of interacting particles lead to a wide variety of possible predictions (e.g., [192–196]).

From a phenomenological perspective, one of the most significant consequences of several QG theories is the violation (LIV) or deformation (DSR) of Lorentz symmetry, which directly changes the energy-momentum dispersion relation [11,197]. A reasonable starting point to describe QG-induced MDRs is to add a term that encapsulates the deviations from Lorentz symmetry, assuming analyticity as energy and momentum approach the special-relativistic limit. This MDR, for a particle a, can be written as:

$$E^2 = m_a^2 c^4 + p^2 c^2 + f_a(E, \vec{p})\,, \tag{31}$$

where the function f_a can be just about anything, depending on the specificities of the QG model. Naturally, there might be formulations which do not fit this parameterisation, although a series-like ansatz combining powers of E and p does tend to be quite general.

Phenomenologically, MDRs like Equation (31) depend on whether the modifications are universal, and whether the usual energy-momentum conservation laws remain unaltered or are themselves deformed in accordance with a modified relativity principle. These two principles help separate two interesting frameworks, LIV and DSR, although there are others.

Assuming small deviations from SR, the function f_a can be expanded in a power series. For rotational invariance in the preferred frame and in the ultrarelativistic limit ($E \approx pc$), this yields:

$$f_a\left(E, \vec{p}\right) \approx f_a\left(p\right) = (pc)^2 \sum_{n=0}^{\infty} \chi_n^{(a)} \left(\frac{pc}{E_{\rm QG}}\right)^n . \tag{32}$$

Although this may sound like a strong assumption, Lorentz symmetry is preserved to very high accuracy, so deviations are expected to be small [198]. More general formulations include anisotropic corrections with preferred spatial directions and mixed energy-momentum powers ($E^j (pc)^{n-j}$) for boost-violating frameworks, though the ultrarelativistic approximation captures the leading-order behaviour for most astrophysical applications.

A common simplification is to consider only the leading-order correction, truncating at finite order (n):

$$f_a\left(p\right) \approx \chi_n^{(a)} \, (pc)^2 \left(\frac{pc}{E_{\rm QG}}\right)^n . \tag{33}$$

Phenomenological MDRs inspired by EFT, such as the SME [98], typically consider only $n = 1, 2$, as higher-order operators are increasingly suppressed by $E_{\rm QG}$.

Different QG approaches yield specific forms of MDRs. Non-commutative spacetimes introduce corrections with inverse powers and logarithmic terms in the four-momentum [135]. Hořava-Lifshitz gravity [199] leads to even powers in momentum due to anisotropic scaling between space and time. Rainbow gravity [200] produces energy-dependent metrics that modify the dispersion relation through the Casimir invariant. In DSR scenarios, the

MDR preserves a modified relativity principle and is typically universal ($f_a = f$ for all particles), often taking forms like [185]:

$$E^2 f_1^2(E) - p^2c^2 f_2^2(E) = m^2c^4\,, \tag{34}$$

with model-dependent functions $f_1(E)$ and $f_2(E)$.

A common phenomenological parameterisation in DSR is the first-order approximation [188,201]:

$$f(E,\vec{p}) = \chi_1 \frac{pc}{E_{\rm QG}} p^2c^2\,, \tag{35}$$

which arises naturally in κ-Minkowski spacetime [202–204] and geometric approaches involving curved momentum spaces [186, 205, 206]. Stochastic modifications inspired by spacetime foam [207–209] take similar forms but treat the coefficient as a stochastic variable [210–212]. It should be emphasised that in DSR, the deformation is accompanied by non-trivial composition laws for energy and momentum, as discussed in Section 3.2.2, so phenomenological effects cannot be inferred from the MDR alone.

It is not my goal to provide an exhaustive list of MDRs arising from various QG approaches found in the literature. Instead, I focused on connecting the underlying theoretical frameworks with their phenomenological consequences, namely the modifications of the dispersion relation.

Given the importance of interaction thresholds in interpreting multi-messenger observations, it is crucial to understand how they are affected by MDRs. Some threshold theorems [194] ensure that under LIV, minimum and maximum thresholds occur for head-on and rear-end collisions if: (i) energy depends only on momentum magnitude (rotational invariance); (ii) energy increases monotonically with momentum; (iii) energy and momentum are additive and conserved. In the general case, forfeiting these assumptions, the situation can be much more complex [196]. For DSR, the picture is completely different, as both dispersion relations and conservation laws are modified, leading to non-linear effects that can significantly alter interaction kinematics [195].

3.2.2. Altered Composition Laws

Some QG approaches, particularly those based on DSR, predict modifications not only to the dispersion relations of particles but also to the laws governing the composition of momenta. These altered composition laws reflect the non-trivial geometry of momentum space in these theories, leading to non-linear and energy-dependent addition rules for momenta.

In general, the composition of two momenta p_1^μ and p_2^μ is denoted as $p_1^\mu \oplus p_2^\mu$, where '$\oplus$' represents the deformed addition operation. Unlike standard momentum addition, which is linear and commutative, these deformed laws can be non-linear, non-commutative, and even non-associative, depending on the specific DSR model, leading to relations such as:

$$p_1^\mu \oplus p_2^\mu \neq p_2^\mu \oplus p_1^\mu\,. \tag{36}$$

As a consequence, *relative locality* [186,187] emerges, where the localisation of events in spacetime depends on the observer's frame of reference. This leads to novel phenomenological effects, such as energy-dependent time delays and modified interaction thresholds, which can be probed with high-energy astrophysical observations.

Several explicit formulations of deformed composition laws exist in the literature, each corresponding to different choices of basis in the underlying algebraic structure. They can usually be cast in the general form:

$$E_\oplus = E_1 \oplus E_2 = w_{E_1}(E_1,E_2,\vec{p}_1,\vec{p}_2)\,E_1 + w_{E_2}(E_1,E_2,\vec{p}_1,\vec{p}_2)\,E_2\,, \tag{37}$$

$$\vec{p}_\oplus = \vec{p}_1 \oplus \vec{p}_2 = w_{p_1}(E_1,E_2,\vec{p}_1,\vec{p}_2)\,\vec{p}_1 + w_{p_2}(E_1,E_2,\vec{p}_1,\vec{p}_2)\,\vec{p}_2\,, \tag{38}$$

where the functions w_{E_i} and w_{p_i} encapsulate the deformation effects, which typically depend on the energies and momenta of the individual particles being combined.

The most common bases used in studies include: bicrossproduct [203, 213], Magueijo-Smolin [184, 185], deformed composition law 1 (DCL1) [214], DSR1 [181,215], among others [216]. Note that these different bases are connected to each other by coordinate transformations that redefine energy and momentum variables [183]. In reality, physical predictions should be invariant under such changes of basis, though calculations may be simpler in one basis versus another.

3.2.3. Interaction Thresholds

In the presence of MDRs, the thresholds for particle interactions can be significantly altered. The modified dispersion relations can lead to changes in the kinematic constraints that govern the allowed energy and momentum

configurations for interactions. This can result in new thresholds for processes that were previously forbidden or in the modification of existing thresholds.

Consider the archetypical case of the MDR altered through the term given by Equation (33). It is possible to derive modified threshold conditions for two-particle interactions. Some of the most relevant processes for high-energy astrophysics were already presented in Section 2.2, and are discussed below in the context of modified interaction thresholds due to MDRs.

Breit-Wheeler pair production. Pair production by photons ($\gamma + \gamma_{\rm bg} \to e^+ + e^-$) is one of the most important interactions affecting the propagation of high-energy gamma rays through cosmological distances. The threshold for this process is particularly sensitive to QG-induced MDRs [217]:

$$s_{\rm thr}^{\rm PP} = p_\gamma^2 c^2 \left[4 \left(\frac{m_e c}{p_\gamma} \right)^2 + \frac{\chi_n^e}{2^n} \left(\frac{p_\gamma c}{E_{\rm QG}} \right)^n \right] , \tag{39}$$

where p_γ is the momentum of the incoming high-energy photon, or conversely, for the background photon minimum energy:

$$\varepsilon_{\rm thr}^{\rm PP} = p_\gamma c \left[\frac{m_e^2 c^2}{p_\gamma^2} + \frac{1}{4} \left(\frac{\chi_n^e}{2^n} - \chi_n^\gamma \right) \left(\frac{p_\gamma c}{E_{\rm QG}} \right)^n \right] . \tag{40}$$

It is evident that positive (negative) values of the LIV parameter for photons (χ_n^γ) increase (decrease) the threshold energy for pair production, potentially allowing high-energy photons to propagate further than expected in standard physics. The mean free path for Breit-Wheeler pair production considering LIV effects is shown in Figure 1.

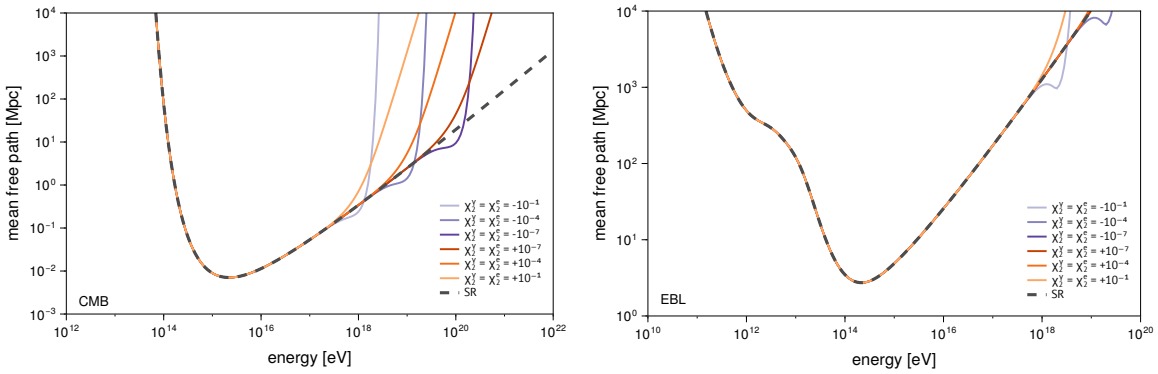

Figure 1. Mean free path for Breit-Wheeler pair production including second-order LIV effects and the MDR given by Equation (33). The left panel shows the results for interactions with CMB photons, whereas the right panel corresponds to interactions with the EBL (model from ref. [218]). Shades of orange represent the superluminal case, whereas shades of purple correspond to the subluminal case. The SR curve is shown as a dashed line. Figure adapted from ref. [217].

Inverse Compton scattering. High-energy electrons can scatter off low-energy background photons, transferring energy to the photons in the process ($e^\pm + \gamma_{\rm bg} \to e^\pm + \gamma$). The threshold for this process is also modified by MDRs [217]:

$$s_{\rm thr}^{\rm ICS} = p_e^2 c^2 \left[\left(\frac{m_e c}{p_e} \right)^2 + \chi_n^e \left(\frac{p_e c}{E_{\rm QG}} \right)^n \right] . \tag{41}$$

In this process, photons of energy ε can interact with the electrons, so $\varepsilon_{\rm thr}^{\rm ICS} = 0$. The mean free path for inverse Compton scattering is shown in Figure 2.

Photoproduction of pions. High-energy protons or neutrons can interact with background photons to produce mesons, as discussed in Section 2.2.3. The two most relevant processes are the photoproduction of neutral and charged pions ($p + \gamma_{\rm bg} \to p + \pi^0$ or $p + \gamma_{\rm bg} \to n + \pi^+$). The threshold for this process is also affected by MDRs, leading to a transcendental equation for the threshold energy. For some partial analytical solutions, see, for instance, refs. [219–223]. The attenuation length[2] for photoproduction of pions considering LIV effects is shown in Figure 3.

[2] The attenuation length is defined as $\left(\frac{1}{E} \frac{{\rm d}E}{{\rm d}x} \right)^{-1}$. It is not necessarily the same as the mean free path, given by Equation (4).

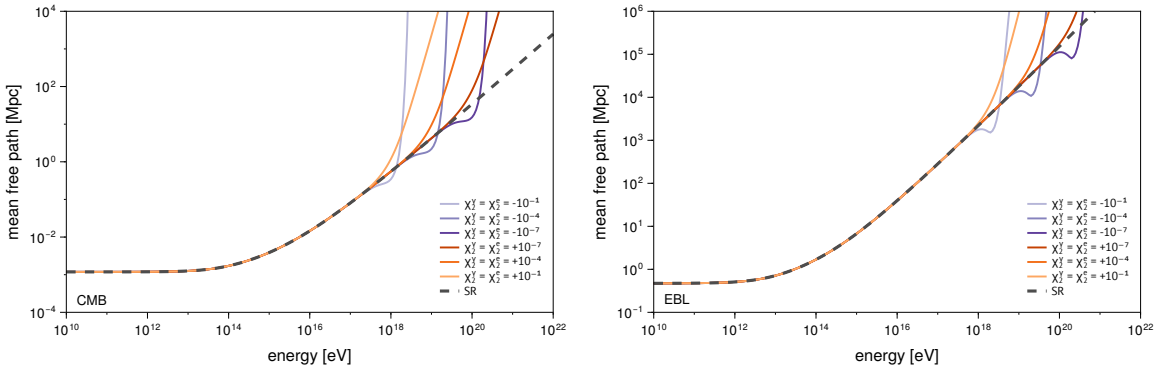

Figure 2. Mean free path for inverse Compton scattering including second-order LIV effects and the MDR given by Equation (33). The left panel shows the results for interactions with CMB photons, whereas the right panel corresponds to interactions with the EBL (model from ref. [218]). Shades of orange represent the superluminal case, whereas shades of purple correspond to the subluminal case. The SR curve is shown as a dashed line. Figure adapted from ref. [217].

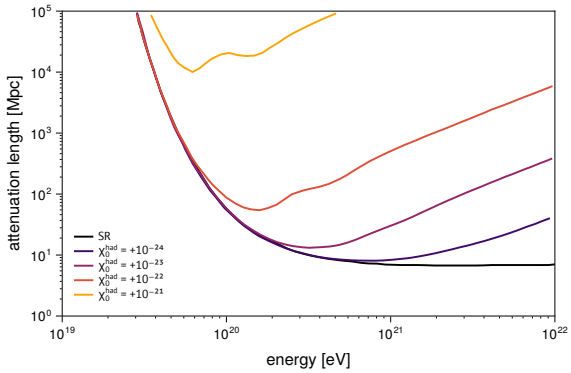

Figure 3. Attenuation length for photoproduction of pions considering LIV effects of order 0, according to Equation (32). Here $\chi_0^{\rm had} = \frac{1}{2}\chi_0^{\pi} = \chi_0^{\rm p}$. Figure adapted from ref. [224].

Photodisintegration. The case of nuclear photodisintegration is more complex due to the composite nature of nuclei. It is not even clear if Lorentz-violating effects should be applied to the nucleus as a whole or to its individual nucleons. The complexities of Lorentz-symmetry breaking in composite systems are discussed in more detail in Section 5.1. Detailed calculations of photodisintegration thresholds under LIV were presented in refs. [225–227], for the MDR given by Equation (33). The energy threshold of the background photon in the nucleus rest frame (ε') is shown in Figure 4 for various LIV coefficients, for two representative nuclei, helium and nitrogen, following the parametrisation from refs. [227,228].

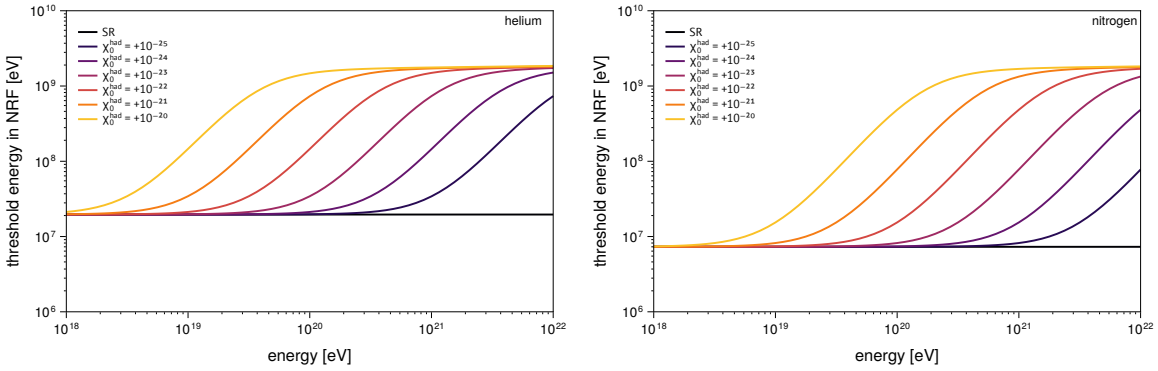

Figure 4. Threshold energy of the target photon (ε'), in the nucleus rest frame, for photodisintegration. Different lines correspond to different LIV coefficients, according to Equation (32) truncated at order $n = 0$. The left panel corresponds to the case of a helium nucleus, and the right is for a nitrogen nucleus. Here $\delta_{\rm had,\,n} = \chi_n^{\rm had} / E_{\rm QG}^n$.

3.2.4. New Processes

A direct consequence of the modified dispersion relations described in Section 3.2.1 is the possibility of new particle processes that are otherwise forbidden in the SM considering SR. In the case of LIV, the explicit breaking of Lorentz symmetry allows for processes that violate standard kinematic constraints, leading to novel decay channels and interactions. In DSR, while Lorentz symmetry is preserved in a deformed sense, single-particle decays like photon decay or vacuum Cherenkov are generically forbidden; threshold anomalies of standard reactions are at most mildly modified.

Below I illustrate several of these processes, following results obtained from EFTs, considering $E_{\rm QG} = E_{\rm Pl}$. The MDR assumed here is the widely-used form given by Equation (33).

Photon decay. In SR, energy-momentum conservation prevents a photon from decaying. However, modifications of the dispersion relation can allow this process to occur above a certain energy threshold. Within extensions of QED, this process can be represented as

$$\gamma \to f^+ + f^- \,, \tag{42}$$

where f is a charged fermion, typically an electron or positron. Threshold conditions are discussed in ref. [192,229], while decay rates and spectra can be found in refs. [192,230].

Vacuum Cherenkov radiation. Depending on the values of the coefficients in MDRs, charged fermions can spontaneously emit photons in vacuum [229,231–233],

$$f^\pm \to f^\pm + \gamma \,. \tag{43}$$

Emission rates and bounds for modified Maxwell and fermion sectors with *non-identical* photon and fermion coefficients have been derived in Rubtsov et al. [230], Kaufhold and Klinkhamer [234, 235], Klinkhamer and Risse [236]. The emission spectrum for a modified Maxwell theory ($n = 2$ in Equation (33)) was obtained in refs. [237,238].

Photon splitting. In SR, photon splitting processes such as

$$\gamma \to \gamma + \gamma \qquad \text{or} \qquad \gamma \to \gamma + \gamma + \gamma \qquad \text{or} \qquad \gamma \to \gamma + \gamma + \gamma + \ldots \tag{44}$$

are forbidden in vacuum for on-shell photons, since they violate energy-momentum conservation. For Lorentz-violating MDRs like Equation (33), the splitting into three photons becomes a viable process, since it can proceed through already-existing multi-photon vertices from QED [192, 239]. Two-photon splitting is also allowed if additional gauge-invariant cubic operators are present in the photon sector; see the discussion in refs. [192].

Neutrino Cherenkov emission. In the Lorentz-invariant SM, neutrinos cannot spontaneously emit photons in vacuum due to their neutral charge and the absence of direct couplings to photons. However, in LIV scenarios with modified neutrino dispersion relations, the process

$$\nu \to \nu + \gamma \tag{45}$$

is kinematically allowed for sufficiently energetic neutrinos. Explicit kinematics and rates are given in refs. [240,241]; threshold analyses can be found in ref. [192].

Neutrino splitting. Another possible process for superluminal neutrinos is the emission of neutrino–anti-neutrino pairs:

$$\nu_i \to \nu_i + \nu_j + \bar{\nu}_j \,, \tag{46}$$

where i and j denote different neutrino flavours or mass eigenstates. The possibility of particle splitting from modified dispersion relations was first noted in general terms by Jacobson et al. [192]. Dedicated calculations for neutrinos have been performed in refs. [242–244].

Neutrino charged-lepton emission. A further possibility is the emission of charged lepton pairs by superluminal neutrinos:

$$\nu_\ell \to \nu_\ell + \ell^+ + \ell^- \,, \tag{47}$$

where ℓ represents a charged lepton. This is primarily a neutral-current process mediated by the Z boson [245], leading to significant energy losses for high-energy neutrinos. Variants of this model have been explored in ref. [246]. Alternative hypotheses, such as tachyonic dispersion relations, have also been considered [247].

Graviton emission. A process theoretically possible in some QG scenarios is the spontaneous emission of gravitons by particles:

$$X \to X + g \,, \tag{48}$$

where g denotes a graviton [248]. This is the gravitational analogue of vacuum Cherenkov radiation: if the maximal attainable velocity of a particle exceeds that of gravity, it can lose energy by emitting a graviton, as first shown by Moore and Nelson [249]. A general description within the gravity sector of the SME, including constraints from CRs and neutrinos, is given in ref. [248]. More recently, a unified framework incorporating modified dispersion relations for both electromagnetic and gravitational channels has been presented by Artola et al. [250].

3.2.5. Chromatic Time Differences

As a consequence of the MDR given by Equation (31), the group velocity of a particle a becomes energy-dependent, and can be expressed as:

$$v_a = \frac{\partial E}{\partial p} = c\left(2pc + \frac{1}{c}\frac{\partial f_a}{\partial p}\right)\left(2E - \frac{\partial f_a}{\partial E}\right)^{-1} . \tag{49}$$

In the limit $f_a \to 0$, one recovers the special-relativistic expression, $v_a = c^2 p/E$.

It follows from Equation (49) that particles with different energies will generally propagate at different speeds, implying chromatic (energy-dependent) time differences. If the correction makes the velocity decrease with energy (*subluminal* case, $v_a < c$), higher-energy particles travel more slowly and therefore arrive at the detector *later* than lower-energy ones. Conversely, if the correction makes the velocity increase with energy (*superluminal* case, $v_a > c$), higher-energy particles propagate faster and arrive *earlier*.

Equation (49) is the phenomenological basis for the search for the speed of particles in QG theories, which ultimately leads to one interesting phenomenological signature of QG: energy-dependent time delays [251–256].

Due to the modified particle velocity in Equation (49), QG models with modified dispersion relations often predict energy-dependent (chromatic) time delays. These effects can become particularly significant in astrophysical sources at high redshift, where cosmological distances amplify tiny QG-scale corrections. For massless particles, the standard energy-momentum relation in an expanding universe reads

$$E(t) = \frac{pc}{a(t)} = pc\,(1 + z(t)) \ , \tag{50}$$

where p is the *comoving* momentum (a conserved quantity for freely propagating particles), and $a(t)$ is the scale factor of the universe, so that $p/a(t)$ is the *physical* momentum. In QG scenarios this relation is modified. For instance, within the LIV framework, it can be expanded in powers of $pc/a(t)E_{\rm QG}$ [255]:

$$E = \frac{pc}{a(t)}\sqrt{1 - \chi_n^\gamma \left(\frac{pc}{a(t)E_{\rm QG}}\right)^n} , \tag{51}$$

where χ_n^γ is a parameter associated with LIV, defined in the context of Equation (33).

The corresponding QG-induced time delay, $\Delta t_{\rm QG}$, in a Friedmann-Lemaître-Robertson-Walker (FLRW) background is given by [11]:

$$\Delta t_{\rm QG} = \chi_n^\gamma \frac{1+n}{2H_0}\left(\frac{E_0}{E_{\rm QG}}\right)^n \int_0^{z_s} \frac{(1+z)^n\, dz}{\sqrt{\Omega_{\rm m}(1+z)^3 + \Omega_\Lambda}} , \tag{52}$$

where E_0 is the observed energy, and the cosmological parameters are those described in Section 2.1.

Beyond the empirical formula by Jacob and Piran [255], several generalisations of the FLRW dispersion relation and corresponding time-delay expressions have been proposed [256–260].

In DSR, relative locality effects further modify the energy-momentum relation and introduce additional terms in $\Delta t_{\rm QG}$, involving more complex integrals [11,258]. In both LIV and DSR, the underlying cosmological model plays a central role in quantifying these delays, making them a promising signature of QG, especially for high-redshift sources.

It should be emphasised that the dispersion relation in Equation (51) is a simplified ansatz. More complete formulations may yield different predictions for the time delays ($\Delta t_{\rm QG}$), which in turn affects the interpretation of observational data.

3.2.6. Neutrino Flavour Transitions

In the SME, the leading-order corrections to neutrino propagation arise from effective operators that violate Lorentz invariance and possibly CPT symmetry. The effective Hamiltonian for neutrino propagation is

$$H_{\alpha\beta}(E,\hat{\varrho}) = \frac{1}{2E}(UM^2U^\dagger)_{\alpha\beta} + \sum_{d\geq 3} E^{d-3}\left[a^{(d)}_{\alpha\beta}(\hat{\varrho}) - c^{(d)}_{\alpha\beta}(\hat{\varrho})\right], \tag{53}$$

where α,β are flavour indices, U is the Pontecorvo-Maki-Nakagawa-Sakata (PMNS) matrix, M^2 is the diagonal mass-squared matrix, and $\hat{\varrho}$ is the neutrino propagation direction. CPT-odd coefficients ($a^{(d)}$) have opposite signs for neutrinos and anti-neutrinos, whereas CPT-even ($c^{(d)}$) have the same sign. Hermiticity requires $a^{(d)} = a^{(d)\dagger}$ and $c^{(d)} = c^{(d)\dagger}$ (in flavour space).

Anisotropic coefficients produce sidereal variations in the event rate, while isotropic ones induce energy-dependent distortions of the oscillation pattern [175,261,262]. At multi-TeV energies and above, atmospheric and astrophysical neutrinos probe operators up to $d \sim 10$, constraining Planck-suppressed LIV terms [263,264].

Direction dependence and the notion of a preferred frame enter the equation through the background-tensor projections, $a^{(d)}(\hat{\varrho})$ and $c^{(d)}(\hat{\varrho})$, which can be expanded in spherical harmonics:

$$a^{(d)}_{\alpha\beta}(\hat{\varrho}) = \sum_{jm} Y_{jm}(\hat{\varrho})\, a^{(d)}_{\alpha\beta,(jm)} \qquad \text{and} \qquad c^{(d)}_{\alpha\beta}(\hat{\varrho}) = \sum_{jm} Y_{jm}(\hat{\varrho})\, c^{(d)}_{\alpha\beta,(jm)}\,, \tag{54}$$

in a given coordinate system, usually the celestial equatorial frame centred at the Sun. The isotropic ($j=0$) components are conventionally denoted by a ring on top of the symbol, $\mathring{a}^{(d)}_{\alpha\beta}$ and $\mathring{c}^{(d)}_{\alpha\beta}$, for the monopole term ($Y_{00} = 1/\sqrt{4\pi}$).

A natural question that arises is how the tensors a and c relate to MDRs like those described in Section 3.2.1. For a flavour eigenstate α, the neutrino and anti-neutrino MDRs implied by the SME Hamiltonian (Equation (53)) are, to leading order in Lorentz violation,

$$\begin{aligned} E_\nu &\simeq pc + \frac{m_\alpha^2 c^3}{2p} + \sum_{\substack{d\geq 3\\ d \text{ odd}}} (pc)^{d-3}\, \mathring{a}^{(d)}_{\alpha\alpha} - \sum_{\substack{d\geq 4\\ d \text{ even}}} (pc)^{d-3}\, \mathring{c}^{(d)}_{\alpha\alpha}\,, \\ E_{\bar{\nu}} &\simeq pc + \frac{m_\alpha^2 c^3}{2p} - \sum_{\substack{d\geq 3\\ d \text{ odd}}} (pc)^{d-3}\, \mathring{a}^{(d)}_{\alpha\alpha} - \sum_{\substack{d\geq 4\\ d \text{ even}}} (pc)^{d-3}\, \mathring{c}^{(d)}_{\alpha\alpha}\,, \end{aligned} \tag{55}$$

where m_α is the effective mass[3] of the flavour eigenstate α. In isotropic cases, Equation (55) reduces to a momentum-power series similar to Equation (32). In this case, anisotropic terms would act like direction-dependent refractive indices.

4. Astrophysical Constraints

In this section, I discuss a few examples of constraints on QG effects derived from the propagation of high-energy astrophysical messengers, namely photons, UHECRs, and neutrinos, considering specific phenomenological observables. When relevant, I address the caveats and limitations of these constraints, as well as possible improvements and future directions.

4.1. Photon Propagation

Several constraints on QG effects have been derived from observations of high-energy photons, particularly gamma rays, focusing on modifications to the energy spectrum due to altered interaction thresholds and cross sections. One of the most common processes considered is pair production, where a high-energy photon interacts with a low-energy background photon to produce an electron-positron pair, as described in Section 2.2.1.

Unless otherwise stated, the constraints from this section assume a modified dispersion relation of the form of Equation (33), possibly with species-dependent coefficients χ^i_n and a common QG energy scale $E_{\rm QG} = E_{\rm Pl}$.

[3] Technically, the notation m_α is a shorthand for the diagonal contribution of the matrix $UM^2U^\dagger$ in flavour space in the ultrarelativistic limit; flavour eigenstates do not, in general, correspond to definite mass eigenstates.

4.1.1. Forbidden Processes

Many constraints on LIV have been derived invoking the new processes allowed under LIV and forbidden in standard physics, such as photon decay, photon splitting, and vacuum Cherenkov radiation, as discussed in Section 3.2.4.

The High-Altitude Water Cherenkov observatory (HAWC) Collaboration derived a very stringent constraint on LIV based on observations of at least four different sources of Galactic gamma rays of energy $E \gtrsim 100$ TeV. The bounds obtained based on photon decay were $\chi_1^\gamma < 5.5 \times 10^{-4}$ and $\chi_2^\gamma < 2.3 \times 10^{10}$, at a 95% C.L. [265]. They also performed a similar analysis for each of the sources considering the splitting of a photon into three (or more) photons. The strongest limit obtained was $\chi_2^\gamma < 1.0 \times 10^8$. These limits assume photon-only LIV, i.e., $\chi_n^e = 0$.

Several constraints exist on LIV in the electron sector from observations of the Crab Nebula [192,266–270], considering vacuum Cherenkov and synchrotron emission. The most stringent ones are $\chi_1^e < 1.3 \times 10^{-7}$ [270].

4.1.2. Universe's Transparency

Several constraints have been derived based on the attenuation of high-energy photon fluxes due to pair production with background photons, such as those from the EBL and CMB. Stringent bounds using several gamma-ray sources were derived in ref. [271] using 111 energy spectra of 38 different sources. The derived LIV coefficients[4], at a 3σ confidence level, are $\chi_1^\gamma > -0.13$ and $\chi_2^\gamma > -5.2 \times 10^{13}$ for an MDR of the form of Equation (33), assuming $E_{\rm QG} = E_{\rm Pl}$. The H.E.S.S. Collaboration derived similar limits using the blazar Mrk 501 during a flaring state in 2014 [273], obtaining $\chi_1^\gamma > -0.46$ and $\chi_2^\gamma > -2.4 \times 10^{14}$ at a 95% confidence level. Note that both of these limits are for the subluminal case ($\chi_n^\gamma < 0$), as this is the scenario that leads to an increase in the pair-production threshold, allowing more high-energy photons to reach Earth. Moreover, they considered modifications to the photon sector only, thus $\chi_n^e = 0$. But according to Equations (39) and (40), the pair-production thresholds depend on the combination $\left(\frac{\chi_n^e}{2^n} - \chi_n^\gamma\right)$, which limits the generality of these results.

An event of great interest that served as a testbed for QG effects was the brightest-ever gamma-ray burst (GRB), GRB 221009A [274–278]. At first, Large High Altitude Air Shower Observatory (LHAASO) reported the detection of photons with energies up to 18 TeV, which was considerably reduced when the results were finally published [275,276]. Since this object was located at a redshift of $z \approx 0.15$, it is extremely unlikely that these particles would have reached Earth due to attenuation from pair production with the EBL. Immediately after the original announcement, several authors [279–281] derived limits on LIV, although a few explanations not involving new physics were proposed [85,282–284]. A detailed analysis was performed by the LHAASO Collaboration [285], who derived the following bounds: $\chi_1^\gamma > -0.1$ and $\chi_2^\gamma > -2.7 \times 10^{14}$, at a 95% confidence level, again assuming $E_{\rm QG} = E_{\rm Pl}$ and $\chi_n^e = 0$. Interestingly, the experiment Carpet-3 reported the detection of a photon-like event with an energy of approximately 300 TeV [286], only a few hours after the burst, consistent with the direction of this GRB within the angular resolution (4.7°, 90% C.L.). If confirmed, this would call for explanations beyond standard physics, including LIV [287,288].

A full treatment of electromagnetic cascades is needed. The widely-used Equation (8) only takes into account pair production, such that photons are absorbed, electron-positron pairs are created, but no other processes are considered. But *what is the fate of those electron-positron pairs?* In reality, they too can interact with background photons via inverse Compton scattering, generating secondary emission (see Section 2.2.2). The secondary photons produced in this way can themselves undergo pair production, creating an *electromagnetic cascade*. The relevance of these secondary photons depends, among other factors, on the spectrum of the emitted high-energy photons. If this information is unavailable, as is often the case, Equation (8) provides a reasonable approximation for the observed flux at the highest energies where pair production dominates, but it may underestimate the flux at lower energies where cascade photons contribute significantly. That could affect constraints based on GeV observations, i.e., the energy range probed by Fermi-LAT [289].

The treatment of electromagnetic cascades is rather complex. To my knowledge, Abdalla and Böttcher [290] were the first to investigate the possible role of inverse Compton scattering in the gamma-ray spectrum in the presence of LIV. They argued that this effect would likely not be significant enough at sub-PeV energies. Nevertheless, they did not perform a full analysis, which would require Monte Carlo simulations of electromagnetic cascades with LIV.

Monte Carlo simulations are the way forward. A recent advance was presented in ref. [291]—the code LIVpropa. It is a plugin for CRPropa [84,85], which enables the simulation of electromagnetic cascades with LIV effects. This

[4] In the literature, it is more common to find constraints on the energy scale $E_{\rm QG}$. However, throughout this review, I opted for the usage of species-dependent coefficients and a single QG scale presumed to be common to all particles. Mathematically, both formulations are obviously equivalent. However, if there is indeed a QG energy scale $E_{\rm QG}$, possible fine-tuning [272] of some coefficients (χ_n) for certain particle species could be hinting towards an even more fundamental theory.

is, to my knowledge, the first public Monte Carlo code that enables full numerical simulations of electromagnetic cascades including LIV effects. Previous works often relied on simplified analytical estimates or semi-analytical models that only considered the primary interaction (pair production) and neglected the subsequent cascade development.

LIVpropa was used in ref. [217] to investigate the impact of LIV on the propagation of high-energy gamma rays from distant astrophysical sources. Figure 5 shows the results of these detailed simulations for two sources, the blazars 1ES 0229+200 and Mrk 421, located at redshifts $z = 0.14$ and $z = 0.030$, respectively. The simulations consider a simple power-law spectrum with a hard cut-off at 1 PeV, and include processes such as pair production and inverse Compton scattering off the CMB and EBL, as well as photon decay and vacuum Cherenkov radiation.

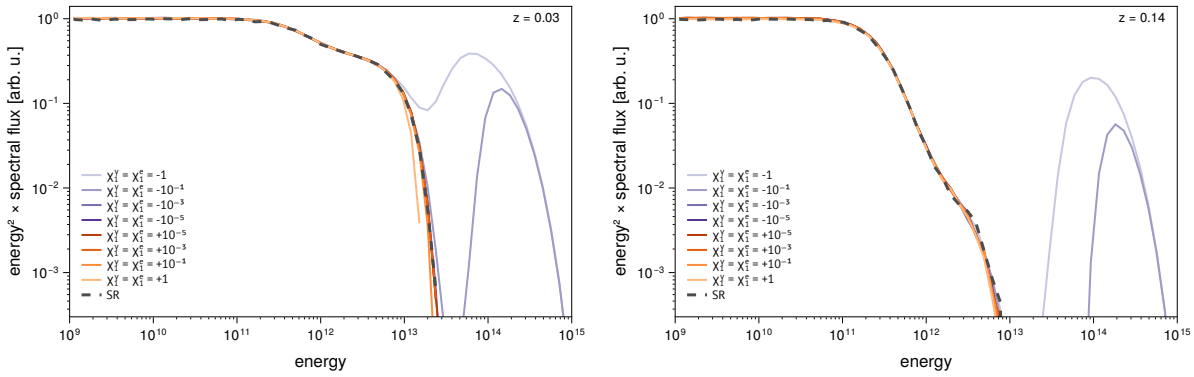

Figure 5. Gamma-ray fluxes expected at Earth, assuming LIV with the parameters indicated in the legend. The left panel depicts a source at redshift $z = 0.03$, and the right one depicts a source at $z = 0.14$, which correspond to the blazars Mrk 421 and 1ES 0229+200, respectively. Shades of orange represent the superluminal case, whereas shades of purple correspond to the subluminal case. The dashed line show the Lorentz-invariant case. Breit-Wheeler pair production and inverse Compton scattering with the CMB and the EBL (model from ref. [218]) are taken into account, alongside photon decay and vacuum Cherenkov radiation. Figure adapted from ref. [217].

The results shown in Figure 5 are rather remarkable because they include in the same simulation processes such as vacuum Cherenkov emission and photon decay (see Section 3.2.4), which are usually treated separately. Therefore, this work provides what is arguably the most complete and self-consistent treatment to date of LIV in the context of high-energy gamma-ray propagation.

Are Lorentz-violating cross sections well known? Uncertainties in the cross section for pair production due to QG effects can significantly impact the interpretation of gamma-ray observations. Carmona et al. [292] recently investigated how different treatments of the pair-production cross section affect the predicted attenuation of high-energy gamma rays traveling through the intergalactic medium. They compared various approximations, some preserving the Breit-Wheeler form of the cross section with modified kinematics, and another one deriving the cross section from first principles within an EFT framework. They found that the choice of cross section model can lead to substantial differences in the predicted gamma-ray fluxes, especially at energies near the pair-production threshold.

An example in the context of DSR. An interesting investigation of the impact of MDRs in the context of DSR was done by Carmona et al. [293]. They consider the propagation of high-energy photons from distant sources, taking into account not only modified dispersion relations but also altered composition laws. Following the discussion presented in Section 3.2.2, they computed mean free paths (Equation (4)) in two ways: with the kinematics perceived by the high-energy photons, and also as seen by the background photons. They showed that this choice can lead to significantly different predictions for the attenuation of gamma-ray fluxes. In particular, in one case the universe is more transparent to high-energy photons, while in the other case it is less transparent. It is, however, unclear how to choose or combine these two solutions.

4.1.3. Time-of-Flight Effects

Several works have derived constraints on QG effects based on time-of-flight measurements of high-energy photons from distant astrophysical sources, such as GRBs and blazars [251, 254, 273, 276, 294–297]. The basic idea is that if QG effects lead to an energy-dependent speed of light, then photons of different energies emitted simultaneously from a distant source would arrive at Earth at different times.

Bounds from transient sources. One of the first constraints of this kind was derived in ref. [298]: $\chi_1^\gamma > -3.05 \times 10^3$. Several subsequent works improved upon this limit [273, 299, 300], especially using GRB observations. Notably,

Fermi-LAT observations of GRB 090510 led to some of the most stringent limits: $-0.55 < \chi_1^\gamma < 0.31$ and $-9.3 \times 10^{16} < \chi_2^\gamma < 1.7 \times 10^{17}$ at a 95% confidence level [301].

Methodologically, those bounds combined three complementary techniques: limits on total dispersion, dispersion-cancellation, and parametric likelihood fits, with explicit treatment of intrinsic lags. More recently, the detection of GRB 190114C by MAGIC [302] enabled competitive limits on χ_2^γ after careful control of source evolution systematics [300]. Several independent analyses constrained Lorentz violation using observations of the extraordinary GRB 221009A (the "B.O.A.T.") [279–281,303,304], although the treatment of modified thresholds, discussed in Section 3.2.3, has to be taken into account when interpreting these results.

Short-duration active galactic nucleus (AGN) flares can also constrain MDRs. The MAGIC Collaboration introduced common analysis methods when analysing observations of Mrk 501 [295], which were complemented by H.E.S.S.'s observations of PKS 2155−304 [296]. Novel statistical techniques and improved statistics have led to progressively better limits over time, in particular in the context of AGN flares like Mrk 421 [273].

Multi-instrument analyses. An interesting effort by Bolmont et al. [305] combined data from the three operating IACTs – H.E.S.S., MAGIC, and VERITAS – to derive joint constraints on LIV. By combining observations of several objects, together with a rigorous treatment of uncertainties, these will likely become the most robust limits based on IACT observations, until the Cherenkov Telescope Array Observatory (CTAO) [306] starts to operate, which will then have unprecedented sensitivity to LIV effects [307].

Nevertheless, the statistical treatment of the data in searching for time lags is rather intricate, and different methods can lead to different results. A review of various statistical techniques used in QG studies with IACTs can be found in ref. [308].

DSR studies. Given the non-trivial nature of the composition laws of DSR (see Section 3.2.2), it is not straightforward to predict time delays based solely on the modified dispersion relation. Amelino-Camelia et al. [151] investigated this issue in detail, showing that while one might naively expect energy-dependent time delays due to modified photon velocities, time delays may not be as pronounced as one might think when $E_{\rm QG} \gtrsim E_{\rm Pl}$, given the interplay between modified dispersion relations and deformed translation symmetries. In fact, in some realisations of DSR, time lags might be zero even if the dispersion relation is modified. This raises the question of which observables are truly sensitive to DSR effects, and whether time-of-flight measurements are the most suitable probes for this class of models.

4.2. UHECR Propagation

4.2.1. The GZK Effect

Much has been speculated about how QG effects could manifest in the propagation of UHECRs [309,310]. Historically, following the initial reports from the AGASA experiment claiming the non-observation of a spectral cut-off [311,312], many works explored how QG effects could affect UHECR interactions [177,181,231,313–317], which could prevent the onset of the GZK effect, thus explaining the AGASA observations (see Section 2.2.3).

There have also been some studies in the context of DSR. Ref. [318] performs simulations of UHECR propagation considering MDR and modified composition laws, as discussed in Section 3.2.2. They show that the expected UHECR spectrum at Earth can be significantly altered depending on the choice of composition law, similar to what was found for high-energy photons in ref. [293].

4.2.2. Phenomenological Fits

Some works did take into account the actual UHECR composition. Saveliev et al. [226] were one of the first to study the effects of LIV on the propagation of nuclei, focusing on nuclear photodisintegration. While they did not derive explicit limits on LIV parameters, they did show that the presence of LIV could significantly alter the expected UHECR spectrum and composition at Earth, and under which conditions. Moreover, they considered additional processes, such as spontaneous decay and vacuum Cherenkov emission, which are forbidden in SR, but can become kinematically allowed in the presence of LIV.

The Pierre Auger Collaboration [224] has recently investigated the phenomenology of LIV in the hadronic sector considering that UHECRs are nuclei. By performing a combined fit of the energy spectrum and the distribution of the depth of the shower maximum ($X_{\rm max}$) measured at the Pierre Auger Observatory, the impact of LIV on the relevant interactions, including photodisintegration and photoproduction of pions, was studied, for a given astrophysical scenario of UHECR sources, assuming an MDR like Equation (33). Here the definitions are such that $\chi_n^{(a)} = \chi_n^p = \chi_n^\pi/2 = A^n \chi_n^A$, where the superscripts p, π, and A refer to protons, pions, and nuclei, respectively. The best-fit values set limits of $\chi_0^p < 10^{-19}$, $\chi_1^p < 1.2 \times 10^{-10}$, and $\chi_2^p < 0.149$, at a 5σ confidence level. However, the quality of the fit including LIV is worse than the Lorentz-invariant case, such that the standard

scenario is preferred if the astrophysical model for UHECR sources is true — which is unlikely to be correct, given the oversimplified assumptions: a uniform distribution of isoluminous sources with a power-law spectrum and a rigidity-dependent exponential cut-off (see ref. [319] for a discussion on the limitations of these combined fits).

4.2.3. Cosmogenic Particles

The flux of cosmogenic neutrinos and gamma rays produced during the propagation of UHECRs is sensitive to QG effects [224,320–324]. In fact, it can be argued that cosmogenic particles are among the most sensitive probes of LIV in the hadronic sector, albeit indirectly. This is because even tiny modifications to the interaction thresholds can lead to significant changes in the expected fluxes of cosmogenic neutrinos and photons.

Recently, the Pierre Auger Collaboration [224] performed a comprehensive analysis of the expected fluxes of cosmogenic photons in the presence of LIV, considering different astrophysical scenarios for UHECR sources. The results depend strongly on the assumed mass composition of UHECRs at the highest energies, and no constraints are possible if the fraction of protons is negligible beyond 10^{19} eV, as suggested by current data. However, for an alternative scenario in which approximately 31% of the total flux above $10^{18.75}$ eV is composed of protons, it is possible to obtain constraints on LIV parameters in the electromagnetic sector. Assuming the MDR of Equation (32) truncated at order $n = 2$, and $E_{\rm QG} = E_{\rm Pl}$, the resulting limits are $\chi_0^\gamma > -10^{-21}$, $\chi_1^\gamma > -10^{-12}$, and $\chi_2^\gamma > -0.015$. Note that these results were derived under the assumption that the cross section is modified only kinematically, i.e., the functional form of the cross section remains the same as in SR, but with modified thresholds (see Section 3.2.3).

In ref. [324], the authors investigated the impact of LIV on the fluxes of cosmogenic neutrinos. The neutrinos were produced mainly through photoproduction of pions and neutron decays. During propagation, they can undergo non-standard processes (see Section 3.2.4), namely neutrino charged-lepton emission and neutrino splitting. It is not possible to derive strong constraints on LIV parameters in the neutrino sector from current data, given the sensitivity of existing experiments. However, with the expected sensitivity of future detectors like Giant Radio Array for Neutrino Detection (GRAND) [325] or IceCube-Gen2 [326], this method is a promising way to set stringent limits on LIV in the neutrino sector.

4.3. Neutrino Propagation

4.3.1. Time-of-Flight Analyses

Several works have derived constraints on QG effects based on time-of-flight measurements of high-energy neutrinos from distant astrophysical sources, such as GRBs and blazars [251,254,294,327–330]. The basic idea is similar to that for photons (see Section 4.1.3): if QG effects lead to an energy-dependent speed of neutrinos (see Equation (49)), then neutrinos of different energies emitted simultaneously from a distant source would arrive at Earth at different times. By measuring the arrival times of neutrinos with different energies, one can set limits on the parameters characterising the QG-induced modifications to the neutrino dispersion relation.

Constraints based on flaring sources. After the strong evidence for high-energy astrophysical neutrinos from an extragalactic source, the blazar TXS 0506 + 056 [263], many works explored the potential of these observations to constrain QG effects based on time-of-flight measurements [331–334]. Some of the most stringent bounds, obtained using Equation (52) for an MDR like Equation (33), are $\chi_1^\nu < 3.8 \times 10^3$ and $\chi_2^\nu < 1.5 \times 10^{16}$.

Recently, Amelino-Camelia et al. [335] performed an analysis of several neutrino-GRB associations, looking for possible QG-induced time delays, building on their previous works [336–338]. They considered neutrinos with $E \gtrsim 60$ TeV. Their analysis distinguishes between neutrinos arriving "early" (before the associated GRB) and "late" (after the GRB). Out of the ten GRBs considered, only one of them had a measured redshift; for the others, they assumed typical values based on known GRB distributions. They claim evidence for a correlation between neutrino energy and time delay, consistent with a linear modification to the neutrino dispersion relation (see Equation (33) with $n = 1$). A similar analysis was performed by Huang and Ma [337],Huang et al. [338], who also discussed in detail the possible role of neutrino–anti-neutrino asymmetry in CPT-odd LIV scenarios.

While this idea is indeed interesting, there are several caveats to be considered. Firstly, the lack of distance information for nine out of the ten GRBs analysed introduces large errors. Secondly, the associations between neutrinos and GRBs are not firmly established, as the angular uncertainties of the neutrino events are often large. Finally, any claim of QG-induced time-of-flight effects must grapple with the challenge of disentangling these from intrinsic source effects and propagation effects. Nevertheless, with a larger sample and with reliable distance measurements, this approach could indeed be interesting for future studies.

Interplay with interaction thresholds. An interesting analysis by Carmona et al. [339] examined the interplay between neutrino time-of-flight anomalies and neutrino decay rates in the presence of LIV. They show that if neutrinos exceed a certain energy threshold, then they could decay via one of the channels described in Section 3.2.4

faster than they can reach Earth from distant sources. Therefore, any time-of-flight analysis for neutrinos should also include these processes to ensure consistency.

DSR signatures. A complementary DSR signature that is studied in the context of high-energy neutrinos is *dual lensing* – tiny, energy-dependent apparent angular offsets due to momentum-space curvature [340,341]. Ref. [331] used IceCube observations of TXS 0506+056 to set an order-of-magnitude bound on such effects at the Planck scale, obtaining $\chi_1 \lesssim 1000$.

4.3.2. Modified Thresholds

The interest in Lorentz-breaking in the neutrino sector increased in the early 2010s when OPERA reported a superluminal neutrino detection, which turned out to be a fluke [342,343]. Several works employed the Coleman-Glashow LIV framework [177] to derive constraints on superluminal neutrinos in the following years. There were also works employing a different approach, focusing on DSR [344]. For a review, see refs. [345–347].

When IceCube first reported PeV-scale neutrinos [348,349], it was quickly realised that if these neutrinos were superluminal, they would lose energy very rapidly primarily via charged-lepton pair emission (also known as vacuum pair emission, VPE), ($\nu \to \nu\, e^+e^-$; see Section 3.2.4) [177,245]. This process has a threshold energy that implies a spectral cut-off, which was not observed, thus leading to constraints [350,351]. Another process that can lead to energy loss for superluminal neutrinos is neutrino splitting, $\nu \to \nu\nu\bar{\nu}$ [242,243]. The most stringent bounds combining both processes are $\chi_1^\nu < 1.6 \times 10^{-6}$ and $\chi_2^\nu < 9.8 \times 10^6$ [352].

The Glashow resonance. At high energies, the Glashow resonance ($\bar{\nu}_e + e^- \to W^-$) at $E \simeq 6.3$ PeV provides a sensitive probe of energy-dependent kinematics susceptible to Lorentz-breaking changes. Early suggestions that the non-observation of such events could indicate LIV-induced shifts in the resonance [353] were rendered obsolete by IceCube's detection of a Glashow resonance event [354], which confirmed the SM threshold within uncertainties.

4.3.3. Neutrino Flavours and Oscillations

LIV constraints. Neutrinos produced in astrophysical sources carry a flavour composition shown in Table 1. QG effects modify the flavours in an energy-dependent (and possibly direction-dependent) way, causing departures from the flavour composition expected from standard oscillations. Thus, measurements of the flavour composition at Earth can be used to probe QG effects, a topic extensively discussed in the literature [355–359].

The IceCube Collaboration has used high-energy atmospheric and astrophysical neutrinos to set the most stringent limits to date on several QG-induced effects that can affect neutrino flavour propagation, including anomalous decoherence and LIV within the SME framework (see Section 3.2.6). No evidence for such effects has been found in the data so far [360]. Four types of models were considered, each affecting the flavour composition in a distinct way, considering LIV of orders $n = \{0, 1, 2, 3\}$, as defined in Equation (33). For $n < 3$, the results place strong bounds on QG, pushing the limits beyond the Planck scale ($E_{\rm QG} > E_{\rm Pl}$).

In a detailed analysis using 7.5 years of high-energy starting events collected by IceCube, Telalovic and Bustamante [361] carried out the first study of the *directional flavour composition* of astrophysical neutrinos, searching for anisotropies that could indicate direction-dependent QG effects such as LIV. They found no significant evidence for flavour anisotropy and placed improved constraints on flavour-dependent directional effects, thereby strengthening existing limits on LIV-type models that predict different propagation for different flavours along different sky directions.

In a follow-up work, Telalovic and Bustamante [362] performed a remarkable analysis building on the previous one. They started by explicitly interpreting the results within the framework of the SME. Then they derived quantitative limits on a broad set of flavour-dependent LIV coefficients for operator dimensions between $d = 2$ and $d = 8$. They found no significant evidence for directional flavour anomalies, which allowed them to set upper limits on hundreds of LIV parameters. Some of these bounds were derived for the first time, and the obtained limits are orders of magnitude better than previous constraints. These results strongly reinforce Lorentz invariance in the high-energy neutrino sector and substantially reduce the allowed parameter space for flavour-dependent LIV effects.

4.4. Constraints from Air Showers

In recent years, the search for LIV in extensive air showers (EASs) has steadily progressed [237,269,363–369]. This topic is extremely important considering that *all* constraints discussed in this review necessarily rely on the physics of air showers for the detection.

On the consistency of analyses. Any astrophysical deviation from Lorentz symmetry should also manifest in the development of EASs, such that constraints should be derived self-consistently, including LIV effects in both the propagation from the source to Earth and in the shower physics. The Pierre Auger Collaboration has

been systematically including LIV in their analyses, both in the propagation of UHECRs and in the shower development [224]. Nevertheless, most works in the literature overlook the latter aspect, which could lead to inconsistencies in the derived limits on LIV parameters.

Muon lifetime. The lifetime of muons, which are produced in air showers, can also be affected by Lorentz-symmetry breaking. If Lorentz symmetry is violated, this lifetime could become energy-dependent [370–372]. This would lead to a modification of the expected muon decay rates in EASs, potentially impacting the observed shower profiles and the inferred properties of the primary particles. Refs. [373,374] investigated this in the context of DSR, showing that the lifetime (τ) of the particles is modified as follows:

$$\tau = \tau(E) = \tau_0 \frac{E}{mc^2}\left[1 + \frac{1}{2E_{\rm QG}}\left(\frac{m^2c^4}{E} - 2E + \frac{E^3}{m^2c^4}\right)\right] , \tag{56}$$

wherein τ_0 is the rest-frame lifetime of the particle. This applies to all unstable particles, including pions and muons, among others, which are crucial in the development of air showers. Therefore, this could lead to observable effects in the shower profiles given the non-linear nature of the cascade process.

5. Critical Discussion

5.1. Constraints Based on Threshold Effects

Modified interaction thresholds can change interaction horizons, making sources more or less visible at certain energies. However, this often presupposes knowledge of the other ingredients entering the relevant equations (see Section 2), such as cross sections, density of targets, etc., which are not necessarily known. Moreover, there is no obvious way to distinguish between an interaction horizon and a magnetic horizon (if relevant), which adds further ambiguity.

Gamma-ray propagation uncertainties. For gamma rays, the main challenge lies in uncertainties in both the propagation and the source physics. Propagation depends sensitively on the adopted EBL model, as well as on assumptions about modified cross sections, as discussed in ref. [292]. At the source, one typically lacks direct knowledge of the emission spectrum, which is instead reconstructed from observations by inverting Equation (9). If multiple zones contribute to the emission, spectral breaks that mimic QG signatures may appear. Moreover, the precise shape of the HE cut-off may also matter. Furthermore, the cosmological model, which is usually fixed in this type of analysis, can be important, especially for time-of-flight studies [375].

An underappreciated difficulty arises from the fact that gamma-ray propagation can be a non-linear process, especially when electromagnetic cascades are involved. The relevant interactions all generate secondary particles that can further interact, namely:

$$\begin{aligned}
\text{pair production:} &\quad \gamma + \gamma_{\rm bg} \to e^+ + e^- \ , \\
\text{inverse Compton:} &\quad e^\pm + \gamma_{\rm bg} \to e^\pm + \gamma \ , \\
\text{vacuum Cherenkov:} &\quad e^\pm \to e^\pm + \gamma \ , \\
\text{photon decay:} &\quad \gamma \to e^+ + e^- \ , \\
\text{photon splitting:} &\quad \gamma \to \gamma + \cdots + \gamma \ .
\end{aligned}$$

Therefore, the possibility exists of intricate feedback loops that could lead to an "LIV cascade" process. This justifies the Monte Carlo approaches advocated in refs. [217,238]. This is particularly important if both photons and electrons are affected by LIV, that is, if $\chi_n^\gamma \neq 0$ and $\chi_n^e \neq 0$.

The GZK effect. In the case of CRs, most studies [182,189,229,314,376–378] have focused on the modifications of the GZK threshold, as discussed in Section 4.2. Many of them mistakenly attributed the observed spectral suppression in UHECRs to the GZK effect. In fact, HiRes [59] did commit to this interpretation by explicitly referring to the GZK effect in the title of their paper, whereas Auger [60] adopted a more cautious approach of reporting on a flux suppression.

However, it has been known for more than a decade now that protons are a sub-dominant contribution of the UHECR flux at these energies [379–385]. A necessary condition for the UHECR spectral suppression to be the GZK effect is that the CRs at the highest energies are protons, which does not seem to be the case according to current observations (see, for example, refs. [219,386,387] for reviews). But this is not sufficient. Even if this is true, one would still need to prove that the suppression is due to propagation effects, rather than being intrinsic to the sources.

Therefore, while QG effects on the GZK threshold may be interesting in their own right and theoretically more tractable, unless the fraction of protons in UHECRs can be inferred, it is rather difficult to derive meaningful QG constraints. This situation would improve if astrophysical sources of protons above the GZK threshold are identified,

such that their flux can be studied separately. Perhaps the cosmogenic fluxes from UHECR interactions could also be a valuable tool for testing QG [224,322–324,388–390].

The case of UHECR nuclei. One could argue that constraints could be derived from the photodisintegration of UHECR nuclei. Indeed, this has been explored in several works [219, 224, 226, 227, 377, 391, 392]. However, applying QG frameworks developed for fundamental particles directly to composite systems such as atomic nuclei is far from trivial. Multi-particle states, even if strongly bound, may require a different treatment, as in the case of the "soccer ball problem" [151,393–395]. In fact, there is no guarantee that it can be applied to protons. Moreover, it is also unclear that processes such as vacuum Cherenkov (VC) (see Section 3.2.4) would apply to CRs in a straightforward way, as done in refs. [229, 389, 396]. Nevertheless, some studies do take this into account and recompute decay and/or interaction rates for nuclei [177,397–401].

5.2. On Time-of-Flight Constraints

Changes in time of flight are a classic signature of QG, as they can predict tiny deviations from standard physics that accumulate over cosmic distances, making astrophysical observations an appealing testing ground. These modifications are measured by comparing the arrival times of two particles of different energies, say E_1 and E_2, emitted by the same source. The anatomy of the temporal profile of an astrophysical signal can be studied by dissecting its individual components:

$$\Delta t_{\rm obs}(E_1, E_2) = \Delta t_{\rm emi}(E_1, E_2) + \Delta t_{\rm src}(E_1, E_2) + \Delta t_{\rm prop} + \Delta t_{\rm QG}(E_1, E_2)\,, \tag{57}$$

where:

- $\Delta t_{\rm emi}$: intrinsic delays from acceleration and emission at the source, sensitive to the dynamics of the central engine and its immediate surroundings;
- $\Delta t_{\rm src}$: delays due to interactions with the source environment, including any variability in the light curve;
- $\Delta t_{\rm prop}$: propagation delays caused by gravitational (Δt_G) or magnetic fields (Δt_B);
- $\Delta t_{\rm QG}$: the hypothesised QG contribution, which is ultimately the quantity of interest.

Note that this decomposition is somewhat arbitrary, as some components may overlap or be difficult to disentangle in practice. Evidently, if the uncertainties from any of these components are larger than $\Delta t_{\rm QG}$, the latter cannot be meaningfully constrained. The question is, then, if the other components can be sufficiently well understood to isolate $\Delta t_{\rm QG}$.

A condition for using observed time delays is that the detected signal be of primary origin, i.e., emitted directly at the source, rather than composed of secondary particles produced during propagation. Otherwise, $\Delta t_{\rm prop}$ needs to be so well understood that propagation uncertainties cannot be masqueraded as $\Delta t_{\rm QG}$. This issue is particularly relevant for gamma-ray constraints [305], as there is no guarantee that observed photons are primary, and secondaries can be significantly delayed by intergalactic magnetic fields (IGMFs) (see Equation (28)).

In the case of UHECRs, time-of-flight constraints on QG are essentially hopeless because $\Delta t_{\rm prop} \gg \Delta t_{\rm QG}$, even if intervening magnetic fields are small (see Section 2.4). Therefore, for this type of constraint, I will discuss only gamma rays and neutrinos.

The temporal emission profile, $\Delta t_{\rm emi}$, directly translates into the usual lightcurves. This term is not a fundamental time profile per se, like the others in Equation (57). Instead, it is merely a phenomenological estimator for processes occurring at the source, which include the operation time of the mechanism responsible for the emission, the duration of the acceleration processes, diffusion time-scales, etc. Nevertheless, it is useful to simply lump all of these together and use $\Delta t_{\rm emi}$ as a placeholder for all processes happening within the boundaries of a certain region of space that delimits the emitter. A detailed discussion on the role of source-intrinsic effects on LIV studies can be found in ref. [402].

Typical sources used for QG constraints include GRBs. These objects emit a burst of gamma rays, lasting from milliseconds to minutes, often followed by an afterglow that can last for days to weeks [403–408]. The electromagnetic lightcurves of GRBs are often complex, with multiple peaks and substructures, but they share some common features [409–414]. A general parametrisation for the emission profile of GRBs can be written as

$$\phi(E) \equiv \frac{{\rm d}^3 N}{{\rm d}E\,{\rm d}A\,{\rm d}t} \propto t^{-a} E^{-b}\,, \tag{58}$$

where the exact values of a and b depend on the type of GRB (short or long) and the exact stage of emission (prompt, afterglow), with closure relations establishing links between these parameters depending on the underlying physical processes [414–416]. An extensive list was presented by Gao et al. [415]. In the case of neutrinos, since there has been no confirmed detection yet [417–421], one can only speculate about their emission profile, which is expected

to be similar to that of gamma rays, but with some delay due to the different production mechanisms [422].

Another class of source widely used for QG constraints are AGNs. They can exhibit flares lasting from minutes to days [423–427]. Within the AGN paradigm, blazars are a subclass of AGN with jets pointing towards Earth [426,428]. Flaring activity and periodicity have been observed across the whole electromagnetic spectrum in the lightcurves of several blazars such as Mrk 501 [273,429–435], PKS 2155-304 [436,437], among others [438–440]. Unlike GRBs, AGNs do not have a typical electromagnetic lightcurve, with different sub-classes of these objects exhibiting different variability patterns [441–446]. Lightcurves of AGNs are not really well understood, despite the many models proposed (e.g., [447–454]).

The neutrino lightcurves associated with AGNs, too, are unknown. There are indications of association with HE neutrinos from the blazar TXS 0506+056 [328], with repeated activity [263]. Moreover, dozens of neutrinos have been detected coinciding with the AGN NGC 1068 [455], although, to my knowledge, there has been no study reporting on the temporal emission profile of source to date [456], which seems steady in high-energy gamma rays over human timescales. There are also hints of neutrino emission from the flaring blazar PKS 0735 + 178 [457,458].

The few results briefly mentioned above illustrate the complexity of the problem. The intrinsic time profile, $\Delta t_{\rm emi}$, is not well known, not for gamma rays and certainly not for neutrinos, although correlations between these messengers are expected if they are produced through hadronic processes. For GRBs, the common features and the general trend parametrised through Equation (58) provide a somewhat cleaner picture than AGNs, reducing the uncertainties in $\Delta t_{\rm emi}$. In fact, the short duration of the prompt emission phase, typically lasting from milliseconds to minutes, provides a natural upper limit on $\Delta t_{\rm emi}$ which enables more stringent constraints on $\Delta t_{\rm QG}$, especially for cosmologically distant sources. At the moment, this is the most promising class of sources for QG constraints based on time of flight, and until neutrinos are detected from GRBs, gamma rays will continue to be the primary high-energy messenger for these studies.

There is also a geometrical component that goes into the emission term ($\Delta t_{\rm emi}$), which depends on the size of the emission region and the distance to the source. The most evident example is that of a jet with a given opening angle slightly misaligned with respect to the line of sight. The particles emitted from different parts of the jet can arrive at different times due to the finite speed of light. If the instrument can resolve this region or object well, this source will be treated as extended, and the geometrical time delays can be more easily accounted for. But if the source appears point-like, these geometrical time delays may be mistakenly absorbed into another component.

The term $\Delta t_{\rm prop}$ depends on the properties of the intergalactic medium (IGM) and interstellar medium (ISM), which are also poorly constrained. The two contributions to this term are Δt_G and Δt_B, and they will be discussed separately below, under simplifying assumptions. The goal is not to provide accurate estimates, but rather to illustrate the order of magnitude of these effects, and how they compare to $\Delta t_{\rm QG}$, under typical astrophysical conditions.

One might be tempted to conclude that uncertainties are too large, rendering any Lorentz-symmetry constraint based on time of flight meaningless. However, the situation is not as bleak as it may seem, due to the chromatic (energy-dependent) nature of these effects, which can be exploited to disentangle the different components. The individual terms of Equation (57) can be energy-dependent, such that the observed time delay between two particles of different energies, $\Delta t_{\rm obs}(E_1, E_2)$, is not necessarily equal to $\Delta t_{\rm QG}(E_1, E_2)$. For instance, Δt_G is energy-independent (see Equation (29)), but $\Delta t_B \propto E^{-a_{t_B}}$ (see Equations (28) and (26)), wherein $a_{t_B} \sim [-2.5, -2.0]$ may itself be energy-dependent. This is often the case, as higher-energy particles may be accelerated and emitted earlier or later than lower-energy particles, depending on the specific mechanisms involved. Similarly, $\Delta t_{\rm emi}$ can be energy- and position-dependent if the emission region is extended and different parts of it emit particles of different energies at different times.

5.3. Identifying the Underlying Lorentz-Breaking Framework

In previous sections, I discussed extensively how Lorentz-violating effects can manifest in the propagation of high-energy cosmic messengers, and how these effects can be used to constrain the underlying QG frameworks. However, that is not an easy task at the moment. For starters, consider the following question: *can we distinguish between different LIV and DSR frameworks based on observational data?*

Take the Breit-Wheeler pair production process, for instance (see Section 2.2.1). Consider a photon-only modification of the dispersion relation similar to Equation (33). To leading order, the minimum energy ($E_{\rm thr}$) a high-energy photon must have in order to produce an electron-positron pair when interacting with a low-energy background photon of energy ε is [459]:

$$E_{\rm thr}^{\rm SR} = \frac{m_e^2 c^4}{\varepsilon}\,, \tag{59}$$

$$E_{\rm thr}^{\rm LIV} \approx \frac{m_e^2 c^4}{\varepsilon}\left[1 + \eta_{\rm LIV}\frac{m_e^4 c^8}{\varepsilon^3\, E_{\rm QG}}\right]\,, \tag{60}$$

$$E_{\rm thr}^{\rm DSR} \approx \frac{m_e^2 c^4}{\varepsilon}\left[1 + \eta_{\rm DSR}\frac{m_e^2 c^4}{\varepsilon\, E_{\rm QG}}\right]\,, \tag{61}$$

where η_i are dimensionless constants which, in the notation adopted in this review, would translate to χ_1^γ. Note that in the DSR case, the threshold correction arises from the combined effect of the modified dispersion relation and the deformed momentum composition law.

The fact that, for LIV, the correction scales as $m_e^4 c^8/\varepsilon^3$, whereas for DSR it scales as $m_e^2 c^4/\varepsilon$, implies that the former affects lower-energy measurements far more strongly than the latter [12]. Moreover, the different dependence on the background photon energy ε suggests that, in principle, one could discriminate between the two frameworks by systematically mapping the threshold modifications at different energy bands, though degeneracies are to be expected. Additional observables such as those discussed in Section 3.2 should be combined to help break these degeneracies, particularly time-of-flight measurements, which probe complementary aspects of the same kinematical modifications.

Even if one could experimentally distinguish DSR and LIV (and perhaps another type of framework), one would still face the deeper question of interpretation, whether an observed threshold anomaly truly originates from an underlying QG theory, such as those described in 3.1, or instead from something else. Addressing this requires a systematic synthesis of the various phenomenological consequences predicted by competing QG frameworks, followed by a rigorous confrontation with data.

5.4. Quantum Gravity and the Dark Sector

Whether the phenomenon we call dark matter (DM) is an ontic entity in nature (a particle or field), or whether it is an epistemological construct to explain certain phenomena, any consistent QG theory should, in principle, encompass it. QG effects could potentially influence the properties and behaviour of DM, as well as its interactions with SM.

This connection has received surprisingly little attention in the literature, although there have been some attempts to explore it in the context of modified gravity theories (e.g., refs. [460–462]). Nevertheless, very few works have systematically investigated the possible interplay between QG effects and DM phenomenology, especially from an observational perspective. In what follows I entertain some of these hypotheses, making the connection with potential phenomenological signatures in high-energy cosmic messengers.

Axion-like particles (ALPs) are today well-motivated DM candidates [463–465]. Although the original quantum chromodynamics (QCD) axion proposed in the 1970s [466–469] to solve what is known as the strong *CP* "problem"[5] is no longer considered a viable DM candidate, more general ALPs arise naturally in certain extensions of the SM, including string theory [471], some of which are Lorentz-violating.

The main manifestation of ALPs is their coupling to photons in the presence of external magnetic fields [472], in a very similar way to neutrino oscillations (see Section 2.3). The propagation theory discussed in Section 2 can be directly applied to this case, with photons interacting during propagation [473–482], possibly perceiving a more transparent or more opaque universe depending on the MDR and the underlying QG framework.

Therefore, the same theoretical framework that predicts the QG effects discussed here may also predict the existence of ALP DM, and vice versa. This opens up the possibility of using astrophysical observations to simultaneously probe both QG and the nature of DM. In fact, the absence of these signatures might also be a consequence of the treatment of these two phenomenologies in isolation, whereas they might be intimately connected.

There are models that predict that the existence of DM [483,484] and the very structure of spacetime [485] are both emergent phenomena resulting from the spontaneous breaking of local Lorentz invariance. In these models, the vacuum state of the theory does not respect local Lorentz symmetry, leading to the emergence of a preferred frame or direction in spacetime. This spontaneous symmetry breaking gives rise to new degrees of freedom that can be interpreted as DM particles.

[5] This is not a problem per se. It might simply be a coincidence that the QCD *CP*-violating parameter θ is so small. Nevertheless, such apparent fine-tuning [470] may actually point to an yet-unknown mechanism that explains the smallness of this value; the axion solution remains an elegant theoretical proposal.

For instance, aether-type theories [486–488] are based on modification of GR in which spacetime is endowed with a dynamical field—the *aether*—that defines a preferred local rest frame. While general covariance is preserved, some of these theories spontaneously break local Lorentz invariance [178,489]. The aether field introduces additional propagating modes whose collective dynamics can potentially mimic the effects of cold DM [483,488]. Moreover, the dynamics of this field can act as a source of dark energy (DE) [490], providing a unified framework to address both dark components of the universe as emergent phenomena from Lorentz-violating dynamics.

In certain limits, some aether theories become closely related to Hořava-Lifshitz gravity [199], another Lorentz-violating framework, which also predicts MDRs. This framework has been explored as a possible explanation for DM [491–493] and DE [494,495], and it shares conceptual ground with other emergent-gravity approaches, such as mimetic gravity [496]. Frameworks like these provide concrete theoretical laboratories for exploring how Lorentz violation and preferred-frame physics could seed the dark sector.

It is scientifically sound to treat QG-induced Lorentz breaking and dark-sector physics as *coupled* hypotheses rather than independent phenomena. In fact, this provides a stronger constraining power than treating them in isolation. Nevertheless, the two phenomenologies might as well be independent.

For instance, indirect searches for DM signatures based on new QG-motivated particles would benefit from incorporating QG effects into the propagation of these particles from source to observer, and from predicting multi-messenger signatures. One might be tempted to claim that these can be conservatively treated in isolation, but this is not necessarily the case, since, by hypothesis, both phenomena are correlated. Analyses that incorporate both aspects simultaneously, for example, by modelling how MDRs affect the observational signatures of hypothetical DM particles, can take advantage of multi-messenger data to yield tighter and more self-consistent constraints. From an epistemological perspective, this avoids the risk of overclaiming exclusions based on incomplete treatments and provides a more robust and falsifiable approach to these problems.

6. Outlook

Lorentz symmetry is one of the canons of modern physics. It is not merely a convenient postulate, but a structural principle woven into the fabric of both relativity and QFT. To violate it would be to glimpse a deeper structure of spacetime, perhaps one emerging from a fundamental quantum-gravitational substratum where familiar notions such as locality and causality vanish into something more fundamental.

Practical limitations prevent us from probing these ideas directly in terrestrial laboratories, so we turn to the cosmos as a laboratory. High-energy astrophysical messengers reach energies far beyond what human-made accelerators can attain, and traverse large distances, amplifying tiny effects that could carry imprints of new physics.

At the dawn of the era of multi-messenger astrophysics, the opportunity to test these ideas is extraordinary—but so is the need for caution. The astrophysical environments that produce these messengers are complex, and the media through which they travel even more so. Small uncertainties in either the source or the propagation models can easily mimic or conceal the delicate imprints of the new physics being sought. Thus, before interpreting an anomaly as evidence of deviations from Lorentz symmetry or a signature of QG, one must first ensure a deep understanding of the astrophysics itself, including correlated systematics, model degeneracies, and the theoretical assumptions underlying each type of study.

Even in this case, the challenge of underdetermination remains. Data alone rarely points to a single interpretation, as different theoretical frameworks can often explain the same observational anomaly by adjusting a few parameters or assumptions. Genuine progress, then, comes from designing tests that can actually exclude certain hypotheses rather than accommodating potential ambiguities.

The multi-messenger framework, properly understood, is not merely an observational tool but an epistemological strategy. Any single messenger channel is fraught with astrophysical uncertainties and model dependencies that can easily mislead interpretations. Cross-messenger comparisons provide a way to break degeneracies and isolate robust signatures of new physics. Whether Lorentz symmetry withstands further scrutiny or reveals subtle violations under extreme conditions will profoundly influence our understanding of spacetime and, perhaps, of QG. The question is no longer whether to search for these effects, but how to design tests capable of disentangling genuine deviations from the intricate astrophysical backgrounds in which they may be concealed. Ultimately, the quest to test Lorentz symmetry in the cosmos is as much a test of our ability to separate fundamental physics from astrophysical complexity as it is a probe of the ultimate nature of spacetime.

Funding

I acknowledge support from the Agence Nationale de la Recherche (ANR), project ANR-23-CPJ1-0103-01.

Acknowledgments

This work falls within the scope of the COST Action CA23130 “Bridging high and low energies in search of quantum gravity”, funded by the European Cooperation in Science and Technology (COST).

Conflicts of Interest

The author declares no conflict of interest.

Use of AI and AI-Assisted Technologies

No AI tools were utilized for this paper.

References

1. Lämmerzahl, C. Special Relativity and Lorentz Invariance. *Ann. Phys.* **2005**, *517*, 71–102.
2. Will, C.M. The Confrontation between General Relativity and Experiment. *Living Rev. Relativ.* **2014**, *17*, 4.
3. Stachel, J. The Early History of Quantum Gravity (1916–1940). In *Black Holes, Gravitational Radiation and the Universe*; Iyer, B.R., Bhawal, B., Eds.; Springer: Dordrecht, The Netherlands, 1999; pp. 525–534.
4. Rovelli, C. Notes for a Brief History of Quantum Gravity. *arXiv* **2000**, arXiv:gr-qc/0006061.
5. Goenner, H.F.M. On the History of Unified Field Theories. *Living Rev. Relativ.* **2004**, *7*, 2.
6. Brown, H.R. *Physical Relativity. Space-Time Structure from a Dynamical Perspective*; Oxford University Press: Oxford, UK, 2005.
7. Dieks, D. *The Ontology of Spacetime*; Elsevier: Amsterdam, The Netherlands, 2006.
8. Dieks, D. *The Ontology of Spacetime II*; Elsevier: Amsterdam, The Netherlands, 2008.
9. Maudlin, T. *Philosophy of Physics: Space and Time*; Princeton University Press: Princeton, NJ, USA, 2012.
10. Brüning, O.S.; Collier, P.; Lebrun, P.; et al. CERN Yellow Reports: Monographs. In *LHC Design Report*; CERN: Geneva, Switzerland, 2004.
11. Addazi, A.; Alvarez-Muniz, J.; Alves Batista, R.; et al. Quantum gravity phenomenology at the dawn of the multi-messenger era—A review. *Prog. Part. Nucl. Phys.* **2022**, *125*, 103948.
12. Alves Batista, R.; Amelino-Camelia, G.; Boncioli, D.; et al. White paper and roadmap for quantum gravity phenomenology in the multi-messenger era. *Class. Quantum Gravity* **2025**, *42*, 032001.
13. KM3NeT Collaboration. Observation of an ultra-high-energy cosmic neutrino with KM3NeT. *Nature* **2025**, *638*, 376–382.
14. LHAASO Collaboration. Ultrahigh-energy photons up to 1.4 petaelectronvolts from 12 γ-ray Galactic sources. *Nature* **2021**, *594*, 33–36.
15. Fly’s Eye Collaboration. Detection of a cosmic ray with measured energy well beyond the expected spectral cutoff due to cosmic microwave radiation. *Astrophys. J.* **1995**, *441*, 144–150.
16. Telescope Array Collaboration. An extremely energetic cosmic ray observed by a surface detector array. *Science* **2023**, *382*, 903–907.
17. Penzias, A.A.; Wilson, R.W. A Measurement of Excess Antenna Temperature at 4080 Mc/s. *Astrophys. J.* **1965**, *142*, 419–421.
18. Partridge, R.B.; Peebles, P.J.E. Are Young Galaxies Visible? *Astrophys. J.* **1967**, *147*, 868.
19. Puget, J.L.; Abergel, A.; Bernard, J.P.; et al. Tentative detection of a cosmic far-infrared background with COBE. *Astron. Astrophys.* **1996**, *308*, L5.
20. Hauser, M.G.; Arendt, R.G.; Kelsall, T.; et al. The COBE Diffuse Infrared Background Experiment Search for the Cosmic Infrared Background. I. Limits and Detections. *Astrophys. J.* **1998**, *508*, 25–43.
21. Bridle, A.H. The spectrum of the radio background between 13 and 404 MHz. *Mon. Not. R. Astron. Soc.* **1967**, *136*, 219.
22. Clark, T.A.; Brown, L.W.; Alexander, J.K. Spectrum of the Extra-galactic Background Radiation at Low Radio Frequencies. *Nature* **1970**, *228*, 847–849.
23. Habing, H.J. The interstellar radiation density between 912 A and 2400 A. *Bull. Astron. Inst. Neth.* **1968**, *19*, 421.
24. Mathis, J.S.; Mezger, P.G.; Panagia, N. Interstellar radiation field and dust temperatures in the diffuse interstellar medium and in giant molecular clouds. *Astron. Astrophys.* **1983**, *128*, 212–229.
25. Hartmann, J. Investigations on the spectrum and orbit of delta Orionis. *Astrophys. J.* **1904**, *19*, 268–286.
26. Heger, M.L. The occurrence of stationary D lines of sodium in the spectroscopic binaries, β Scorpii and δ Orionis. *Lick Obs. Bull.* **1919**, *326*, 59–63.
27. Strömgren, B. The Physical State of Interstellar Hydrogen. *Astrophys. J.* **1939**, *89*, 526.
28. Meekins, J.F.; Fritz, G.; Chubb, T.A.; et al. Physical Sciences: X-rays from the Coma Cluster of Galaxies. *Nature* **1971**, *231*, 107–108.
29. Fang, K.; Olinto, A.V. High-energy Neutrinos from Sources in Clusters of Galaxies. *Astrophys. J.* **2016**, *828*, 37.
30. Hussain, S.; Alves Batista, R.; de Gouveia Dal Pino, E.M.; et al. High-energy neutrino production in clusters of galaxies. *Mon. Not. R. Astron. Soc.* **2021**, *507*, 1762–1774.

31. Hussain, S.; Alves Batista, R.; de Gouveia Dal Pino, E.M.; et al. The diffuse gamma-ray flux from clusters of galaxies. *Nat. Commun.* **2023**, *14*, 2486.
32. Weinberg, S. Universal Neutrino Degeneracy. *Phys. Rev.* **1962**, *128*, 1457–1473.
33. Seckel, D. Neutrino-Photon Reactions in Astrophysics and Cosmology. *Phys. Rev. Lett.* **1998**, *80*, 900–903.
34. Murase, K.; Beacom, J.F.; Takami, H. Gamma-ray and neutrino backgrounds as probes of the high-energy universe: hints of cascades, general constraints, and implications for TeV searches. *J. Cosmol. Astropart. Phys.* **2012**, *8*, 030.
35. Di Marco, G.; Alves Batista, R.; Sánchez-Conde, M.A. Gamma rays as leptonic portals to energetic neutrinos: A new Monte Carlo approach. *Astropart. Phys.* **2026**, *175*, 103192.
36. Nikishov, A.I. Absorption of high-energy photons in the universe. *J. Exp. Theor. Phys. Lett.* **1962**, *14*, 393.
37. Jelley, J.V. High-Energy γ-Ray Absorption in Space by a 3.5°K Microwave Field. *Phys. Rev. Lett.* **1966**, *16*, 479–481.
38. Gould, R.J.; Schréder, G. Opacity of the Universe to High-Energy Photons. *Phys. Rev. Lett.* **1966**, *16*, 252–254.
39. Bjorken, J.D.; Drell, S.D. Tridents, μ Pairs, and Quantum Electrodynamics at Small Distances. *Phys. Rev.* **1959**, *114*, 1368–1374.
40. Krass, A.S. Photoproduction of Muon Pairs. *Phys. Rev.* **1965**, *138*, 1268–1273.
41. Arteaga-Romero, N.; Jaccarini, A.; Kessler, P.; et al. Photon-Photon Collisions, a New Area of Experimental Investigation in High-Energy Physics. *Phys. Rev. D* **1971**, *3*, 1569–1579.
42. Terazawa, H. Two-Photon Processes for Particle Production at High Energies. *Rev. Mod. Phys.* **1973**, *45*, 615–662.
43. Brodsky, S.J.; Kinoshita, T.; Terazawa, H. Two-Photon Mechanism of Particle Production by High-Energy Colliding Beams. *Phys. Rev. D* **1971**, *4*, 1532–1557.
44. Cheng, H.; Wu, T.T. Cross Sections for Two-Pair Production at Infinite Energy. *Phys. Rev. D* **1970**, *2*, 2103–2104.
45. Brown, R.W.; Hunt, W.F.; Mikaelian, K.O.; et al. Role of $\gamma + \gamma \to e^- + e^+$ in Photoproduction, Colliding Beams, and Cosmic Photon Absorption. *Phys. Rev. D* **1973**, *8*, 3083–3102.
46. Compton, A.H. A Quantum Theory of the Scattering of X-rays by Light Elements. *Phys. Rev.* **1923**, *21*, 483–502.
47. Hayakawa, S. Electron-Photon Cascade Process in Intergalactic Space. *Prog. Theor. Phys. Suppl.* **1966**, *37*, 594–597.
48. Davies, H.; Bethe, H.A.; Maximon, L.C. Theory of Bremsstrahlung and Pair Production. II. Integral Cross Section for Pair Production. *Phys. Rev.* **1954**, *93*, 788–795.
49. Motz, J.W.; Olsen, H.A.; Koch, H.W. Pair Production by Photons. *Rev. Mod. Phys.* **1969**, *41*, 581–639.
50. Bonometto, S.A.; Marcolungo, P. Metagalactic opacity to photons of energy larger than 10^{17} eV. *Nuovo C. Lett.* **1972**, *5*, 595–603.
51. Bonometto, S.A.; Lucchin, F.; Marcolungo, P. Induced Pair Production and Opacity Due to Black-body Radiation. *Astron. Astrophys.* **1974**, *31*, 41.
52. Bethe, H.; Heitler, W. On the Stopping of Fast Particles and on the Creation of Positive Electrons. *Proc. R. Soc. Lond. Ser.* **1934**, *146*, 83–112.
53. Blumenthal, G.R. Energy Loss of High-Energy Cosmic Rays in Pair-Producing Collisions with Ambient Photons. *Phys. Rev. D* **1970**, *1*, 1596–1602.
54. Chodorowski, M.J.; Zdziarski, A.A.; Sikora, M. Reaction Rate and Energy-Loss Rate for Photopair Production by Relativistic Nuclei. *Astrophys. J.* **1992**, *400*, 181.
55. Greisen, K. End to the Cosmic-Ray Spectrum? *Phys. Rev. Lett.* **1966**, *16*, 748–750.
56. Zatsepin, G.T.; Kuz'min, V.A. Upper Limit of the Spectrum of Cosmic Rays. *Sov. J. Exp. Theor. Phys. Lett.* **1966**, *4*, 78.
57. Karakula, S.; Tkaczyk, W. The formation of the cosmic ray energy spectrum by a photon field. *Astropart. Phys.* **1993**, *1*, 229–237.
58. Morejon, L.; Fedynitch, A.; Boncioli, D.; et al. Improved photomeson model for interactions of cosmic ray nuclei. *J. Cosmol. Astropart. Phys.* **2019**, *11*, 007.
59. HiRes Collaboration. First Observation of the Greisen-Zatsepin-Kuzmin Suppression. *Phys. Rev. Lett.* **2008**, *100*, 101101.
60. Pierre Auger Collaboration. Observation of the Suppression of the Flux of Cosmic Rays above 4×10^{19} eV. *Phys. Rev. Lett.* **2008**, *101*, 061101.
61. Stecker, F.W. Photodisintegration of Ultrahigh-Energy Cosmic Rays by the Universal Radiation Field. *Phys. Rev.* **1969**, *180*, 1264–1266.
62. Puget, J.L.; Stecker, F.W.; Bredekamp, J.H. Photonuclear interactions of ultrahigh energy cosmic rays and their astrophysical consequences. *Astrophys. J.* **1976**, *205*, 638–654.
63. Alves Batista, R.; Boncioli, D.; di Matteo, A.; et al. Effects of uncertainties in simulations of extragalactic UHECR propagation, using CRPropa and SimProp. *J. Cosmol. Astropart. Phys.* **2015**, *10*, 063.
64. Boncioli, D.; Fedynitch, A.; Winter, W. Nuclear Physics Meets the Sources of the Ultra-High Energy Cosmic Rays. *Sci. Rep.* **2017**, *7*, 4882.
65. Soriano, J.F.; Anchordoqui, L.A.; Torres, D.F. Photo-disintegration of ^{4}He on the cosmic microwave background is less severe than earlier thought. *Phys. Rev. D* **2018**, *98*, 043001.
66. Alves Batista, R.; Boncioli, D.; di Matteo, A.; et al. Secondary neutrino and gamma-ray fluxes from SimProp and CRPropa. *J. Cosmol. Astropart. Phys.* **2019**, *5*, 006.

67. Dicus, D.A.; Repko, W.W. Photon neutrino scattering. *Phys. Rev. D* **1993**, *48*, 5106–5108.
68. Abbasabadi, A.; Devoto, A.; Dicus, D.A.; et al. High energy photon-neutrino interactions. *Phys. Rev. D* **1998**, *59*, 013012.
69. Abbasabadi, A.; Devoto, A.; Repko, W.W. High energy photon-neutrino elastic scattering. *Phys. Rev. D* **2001**, *63*, 093001.
70. Bahcall, J.N. Neutrino Opacity I. Neutrino-Lepton Scattering. *Phys. Rev.* **1964**, *136*, 1164–1171.
71. Yoshida, S. Propagation of ultrahigh energy neutrinos in the black-body neutrino field. *Astropart. Phys.* **1994**, *2*, 187–198.
72. Pontecorvo, B. Mesonium and Antimesonium. *Sov. J. Exp. Theor. Phys.* **1958**, *6*, 429.
73. Maki, Z.; Nakagawa, M.; Sakata, S. Remarks on the Unified Model of Elementary Particles. *Prog. Theor. Phys.* **1962**, *28*, 870–880.
74. Giunti, C.; Kim, C.W. Coherence of neutrino oscillations in the wave packet approach. *Phys. Rev. D* **1998**, *58*, 017301.
75. Giunti, C. Coherence and Wave Packets in Neutrino Oscillations. *Found. Phys. Lett.* **2004**, *17*, 103–124.
76. Beuthe, M. Oscillations of neutrinos and mesons in quantum field theory. *Phys. Rep.* **2003**, *375*, 105–218.
77. Akhmedov, E.K.; Smirnov, A.Y. Paradoxes of neutrino oscillations. *Phys. At. Nucl.* **2009**, *72*, 1363–1381.
78. Esteban, I.; Gonzalez-Garcia, M.C.; Maltoni, M.; et al. NuFit-6.0: updated global analysis of three-flavor neutrino oscillations. *J. High Energy Phys.* **2024**, *12*, 216.
79. Bhattacharjee, P.; Sigl, G. Origin and propagation of extremely high energy cosmic rays. *Phys. Rep.* **2000**, *327*, 109–247.
80. Neronov, A.; Semikoz, D.V. Sensitivity of γ-ray telescopes for detection of magnetic fields in the intergalactic medium. *Phys. Rev. D* **2009**, *80*, 123012.
81. Lipari, P.; Vernetto, S. Diffuse Galactic gamma-ray flux at very high energy. *Phys. Rev. D* **2018**, *98*, 043003.
82. Di Marco, G.; Alves Batista, R.; Sánchez-Conde, M.Á. Revisiting the propagation of highly-energetic gamma rays in the Galaxy. *Phys. Rev. D* **2025**, *111*, 083004.
83. Shapiro, I.I. Fourth Test of General Relativity. *Phys. Rev. Lett.* **1964**, *13*, 789–791.
84. Alves Batista, R.; Dundovic, A.; Erdmann, M.; et al. CRPropa 3—A public astrophysical simulation framework for propagating extraterrestrial ultra-high energy particles. *J. Cosmol. Astropart. Phys.* **2016**, *5*, 038.
85. Alves Batista, R.; Becker Tjus, J.; Dörner, J.; et al. CRPropa 3.2—An advanced framework for high-energy particle propagation in extragalactic and galactic spaces. *J. Cosmol. Astropart. Phys.* **2022**, *09*, 035.
86. Kachelrieß, M.; Ostapchenko, S.; Tomàs, R. ELMAG: A Monte Carlo simulation of electromagnetic cascades on the extragalactic background light and in magnetic fields. *Comput. Phys. Commun.* **2012**, *183*, 1036–1043.
87. Blytt, M.; Kachelrieß, M.; Ostapchenko, S. ELMAG 3.01: A three-dimensional Monte Carlo simulation of electromagnetic cascades on the extragalactic background light and in magnetic fields. *Comput. Phys. Commun.* **2020**, *252*, 107163.
88. Kalashev, O.; Korochkin, A.; Neronov, A.; et al. Modeling the propagation of very-high-energy γ-rays with the CRbeam code: Comparison with CRPropa and ELMAG codes. *Astron. Astrophys.* **2023**, *675*, A132.
89. Settimo, M.; De Domenico, M. Propagation of extragalactic photons at ultra-high energy with the EleCa code. *Astropart. Phys.* **2015**, *62*, 92–99.
90. Armengaud, E.; Sigl, G.; Beau, T.; et al. CRPropa: A numerical tool for the propagation of UHE cosmic rays, γ-rays and neutrinos. *Astropart. Phys.* **2007**, *28*, 463–471.
91. Kampert, K.H.; Kulbartz, J.; Maccione, L.; et al. CRPropa 2.0—A public framework for propagating high energy nuclei, secondary gamma rays and neutrinos. *Astropart. Phys.* **2013**, *42*, 41–51.
92. Aloisio, R.; Boncioli, D.; Grillo, A.F.; et al. SimProp: a simulation code for ultra high energy cosmic ray propagation. *J. Cosmol. Astropart. Phys.* **2012**, *10*, 007.
93. Aloisio, R.; Boncioli, D.; di Matteo, A.; et al. SimProp v2r4: Monte Carlo simulation code for UHECR propagation. *J. Cosmol. Astropart. Phys.* **2017**, *11*, 009.
94. Moskalenko, I. GALPROP Code for Galactic Cosmic Ray Propagation and Associated Photon Emissions. In Proceedings of the 32nd International Cosmic Ray Conference (ICRC2011), Beijing, China, 11–18 August, 2011; Volume 6, p. 279.
95. Porter, T.A.; Jóhannesson, G.; Moskalenko, I.V. The GALPROP Cosmic-ray Propagation and Nonthermal Emissions Framework: Release v57. *Astrophys. J. Suppl. Ser.* **2022**, *262*, 30.
96. Evoli, C.; Gaggero, D.; Vittino, A.; et al. Cosmic-ray propagation with DRAGON2: I. numerical solver and astrophysical ingredients. *J. Cosmol. Astropart. Phys.* **2017**, *2*, 015.
97. Evoli, C.; Gaggero, D.; Vittino, A.; et al. Cosmic-ray propagation with DRAGON2: II. Nuclear interactions with the interstellar gas. *J. Cosmol. Astropart. Phys.* **2018**, *7*, 006.
98. Colladay, D.; Kostelecký, V.A. Lorentz-violating extension of the standard model. *Phys. Rev. D* **1998**, *58*, 116002.
99. Earman, J.; Glymour, C.; Rynasiewicz, R. On Writing the History of Special Relativity. In *PSA: Proceedings of the Biennial Meeting of the Philosophy of Science Association*; Cambridge University Press: Cambridge, UK, 1982; pp. 403–416.
100. Will, C.M. Special Relativity: A Centenary Perspective. In *Einstein, 1905–2005: Poincaré Seminar 2005*; Damour, T., Darrigol, O., Duplantier, B., et al., Eds.; Birkhäuser: Basel, Switzerland, 2006; Volume 47, p. 33.
101. Schwarz, J.H. Superstring theory. *Phys. Rep.* **1982**, *89*, 223–322.
102. Polchinski, J. String duality. *Rev. Mod. Phys.* **1996**, *68*, 1245–1258.
103. Aharony, O.; Gubser, S.S.; Maldacena, J.; et al. Large N field theories, string theory and gravity. *Phys. Rep.* **2000**,

323, 183–386.
104. Mukhi, S. String theory: a perspective over the last 25 years. *Class. Quantum Gravity* **2011**, *28*, 153001.
105. Polchinski, J. TASI Lectures on D-Branes. *arXiv* **1996**, arXiv:hep-th/9611050.
106. Scherk, J.; Schwarz, J.H. Dual models for non-hadrons. *Nucl. Phys. B* **1974**, *81*, 118–144.
107. Witten, E. String theory dynamics in various dimensions. *Nucl. Phys. B* **1995**, *443*, 85–126.
108. Maldacena, J.M. The Large N Limit of Superconformal Field Theories and Supergravity. *Adv. Theor. Math. Phys.* **1998**, *2*, 231.
109. Hubeny, V.E. The AdS/CFT correspondence. *Class. Quantum Gravity* **2015**, *32*, 124010.
110. Kostelecký, V.A.; Samuel, S. Spontaneous breaking of Lorentz symmetry in string theory. *Phys. Rev. D* **1989**, *39*, 683–685.
111. Kostelecký, V.A.; Samuel, S. Gravitational phenomenology in higher-dimensional theories and strings. *Phys. Rev. D* **1989**, *40*, 1886–1903.
112. Kostelecký, V.A.; Samuel, S. Phenomenological gravitational constraints on strings and higher-dimensional theories. *Phys. Rev. Lett.* **1989**, *63*, 224–227.
113. Potting, R. Symmetry breaking in string theory. *Phys. At. Nucl.* **1998**, *61*, 1914–1917.
114. Frey, A.R. String theoretic bounds on Lorentz-violating warped compactification. *J. High Energy Phys.* **2003**, *4*, 012.
115. Sudarsky, D.; Urrutia, L.; Vucetich, H. Bounds on stringy quantum gravity from low energy existing data. *Phys. Rev. D* **2003**, *68*, 024010.
116. Mavromatos, N.E. Quantum-gravity induced Lorentz violation and dynamical mass generation. *Phys. Rev. D* **2011**, *83*, 025018.
117. Chang, Z.; Wang, S. Lorentz invariance violation and electromagnetic field in an intrinsically anisotropic spacetime. *Eur. Phys. J. C* **2012**, *72*, 2165.
118. Ellis, G.; Silk, J. Scientific method: Defend the integrity of physics. *Nature* **2014**, *516*, 321–323.
119. Ritson, S.; Camilleri, K. Contested Boundaries: The String Theory Debates and Ideologies of Science. *Perspect. Sci.* **2015**, *23*, 192–227.
120. Hewett, J.L.; Rizzo, T.G. Low-energy phenomenology of superstring-inspired E_6 models. *Phys. Rep.* **1989**, *183*, 193–381.
121. Vafa, C. The String Landscape and the Swampland. *arXiv* **2005**, arXiv:hep-th/0509212.
122. Acharya, B.S.; Kane, G.; Kumar, P. Compactified String Theories – Generic Predictions for Particle Physics. *Int. J. Mod. Phys. A* **2012**, *27*, 1230012.
123. Halverson, J.; Langacker, P. TASI Lectures on Remnants from the String Landscape. *arXiv* **2018**, arXiv:1801.03503.
124. Dawid, R. *String Theory and the Scientific Method*; Cambridge University Press: Cambridge, UK, 2013.
125. Dawid, R. The Significance of Non-Empirical Confirmation in Fundamental Physics. In *Why Trust a Theory? Epistemology of Fundamental Physics*; Cambridge University Press: Cambridge, UK, 2019; pp. 99–119.
126. Carroll, S.M., Beyond Falsifiability: Normal Science in a Multiverse. In *Why Trust a Theory? Epistemology of Fundamental Physics*; Cambridge University Press: Cambridge, UK, 2019; pp. 300–314.
127. Greenberg, O.W. CPT Violation Implies Violation of Lorentz Invariance. *Phys. Rev. Lett.* **2002**, *89*, 231602.
128. Mavromatos, N.E. Lorentz Symmetry Violation in String-Inspired Effective Modified Gravity Theories. In *Modified and Quantum Gravity: From Theory to Experimental Searches on All Scales*; Springer: Cham, Switzerland, 2023; Volume 1017, pp. 3–48.
129. Seiberg, N.; Witten, E. String theory and noncommutative geometry. *J. High Energy Phys.* **1999**, *9*, 032.
130. Doplicher, S.; Fredenhagen, K.; Roberts, J.E. The quantum structure of spacetime at the Planck scale and quantum fields. *Commun. Math. Phys.* **1995**, *172*, 187–220.
131. Szabo, R.J. Quantum field theory on noncommutative spaces. *Phys. Rep.* **2003**, *378*, 207–299.
132. Connes, A. Noncommutative geometry and reality. *J. Math. Phys.* **1995**, *36*, 6194–6231.
133. Snyder, H.S. Quantized Space-Time. *Phys. Rev.* **1947**, *71*, 38–41.
134. Carroll, S.M.; Harvey, J.A.; Kostelecký, V.A.; et al. Noncommutative Field Theory and Lorentz Violation. *Phys. Rev. Lett.* **2001**, *87*, 141601.
135. Douglas, M.R.; Nekrasov, N.A. Noncommutative field theory. *Rev. Mod. Phys.* **2001**, *73*, 977–1029.
136. Ashtekar, A.; Lewandowski, J. Background independent quantum gravity: A status report. *Class. Quantum Gravity* **2004**, *21*, R53–R152.
137. Oriti, D. The microscopic dynamics of quantum space as a group field theory. In *Foundations of Space and Time*; Murugan, J., Weltman, A., Ellis, G.F.R., Eds.; Cambridge University Press: Cambridge, UK, 2012; pp. 257–320.
138. Rovelli, C. Loop Quantum Gravity. *Living Rev. Relativ.* **2008**, *11*, 5.
139. Ashtekar, A.; Bianchi, E. A short review of loop quantum gravity. *Rep. Prog. Phys.* **2021**, *84*, 042001.
140. Ashtekar, A.; Fairhurst, S.; Willis, J.L. Quantum gravity, shadow states and quantum mechanics. *Class. Quantum Gravity* **2003**, *20*, 1031–1061.
141. Ashtekar, A.; Rovelli, C.; Smolin, L. Weaving a classical metric with quantum threads. *Phys. Rev. Lett.* **1992**, *69*, 237–240.
142. Rovelli, C.; Smolin, L. Spin networks and quantum gravity. *Phys. Rev. D* **1995**, *52*, 5743–5759.

143. Bojowald, M. Absence of a Singularity in Loop Quantum Cosmology. *Phys. Rev. Lett.* **2001**, *86*, 5227–5230.
144. Ashtekar, A.; Pawlowski, T.; Singh, P. Quantum Nature of the Big Bang. *Phys. Rev. Lett.* **2006**, *96*, 141301.
145. Gambini, R.; Pullin, J. Nonstandard optics from quantum space-time. *Phys. Rev. D* **1999**, *59*, 124021.
146. Alfaro, J.; Morales-Técotl, H.A.; Urrutia, L.F. Loop quantum gravity and light propagation. *Phys. Rev. D* **2002**, *65*, 103509.
147. Bojowald, M.; Paily, G.M. Deformed general relativity. *Phys. Rev. D* **2013**, *87*, 044044.
148. Freidel, L. Group Field Theory: An Overview. *Int. J. Theor. Phys.* **2005**, *44*, 1769–1783.
149. Reisenberger, M.P.; Rovelli, C. "Sum over surfaces" form of loop quantum gravity. *Phys. Rev. D* **1997**, *56*, 3490–3508.
150. Girelli, F.; Konopka, T.; Kowalski-Glikman, J.; et al. Free particle in deformed special relativity. *Phys. Rev. D* **2006**, *73*, 045009.
151. Amelino-Camelia, G.; Freidel, L.; Kowalski-Glikman, J.; et al. Relative locality and the soccer ball problem. *Phys. Rev. D* **2011**, *84*, 087702.
152. Surya, S. The causal set approach to quantum gravity. *Living Rev. Relativ.* **2019**, *22*, 5.
153. Bombelli, L.; Lee, J.; Meyer, D.; et al. Space-time as a causal set. *Phys. Rev. Lett.* **1987**, *59*, 521–524.
154. Ambjørn, J.; Jurkiewicz, J.; Loll, R. Causal dynamical triangulations and the quest for quantum gravity. In *Foundations of Space and Time*; Cambridge University Press: Cambridge, UK, 2012; pp. 321–337.
155. Loll, R. Quantum gravity from causal dynamical triangulations: a review. *Class. Quantum Gravity* **2020**, *37*, 013002.
156. Tawfik, A.; Diab, A. Generalized uncertainty principle: Approaches and applications. *Int. J. Mod. Phys. D* **2014**, *23*, 1430025.
157. Bosso, P.; Gaetano Luciano, G.; Petruzziello, L.; et al. 30 years in: Quo vadis generalized uncertainty principle? *Class. Quantum Gravity* **2023**, *40*, 195014.
158. Maggiore, M. A generalized uncertainty principle in quantum gravity. *Phys. Lett. B* **1993**, *304*, 65–69.
159. Maggiore, M. Quantum groups, gravity, and the generalized uncertainty principle. *Phys. Rev. D* **1994**, *49*, 5182–5187.
160. Kempf, A.; Mangano, G.; Mann, R.B. Hilbert space representation of the minimal length uncertainty relation. *Phys. Rev. D* **1995**, *52*, 1108–1118.
161. Garay, L.J. Quantum Gravity and Minimum Length. *Int. J. Mod. Phys. A* **1995**, *10*, 145–165.
162. Ali, A.F.; Das, S.; Vagenas, E.C. Discreteness of space from the generalized uncertainty principle. *Phys. Lett. B* **2009**, *678*, 497–499.
163. Eichhorn, A. An asymptotically safe guide to quantum gravity and matter. *Front. Astron. Space Sci.* **2018**, *5*, 47.
164. Eichhorn, A.; Schiffer, M., Asymptotic Safety of Gravity with Matter. In *Handbook of Quantum Gravity*; Bambi, C., Modesto, L., Shapiro, I., Eds.; Springer Nature: Singapore, 2024; pp. 915–1001.
165. Platania, A. From renormalization group flows to cosmology. *Front. Phys.* **2020**, *8*, 188.
166. Weinberg, S. Ultraviolet divergences in quantum theories of gravitation. In *General Relativity*; Cambridge University Press: Cambridge, UK, 1979; pp. 790–831.
167. Reuter, M. Nonperturbative evolution equation for quantum gravity. *Phys. Rev. D* **1998**, *57*, 971–985.
168. Niedermaier, M. The asymptotic safety scenario in quantum gravity: An introduction. *Class. Quantum Gravity* **2007**, *24*, R171–R230.
169. Eichhorn, A.; Held, A.; Wetterich, C. Predictive power of grand unification from quantum gravity. *J. High Energy Phys.* **2020**, *8*, 111.
170. Reuter, M.; Weyer, H. Quantum gravity at astrophysical distances? *J. Cosmol. Astropart. Phys.* **2004**, *12*, 001.
171. Eichhorn, A.; Platania, A.; Schiffer, M. Lorentz invariance violations in the interplay of quantum gravity with matter. *Phys. Rev. D* **2020**, *102*, 026007.
172. Donoghue, J.F. Leading quantum correction to the Newtonian potential. *Phys. Rev. Lett.* **1994**, *72*, 2996–2999.
173. Donoghue, J.F. General relativity as an effective field theory: The leading quantum corrections. *Phys. Rev. D* **1994**, *50*, 3874–3888.
174. Donoghue, J.F. Quantum General Relativity and Effective Field Theory. In *Handbook of Quantum Gravity*; Bambi, C., Modesto, L., Shapiro, I., Eds.; Springer Nature: Singapore, 2024; pp. 3–26.
175. Kostelecký, V.A. Gravity, Lorentz violation, and the standard model. *Phys. Rev. D* **2004**, *69*, 105009.
176. Chaichian, M.; Dolgov, A.D.; Novikov, V.A.; et al. CPT violation does not lead to violation of Lorentz invariance and vice versa. *Phys. Lett. B* **2011**, *699*, 177–180.
177. Coleman, S.; Glashow, S.L. High-energy tests of Lorentz invariance. *Phys. Rev. D* **1999**, *59*, 116008.
178. Mattingly, D. Modern Tests of Lorentz Invariance. *Living Rev. Relativ.* **2005**, *8*, 5.
179. Liberati, S.; Maccione, L. Lorentz Violation: Motivation and New Constraints. *Annu. Rev. Nucl. Part. Sci.* **2009**, *59*, 245–267.
180. Tasson, J.D. What do we know about Lorentz invariance? *Rep. Prog. Phys.* **2014**, *77*, 062901.
181. Amelino-Camelia, G. Testable scenario for relativity with minimum length. *Phys. Lett. B* **2001**, *510*, 255–263.
182. Amelino-Camelia, G. Relativity: Special treatment. *Nature* **2002**, *418*, 34–35.
183. Kowalski-Glikman, J.; Nowak, S. Doubly special relativity theories as different bases of κ-Poincaré algebra. *Phys. Lett. B* **2002**, *539*, 126–132.

184. Magueijo, J.; Smolin, L. Lorentz Invariance with an Invariant Energy Scale. *Phys. Rev. Lett.* **2002**, *88*, 190403.
185. Magueijo, J.; Smolin, L. Generalized Lorentz invariance with an invariant energy scale. *Phys. Rev. D* **2003**, *67*, 044017.
186. Amelino-Camelia, G.; Freidel, L.; Kowalski-Glikman, J.; et al. Principle of relative locality. *Phys. Rev. D* **2011**, *84*, 084010.
187. Amelino-Camelia, G.; Freidel, L.; Kowalski-Glikman, J.; et al. Relative locality: a deepening of the relativity principle. *Gen. Relativ. Gravit.* **2011**, *43*, 2547–2553.
188. Kowalski-Glikman, J. Introduction to Doubly Special Relativity. In *Planck Scale Effects in Astrophysics and Cosmology*; Springer: Berlin/Heidelberg, Germany, 2005; Volume 669, p. 131.
189. Amelino-Camelia, G. Doubly-Special Relativity: Facts, Myths and Some Key Open Issues. *Symmetry* **2010**, *2*, 230–271.
190. Amelino-Camelia, G. Quantum-Spacetime Phenomenology. *Living Rev. Relativ.* **2013**, *16*, 5.
191. Arzano, M.; Gubitosi, G.; Relancio, J.J. Deformed Relativistic Symmetry Principles. In *Modified and Quantum Gravity: From Theory to Experimental Searches on All Scales*; Springer: Cham, Switzerland, 2023; Volume 1017, pp. 49–103.
192. Jacobson, T.; Liberati, S.; Mattingly, D. Threshold effects and Planck scale Lorentz violation: Combined constraints from high energy astrophysics. *Phys. Rev. D* **2003**, *67*, 124011.
193. Lehnert, R. Threshold analyses and Lorentz violation. *Phys. Rev. D* **2003**, *68*, 085003.
194. Mattingly, D.; Jacobson, T.; Liberati, S. Threshold configurations in the presence of Lorentz violating dispersion relations. *Phys. Rev. D* **2003**, *67*, 124012.
195. Heyman, D.; Major, S.; Hinteleitner, F. Reaction thresholds in doubly special relativity. *Phys. Rev. D* **2004**, *69*, 105016.
196. Baccetti, V.; Tate, K.; Visser, M. Lorentz violating kinematics: Threshold theorems. *J. High Energy Phys.* **2012**, *2012*, 87.
197. Amelino-Camelia, G. Quantum Space-Time Deformed Symmetries Versus Broken Symmetries. In *CPT and Lorentz Symmetry*; Kostelecký, V.A., Ed.; World Scientific: Singapore, 2002, pp. 254–261.
198. Kostelecký, V.A.; Russell, N. Data tables for Lorentz and CPT violation. *Rev. Mod. Phys.* **2011**, *83*, 11–32.
199. Hořava, P. Quantum gravity at a Lifshitz point. *Phys. Rev. D* **2009**, *79*, 084008.
200. Magueijo, J.; Smolin, L. Gravity's rainbow. *Class. Quantum Gravity* **2004**, *21*, 1725–1736.
201. Amelino-Camelia, G. Phenomenology of Planck-scale Lorentz-symmetry test theories. *New J. Phys.* **2004**, *6*, 188.
202. Lukierski, J.; Ruegg, H.; Nowicki, A.; et al. q-deformation of Poincaré algebra. *Phys. Lett. B* **1991**, *264*, 331–338.
203. Majid, S.; Ruegg, H. Bicrossproduct structure of κ-Poincare group and non-commutative geometry. *Phys. Lett. B* **1994**, *334*, 348–354.
204. Lukierski, J. Kappa-deformations: historical developments and recent results. *J. Phys. Conf. Ser.* **2017**, *804*, 012028.
205. Girelli, F.; Liberati, S.; Sindoni, L. Planck-scale modified dispersion relations and Finsler geometry. *Phys. Rev. D* **2007**, *75*, 064015.
206. Barcaroli, L.; Brunkhorst, L.K.; Gubitosi, G.; et al. Hamilton geometry: Phase space geometry from modified dispersion relations. *Phys. Rev. D* **2015**, *92*, 084053.
207. Wheeler, J.A. Geons. *Phys. Rev.* **1955**, *97*, 511–536.
208. Hawking, S.W. Spacetime foam. *Nucl. Phys. B* **1978**, *144*, 349–362.
209. Carlip, S. Spacetime foam: A review. *Rep. Prog. Phys.* **2023**, *86*, 066001.
210. Jack Ng, Y.; van Dam, H. Limit to Space-Time Measurement. *Mod. Phys. Lett. A* **1994**, *9*, 335–340.
211. Schreck, M.; Sorba, F.; Thambyahpillai, S. Simple model of pointlike spacetime defects and implications for photon propagation. *Phys. Rev. D* **2013**, *88*, 125011.
212. Hossenfelder, S. Phenomenology of space-time imperfection. II. Local defects. *Phys. Rev. D* **2013**, *88*, 124031.
213. Borowiec, A.; Pachol, A. κ-Minkowski Spacetimes and DSR Algebras: Fresh Look and Old Problems. *Symmetry Integr. Geom. Methods Appl.* **2010**, *6*, 086.
214. Carmona, J.M.; Cortés, J.L.; Relancio, J.J. Relativistic deformed kinematics from locality conditions in a generalized spacetime. *Phys. Rev. D* **2020**, *101*, 044057.
215. Amelino-Camelia, G.; Ahluwalia, D.V. Relativity in Spacetimes with Short-Distance Structure Governed by an Observer-Independent (Planckian) Length Scale. *Int. J. Mod. Phys. D* **2002**, *11*, 35–59.
216. Kosiński, P.; Lukierski, J.; Sobczyk, J.; et al. The Classical Basis for κ-deformed Poincaré Algebra and Superalgebra. *Mod. Phys. Lett. A* **1995**, *10*, 2599–2606.
217. Saveliev, A.; Alves Batista, R. Simulating electromagnetic cascades with Lorentz invariance violation. *Class. Quantum Gravity* **2024**, *41*, 115011.
218. Saldana-Lopez, A.; Domínguez, A.; Pérez-González, P.G.; et al. An observational determination of the evolving extragalactic background light from the multiwavelength HST/CANDELS survey in the Fermi and CTA era. *Mon. Not. R. Astron. Soc.* **2021**, *507*, 5144–5160.
219. Anchordoqui, L.A.; Soriano, J.F. New test of Lorentz symmetry using ultrahigh-energy cosmic rays. *Phys. Rev. D* **2018**, *97*, 043010.
220. Li, H.; Ma, B.Q. Threshold anomalies of ultra-high energy cosmic photons due to Lorentz invariance violation. *J. High Energy Astrophys.* **2021**, *32*, 1–5.
221. Burde, G.I. Particle dynamics and GZK limit in relativity with a preferred frame. *Astropart. Phys.* **2021**, *126*, 102526.

222. Burde, G.I. Lorentz Violation by the Preferred Frame Effects and Cosmic and Gamma Ray Propagation. *Galaxies* **2021**, *9*, 119.
223. He, P.; Ma, B.Q. Abnormal threshold behaviors of photo-pion production off the proton in the GZK region. *Eur. Phys. J. C* **2024**, *84*, 401.
224. Pierre Auger Collaboration. Testing effects of Lorentz invariance violation in the propagation of astroparticles with the Pierre Auger Observatory. *J. Cosmol. Astropart. Phys.* **2022**, *1*, 023.
225. Galaverni, M.; Sigl, G. Lorentz violation and ultrahigh-energy photons. *Phys. Rev. D* **2008**, *78*, 063003.
226. Saveliev, A.; Maccione, L.; Sigl, G. Lorentz invariance violation and chemical composition of ultra high energy cosmic rays. *J. Cosmol. Astropart. Phys.* **2011**, *3*, 046.
227. Lang, R.G.; Martínez-Huerta, H.; de Souza, V. Ultra-High-Energy Astroparticles as Probes for Lorentz Invariance Violation. *Universe* **2022**, *8*, 435.
228. Guedes Lang, R.; Martínez-Huerta, H.; de Souza, V. Limits on the Lorentz Invariance Violation from UHECR Astrophysics. *Astrophys. J.* **2018**, *853*, 23.
229. Coleman, S.; Glashow, S.L. Cosmic ray and neutrino tests of special relativity. *Phys. Lett. B* **1997**, *405*, 249–252.
230. Rubtsov, G.; Satunin, P.; Sibiryakov, S. Calculation of cross sections in Lorentz-violating theories. *Phys. Rev. D* **2012**, *86*, 085012.
231. Jacobson, T.; Liberati, S.; Mattingly, D. TeV astrophysics constraints on Planck scale Lorentz violation. *Phys. Rev. D* **2002**, *66*, 081302.
232. Lehnert, R.; Potting, R. Vacuum Čerenkov Radiation. *Phys. Rev. Lett.* **2004**, *93*, 110402.
233. Lehnert, R.; Potting, R. Čerenkov effect in Lorentz-violating vacua. *Phys. Rev. D* **2004**, *70*, 125010.
234. Kaufhold, C.; Klinkhamer, F.R. Vacuum Cherenkov radiation and photon triple-splitting in a Lorentz-noninvariant extension of quantum electrodynamics. *Nucl. Phys. B* **2006**, *734*, 1–23.
235. Kaufhold, C.; Klinkhamer, F.R. Vacuum Cherenkov radiation in spacelike Maxwell-Chern-Simons theory. *Phys. Rev. D* **2007**, *76*, 025024.
236. Klinkhamer, F.R.; Risse, M. Ultrahigh-energy cosmic-ray bounds on nonbirefringent modified Maxwell theory. *Phys. Rev. D* **2008**, *77*, 016002.
237. Díaz, J.S.; Klinkhamer, F.R.; Risse, M. Changes in extensive air showers from isotropic Lorentz violation in the photon sector. *Phys. Rev. D* **2016**, *94*, 085025.
238. Saveliev, A.; Alves Batista, R.; Mishin, F. Spectra for reactions in astrophysical electromagnetic cascades with Lorentz invariance violation: The vacuum Cherenkov effect. *Phys. Rev. D* **2025**, *111*, 083001.
239. Kostelecký, V.A.; Pickering, A.G. Vacuum Photon Splitting in Lorentz-Violating Quantum Electrodynamics. *Phys. Rev. Lett.* **2003**, *91*, 031801.
240. Anselmi, D.; Taiuti, M. Vacuum Cherenkov radiation in quantum electrodynamics with high-energy Lorentz violation. *Phys. Rev. D* **2011**, *83*, 056010.
241. Schreck, M. Vacuum Cherenkov radiation for Lorentz-violating fermions. *Phys. Rev. D* **2017**, *96*, 095026.
242. Carmona, J.M.; Cortes, J.L. Constraints from Neutrino Decay on Superluminal Velocities. *arXiv* **2011**, arXiv:hep-ph/1110.0430.
243. Somogyi, G.; Nándori, I.; Jentschura, U.D. Neutrino splitting for Lorentz-violating neutrinos: Detailed analysis. *Phys. Rev. D* **2019**, *100*, 035036.
244. Carmona, J.M.; Cortés, J.L.; Relancio, J.J.; et al. Decay of superluminal neutrinos in the collinear approximation. *Phys. Rev. D* **2023**, *107*, 043001.
245. Cohen, A.G.; Glashow, S.L. Pair Creation Constrains Superluminal Neutrino Propagation. *Phys. Rev. Lett.* **2011**, *107*, 181803.
246. Bezrukov, F.; Lee, H.M. Model dependence of the bremsstrahlung effects from the superluminal neutrino at OPERA. *Phys. Rev. D* **2012**, *85*, 031901.
247. Jentschura, U.D. Squeezing the Parameter Space for Lorentz Violation in the Neutrino Sector with Additional Decay Channels. *Particles* **2020**, *3*, 630–641.
248. Kostelecký, V.A.; Tasson, J.D. Constraints on Lorentz violation from gravitational Čerenkov radiation. *Phys. Lett. B* **2015**, *749*, 551–559.
249. Moore, G.D.; Nelson, A.E. Lower bound on the propagation speed of gravity from gravitational Cherenkov radiation. *J. High Energy Phys.* **2001**, *9*, 023.
250. Artola, M.; Cembranos, J.A.R.; Martín-Moruno, P. Gravitational and electromagnetic Cherenkov radiation constraints in modified dispersion relations. *Phys. Rev. D* **2024**, *110*, 124060.
251. Amelino-Camelia, G.; Ellis, J.; Mavromatos, N.E.; et al. Tests of quantum gravity from observations of γ-ray bursts. *Nature* **1998**, *393*, 763–765.
252. Schaefer, B.E. Severe Limits on Variations of the Speed of Light with Frequency. *Phys. Rev. Lett.* **1999**, *82*, 4964–4966.
253. Ellis, J.; Mavromatos, N.E.; Nanopoulos, D.V. Quantum-Gravitational Diffusion and Stochastic Fluctuations in the Velocity of Light. *Gen. Relativ. Gravit.* **2000**, *32*, 127–144.

254. Ellis, J.; Mavromatos, N.E.; Nanopoulos, D.V.; et al. Quantum-gravity analysis of gamma-ray bursts using wavelets. *Astron. Astrophys.* **2003**, *402*, 409–424.
255. Jacob, U.; Piran, T. Lorentz-violation-induced arrival delays of cosmological particles. *J. Cosmol. Astropart. Phys.* **2008**, *1*, 031.
256. Rosati, G.; Amelino-Camelia, G.; Marcianò, A.; et al. Planck-scale-modified dispersion relations in FRW spacetime. *Phys. Rev. D* **2015**, *92*, 124042.
257. Li, T.; Mavromatos, N.E.; Nanopoulos, D.V.; et al. Time delays of strings in D-particle backgrounds and vacuum refractive indices. *Phys. Lett. B* **2009**, *679*, 407–413.
258. Amelino-Camelia, G.; Matassa, M.; Mercati, F.; et al. Taming Nonlocality in Theories with Planck-Scale Deformed Lorentz Symmetry. *Phys. Rev. Lett.* **2011**, *106*, 071301.
259. Amelino-Camelia, G.; Rosati, G.; Bedić, S. Phenomenology of curvature-induced quantum-gravity effects. *Phys. Lett. B* **2021**, *820*, 136595.
260. Lobo, I.P. Time delay in κ-anti-de Sitter spacetime. *Phys. Lett. B* **2024**, *855*, 138864.
261. Kostelecký, V.A.; Mewes, M. Neutrinos with Lorentz-violating operators of arbitrary dimension. *Phys. Rev. D* **2012**, *85*, 096005.
262. Kostelecký, V.A.; Li, Z. Backgrounds in gravitational effective field theory. *Phys. Rev. D* **2021**, *103*, 024059.
263. IceCube Collaboration. Neutrino emission from the direction of the blazar TXS 0506+056 prior to the IceCube-170922A alert. *Science* **2018**, *361*, 147–151.
264. IceCube Collaboration. A Search for IceCube Events in the Direction of ANITA Neutrino Candidates. *Astrophys. J.* **2020**, *892*, 53.
265. HAWC Collaboration. Constraints on Lorentz Invariance Violation from HAWC Observations of Gamma Rays above 100 TeV. *Phys. Rev. Lett.* **2020**, *124*, 131101.
266. Jacobson, T.; Liberati, S.; Mattingly, D. Lorentz violation at high energy: Concepts, phenomena, and astrophysical constraints. *Ann. Phys.* **2006**, *321*, 150–196.
267. Maccione, L.; Liberati, S.; Celotti, A.; et al. New constraints on Planck-scale Lorentz violation in QED from the Crab Nebula. *J. Cosmol. Astropart. Phys.* **2007**, *10*, 013.
268. Liberati, S.; Maccione, L.; Sotiriou, T.P. Scale Hierarchy in Hořava-Lifshitz Gravity: Strong Constraint from Synchrotron Radiation in the Crab Nebula. *Phys. Rev. Lett.* **2012**, *109*, 151602.
269. Rubtsov, G.; Satunin, P.; Sibiryakov, S. Constraints on violation of Lorentz invariance from atmospheric showers initiated by multi-TeV photons. *J. Cosmol. Astropart. Phys.* **2017**, *5*, 049.
270. Li, C.; Ma, B.Q. Testing Lorentz invariance of electrons with LHAASO observations of PeV gamma-rays from the Crab Nebula. *Phys. Lett. B* **2022**, *829*, 137034.
271. Lang, R.G.; Martínez-Huerta, H.; de Souza, V. Improved limits on Lorentz invariance violation from astrophysical gamma-ray sources. *Phys. Rev. D* **2019**, *99*, 043015.
272. Sloan, D.; Alves Batista, R.; Hicks, M.; et al. *Fine-Tuning in the Physical Universe*, 1 ed.; Cambridge University Press: Cambridge, UK, 2020.
273. H.E.S.S. Collaboration. The 2014 TeV γ-Ray Flare of Mrk 501 Seen with H.E.S.S.: Temporal and Spectral Constraints on Lorentz Invariance Violation. *Astrophys. J.* **2019**, *870*, 93.
274. Lesage, S.; Veres, P.; Briggs, M.S.; et al. Fermi-GBM Discovery of GRB 221009A: An Extraordinarily Bright GRB from Onset to Afterglow. *Astrophys. J. Lett.* **2023**, *952*, L42.
275. LHAASO Collaboration. A tera-electron volt afterglow from a narrow jet in an extremely bright gamma-ray burst. *Science* **2023**, *380*, 1390–1396.
276. LHAASO Collaboration. Very high-energy gamma-ray emission beyond 10 TeV from GRB 221009A. *Sci. Adv.* **2023**, *9*, eadj2778.
277. H.E.S.S. Collaboration. H.E.S.S. Follow-up Observations of GRB 221009A. *Astrophys. J. Lett.* **2023**, *946*, L27.
278. Burns, E.; Svinkin, D.; Fenimore, E.; et al. GRB 221009A: The BOAT. *Astrophys. J. Lett.* **2023**, *946*, L31.
279. Finke, J.D.; Razzaque, S. Possible Evidence for Lorentz Invariance Violation in Gamma-Ray Burst 221009A. *Astrophys. J. Lett.* **2023**, *942*, L21.
280. Li, H.; Ma, B.Q. Lorentz invariance violation induced threshold anomaly versus very-high energy cosmic photon emission from GRB 221009A. *Astropart. Phys.* **2023**, *148*, 102831.
281. Piran, T.; Ofengeim, D.D. Lorentz invariance violation limits from GRB 221009A. *Phys. Rev. D* **2024**, *109*, L081501.
282. Das, S.; Razzaque, S. Ultrahigh-energy cosmic-ray signature in GRB 221009A. *Astron. Astrophys.* **2023**, *670*, L12.
283. Mirabal, N. Secondary GeV-TeV emission from ultra-high-energy cosmic rays accelerated by GRB 221009A. *Mon. Not. R. Astron. Soc.* **2023**, *519*, L85–L86.
284. He, H.N.; Zhang, B.T.; Fan, Y.Z. A Detectable Ultra-high-energy Cosmic-Ray Outburst from GRB 221009A. *Astrophys. J.* **2024**, *963*, 109.
285. Cao, Z.; Aharonian, F.; Axikegu; et al. Stringent Tests of Lorentz Invariance Violation from LHAASO Observations of GRB 221009A. *Phys. Rev. Lett.* **2024**, *133*, 071501.

286. Carpet-3 Group. Carpet-3 detection of a photonlike air shower with estimated primary energy above 100 TeV in a spatial and temporal coincidence with GRB 221009A. *Phys. Rev. D* **2025**, *111*, 102005.
287. Ofengeim, D.D.; Piran, T. 300 TeV photon from GRB 221009A: A hint at nonlinear Lorentz invariance violation? *Phys. Rev. D* **2025**, *112*, 083055.
288. Song, H.; Ma, B.Q. Carpet-3 300 TeV photon event as an evidence for Lorentz violation. *Phys. Lett. B* **2025**, *870*, 139959.
289. Fermi-LAT Collaboration (Atwood, W. B. et al.). The Large Area Telescope on the Fermi Gamma-Ray Space Telescope Mission. *Astrophys. J.* **2009**, *697*, 1071–1102.
290. Abdalla, H.; Böttcher, M. Lorentz Invariance Violation Effects on Gamma-Gamma Absorption and Compton Scattering. *Astrophys. J.* **2018**, *865*, 159.
291. Saveliev, A.; Alves Batista, R. On Numerical Simulations of Intergalactic Electromagnetic Cascades with Lorentz Invariance Violation. *arXiv* **2023**, arXiv:2307.11421.
292. Carmona, J.M.; Cortés, J.L.; Rescic, F.; et al. Approaches to photon absorption in a Lorentz invariance violation scenario. *Phys. Rev. D* **2024**, *110*, 063035.
293. Carmona, J.M.; Cortés, J.L.; Relancio, J.J.; et al. Modification of the mean free path of very high-energy photons due to a relativistic deformed kinematics. *Eur. Phys. J. Plus* **2022**, *137*, 768.
294. Ellis, J.; Mavromatos, N.E.; Nanopoulos, D.V. Probing models of quantum space-time foam. *arXiv* **1999**, arXiv:gr-qc/9909085.
295. MAGIC Collaboration. Probing quantum gravity using photons from a flare of the active galactic nucleus Markarian 501 observed by the MAGIC telescope. *Phys. Lett. B* **2008**, *668*, 253–257.
296. H.E.S.S. Collaboration. Search for Lorentz Invariance breaking with a likelihood fit of the PKS 2155-304 flare data taken on MJD 53944. *Astropart. Phys.* **2011**, *34*, 738–747.
297. H.E.S.S. Collaboration; Fermi-LAT Collaboration. Constraints on the Intergalactic Magnetic Field Using Fermi-LAT and H.E.S.S. Blazar Observations. *Astrophys. J. Lett.* **2023**, *950*, L16.
298. Biller, S.D.; Breslin, A.C.; Buckley, J.; et al. Limits to Quantum Gravity Effects on Energy Dependence of the Speed of Light from Observations of TeV Flares in Active Galaxies. *Phys. Rev. Lett.* **1999**, *83*, 2108–2111.
299. MAGIC Collaboration. Constraining Lorentz Invariance Violation Using the Crab Pulsar Emission Observed up to TeV Energies by MAGIC. *Astrophys. J. Suppl. Ser.* **2017**, *232*, 9.
300. MAGIC Collaboration. Bounds on Lorentz Invariance Violation from MAGIC Observation of GRB 190114C. *Phys. Rev. Lett.* **2020**, *125*, 021301.
301. Vasileiou, V.; Jacholkowska, A.; Piron, F.; et al. Constraints on Lorentz invariance violation from Fermi-Large Area Telescope observations of gamma-ray bursts. *Phys. Rev. D* **2013**, *87*, 122001.
302. MAGIC Collaboration. Teraelectronvolt emission from the γ-ray burst GRB 190114C. *Nature* **2019**, *575*, 455–458.
303. Zhu, J.; Ma, B.Q. Light speed variation from GRB 221009A. *J. Phys. Nucl. Phys.* **2023**, *50*, 06LT01.
304. LHAASO Collaboration. The First LHAASO Catalog of Gamma-Ray Sources. *Astrophys. J. Suppl. Ser.* **2024**, *271*, 25.
305. Bolmont, J.; Caroff, S.; Gaug, M.; et al. First Combined Study on Lorentz Invariance Violation from Observations of Energy-dependent Time Delays from Multiple-type Gamma-Ray Sources. I. Motivation, Method Description, and Validation through Simulations of H.E.S.S., MAGIC, and VERITAS Data Sets. *Astrophys. J.* **2022**, *930*, 75.
306. CTA Consortium. *Science with the Cherenkov Telescope Array*; World Scientific: Singapore, 2019.
307. CTA Consortium. Sensitivity of the Cherenkov Telescope Array for probing cosmology and fundamental physics with gamma-ray propagation. *J. Cosmol. Astropart. Phys.* **2021**, *02*, 048.
308. Terzić, T.; Kerszberg, D.; Strišković, J. Probing Quantum Gravity with Imaging Atmospheric Cherenkov Telescopes. *Universe* **2021**, *7*, 345.
309. Kirzhnits, D.A.; Chechin, V.A. Cosmic Rays and the Elementary Length. *JETP Lett.* **1971**, *14*, 261.
310. Gonzalez-Mestres, L. Physics opportunities above the Greisen-Zatsepin-Kuzmin cutoff: Lorentz symmetry violation at the Planck scale. In Proceedings of the Workshop on Observing Giant Cosmic Ray Air Showers From $>$10(20) eV Particles From Space, College Park, MD, USA, 13–15 November 1998; Volume 433, pp. 148–158.
311. AGASA Collaboration. The cosmic ray energy spectrum above 3×10^{18} eV measured by the Akeno Giant Air Shower Array. *Astropart. Phys.* **1995**, *3*, 105–123.
312. AGASA Collaboration. Extension of the cosmic ray energy spectrum beyond the predicted Greisen-Zatsepin-Kuz'min cutoff. *Phys. Rev. Lett.* **1998**, *81*, 1163–1166.
313. Kifune, T. Invariance Violation Extends the Cosmic-Ray Horizon? *Astrophys. J. Lett.* **1999**, *518*, L21–L24.
314. Bertolami, O.; Carvalho, C.S. Proposed astrophysical test of Lorentz invariance. *Phys. Rev. D* **2000**, *61*, 103002.
315. Aloisio, R.; Blasi, P.; Ghia, P.L.; et al. Probing the structure of space-time with cosmic rays. *Phys. Rev. D* **2000**, *62*, 053010.
316. Ellis, J.; Mavromatos, N.E.; Nanopoulos, D.V. Space-time foam effects on particle interactions and the Greisen-Zatsepin-Kuzmin cutoff. *Phys. Rev. D* **2001**, *63*, 124025.
317. Aloisio, R.; Blasi, P.; Galante, A.; et al. Space-time fluctuations and ultra-high energy cosmic ray interactions. *Astropart. Phys.* **2003**, *19*, 127–133.
318. Torri, M.D.C.; Caccianiga, L.; di Matteo, A.; et al. Predictions of Ultra-High Energy Cosmic Ray Propagation in the

Context of Homogeneously Modified Special Relativity. *Symmetry* **2020**, *12*, 1961.
319. Alves Batista, R. The Quest for the Origins of Ultra-High-Energy Cosmic Rays. *arXiv* **2024**, arXiv:2412.17201.
320. Maccione, L.; Liberati, S. GZK photon constraints on Planck-scale Lorentz violation in QED. *J. Cosmol. Astropart. Phys.* **2008**, *8*, 027.
321. Mattingly, D.M.; Maccione, L.; Galaverni, M.; et al. Possible cosmogenic neutrino constraints on Planck-scale Lorentz violation. *J. Cosmol. Astropart. Phys.* **2010**, *2*, 007.
322. Scully, S.T.; Stecker, F.W. Testing Lorentz invariance with neutrinos from ultrahigh energy cosmic ray interactions. *Astropart. Phys.* **2011**, *34*, 575–580.
323. Gorham, P.W.; Connolly, A.; Allison, P.; et al. Implications of ultrahigh energy neutrino flux constraints for Lorentz-invariance violating cosmogenic neutrinos. *Phys. Rev. D* **2012**, *86*, 103006.
324. Reyes, M.A.; Boncioli, D.; Carmona, J.M.; et al. Testing Lorentz invariance violation using cosmogenic neutrinos. *arXiv* **2023**, arXiv:hep-ph/2309.02103.
325. GRAND Collaboration. The Giant Radio Array for Neutrino Detection (GRAND): Science and design. *Sci. China Phys. Mech. Astron.* **2020**, *63*, 219501.
326. IceCube-Gen2 Collaboration. IceCube-Gen2: the window to the extreme Universe. *J. Phys. Nucl. Phys.* **2021**, *48*, 060501.
327. Fermi-LAT Collaboration. A limit on the variation of the speed of light arising from quantum gravity effects. *Nature* **2009**, *462*, 331–334.
328. IceCube Collaboration; Fermi-LAT Collaboration; MAGIC Collaboration; et al. Multimessenger observations of a flaring blazar coincident with high-energy neutrino IceCube-170922A. *Science* **2018**, *361*, eaat1378.
329. IceCube Collaboration. Search for steady point-like sources in the astrophysical muon neutrino flux with 8 years of IceCube data. *Eur. Phys. J. C* **2019**, *79*, 234.
330. IceCube Collaboration. LeptonInjector and LeptonWeighter: A neutrino event generator and weighter for neutrino observatories. *Comput. Phys. Commun.* **2021**, *266*, 108018.
331. Laha, R. Constraints on neutrino speed, weak equivalence principle violation, Lorentz invariance violation, and dual lensing from the first high-energy astrophysical neutrino source TXS 0506+056. *Phys. Rev. D* **2019**, *100*, 103002.
332. Ellis, J.; Mavromatos, N.E.; Sakharov, A.S.; et al. Limits on neutrino Lorentz violation from multimessenger observations of TXS 0506+056. *Phys. Lett. B* **2019**, *789*, 352–355.
333. Wei, J.J.; Zhang, B.B.; Shao, L.; et al. Multimessenger tests of Einstein's weak equivalence principle and Lorentz invariance with a high-energy neutrino from a flaring blazar. *J. High Energy Astrophys.* **2019**, *22*, 1–4.
334. Wang, K.; Xi, S.Q.; Shao, L.; et al. Limiting superluminal neutrino velocity and Lorentz invariance violation by neutrino emission from the blazar TXS 0506+056. *Phys. Rev. D* **2020**, *102*, 063027.
335. Amelino-Camelia, G.; Di Luca, M.G.; Gubitosi, G.; et al. Could quantum gravity slow down neutrinos? *Nat. Astron.* **2023**, *7*, 996–1001.
336. Amelino-Camelia, G.; D'Amico, G.; Rosati, G.; et al. In vacuo dispersion features for gamma-ray-burst neutrinos and photons. *Nat. Astron.* **2017**, *1*, 0139.
337. Huang, Y.; Ma, B.Q. Lorentz violation from gamma-ray burst neutrinos. *Commun. Phys.* **2018**, *1*, 62.
338. Huang, Y.; Li, H.; Ma, B.Q. Consistent Lorentz violation features from near-TeV IceCube neutrinos. *Phys. Rev. D* **2019**, *99*, 123018.
339. Carmona, J.M.; Cortés, J.L.; Reyes, M.A. Consistency of Lorentz-invariance violation neutrino scenarios in time delay analyses. *Class. Quantum Gravity* **2024**, *41*, 075012.
340. Amelino-Camelia, G.; Barcaroli, L.; D'Amico, G.; et al. IceCube and GRB neutrinos propagating in quantum spacetime. *Phys. Lett. B* **2016**, *761*, 318–325.
341. Amelino-Camelia, G.; Barcaroli, L.; D'Amico, G.; et al. Quantum-gravity-induced dual lensing and IceCube neutrinos. *Int. J. Mod. Phys. D* **2017**, *26*, 1750076.
342. OPERA Collaboration. Measurement of the neutrino velocity with the OPERA detector in the CNGS beam. *J. High Energy Phys.* **2012**, *2012*, 93.
343. OPERA Collaboration. Measurement of the neutrino velocity with the OPERA detector in the CNGS beam using the 2012 dedicated data. *J. High Energy Phys.* **2013**, *2013*, 153.
344. Amelino-Camelia, G.; Freidel, L.; Kowalski-Glikman, J.; et al. Opera Neutrinos and Deformed Special Relativity. *Mod. Phys. Lett. A* **2012**, *27*, 1250063.
345. Stecker, F. Testing Lorentz Symmetry Using High Energy Astrophysics Observations. *Symmetry* **2017**, *9*, 201.
346. Torri, M.D.C.; Miramonti, L. Neutrinos as possible probes for quantum gravity. *Class. Quantum Gravity* **2024**, *41*, 153001.
347. Li, C.; Ma, B.Q. Probes for String-Inspired Foam, Lorentz, and CPT Violations in Astrophysics. *Symmetry* **2025**, *17*, 974.
348. IceCube Collaboration. First Observation of PeV-Energy Neutrinos with IceCube. *Phys. Rev. Lett.* **2013**, *111*, 021103.
349. IceCube Collaboration. Evidence for High-Energy Extraterrestrial Neutrinos at the IceCube Detector. *Science* **2013**, *342*, 1242856.
350. Borriello, E.; Chakraborty, S.; Mirizzi, A.; et al. Stringent constraint on neutrino Lorentz invariance violation from the two IceCube PeV neutrinos. *Phys. Rev. D* **2013**, *87*, 116009.

351. Stecker, F.W.; Scully, S.T.; Liberati, S.; et al. Searching for traces of Planck-scale physics with high energy neutrinos. *Phys. Rev. D* **2015**, *91*, 045009.
352. Carmona, J.M.; Cortés, J.L.; Relancio, J.J.; et al. Lorentz Violation Footprints in the Spectrum of High-Energy Cosmic Neutrinos – Deformation of the Spectrum of Superluminal Neutrinos from Electron-Positron Pair Production in Vacuum. *Symmetry* **2019**, *11*, 1419.
353. Tomar, G.; Mohanty, S.; Pakvasa, S. Lorentz invariance violation and IceCube neutrino events. *J. High Energy Phys.* **2015**, *2015*, 22.
354. IceCube Collaboration. Detection of a particle shower at the Glashow resonance with IceCube. *Nature* **2021**, *591*, 220–224.
355. Brustein, R.; Eichler, D.; Foffa, S. Probing the Planck scale with neutrino oscillations. *Phys. Rev. D* **2002**, *65*, 105006.
356. Beacom, J.F.; Bell, N.F.; Hooper, D.; et al. Decay of High-Energy Astrophysical Neutrinos. *Phys. Rev. Lett.* **2003**, *90*, 181301.
357. Hooper, D.; Morgan, D.; Winstanley, E. Lorentz and CPT invariance violation in high-energy neutrinos. *Phys. Rev. D* **2005**, *72*, 065009.
358. Argüelles, C.A.; Katori, T.; Salvado, J. Effect of New Physics in Astrophysical Neutrino Flavor. *Phys. Rev. Lett.* **2015**, *115*, 161303.
359. Bustamante, M.; Ahlers, M. Inferring the Flavor of High-Energy Astrophysical Neutrinos at Their Sources. *Phys. Rev. Lett.* **2019**, *122*, 241101.
360. IceCube Collaboration. Characterization of the astrophysical diffuse neutrino flux using starting track events in IceCube. *Phys. Rev. D* **2024**, *110*, 022001.
361. Telalovic, B.; Bustamante, M. Flavor anisotropy in the high-energy astrophysical neutrino sky. *J. Cosmol. Astropart. Phys.* **2025**, *5*, 013.
362. Telalovic, B.; Bustamante, M. No Flavor Anisotropy in the High-Energy Neutrino Sky Upholds Lorentz Invariance. *arXiv* **2025**, arXiv:2503.15468.
363. Antonov, E.E.; Dedenko, L.G.; Kirillov, A.A.; et al. Test of Lorentz Invariance through Observation of the Longitudinal Development of Ultrahigh-Energy Extensive Air Showers. *Sov. J. Exp. Theor. Phys. Lett.* **2001**, *73*, 446–450.
364. Dedenko, L.G.; Fedorova, G.F.; Fedunin, E.Y.; et al. Test of Lorentz invariance through observation of the maximum depths in giant air showers. *Nucl. Phys. Proc. Suppl.* **2003**, *122*, 321–324.
365. Klinkhamer, F.R.; Niechciol, M.; Risse, M. Improved bound on isotropic Lorentz violation in the photon sector from extensive air showers. *Phys. Rev. D* **2017**, *96*, 116011.
366. Duenkel, F.; Niechciol, M.; Risse, M. Photon decay in ultrahigh-energy air showers: Stringent bound on Lorentz violation. *Phys. Rev. D* **2021**, *104*, 015010.
367. Duenkel, F.; Niechciol, M.; Risse, M. New bound on Lorentz violation based on the absence of vacuum Cherenkov radiation in ultrahigh energy air showers. *Phys. Rev. D* **2023**, *107*, 083004.
368. Risse, M. Using Ultrahigh-Energy Cosmic Rays and Air Showers to Test Lorentz Invariance Within Modified Maxwell Theory. *arXiv* **2023**, arXiv:hep-ph/2208.08747.
369. Martynenko, N.S.; Rubtsov, G.I.; Satunin, P.S.; et al. Hypothetical Lorentz invariance violation and the muon content of extensive air showers. *Phys. Rev. D* **2025**, *111*, 063010.
370. Lobo, I.P.; Pfeifer, C. Reaching the Planck scale with muon lifetime measurements. *Phys. Rev. D* **2021**, *103*, 106025.
371. Lobo, I.P.; Pfeifer, C. Muon accelerators-muon lifetime measurements as window to Planck scale physics. *Class. Quantum Gravity* **2024**, *41*, 015008.
372. Lobo, I.P.; Pfeifer, C.; Morais, P.H. Experimental bounds on deformed muon lifetime dilation. *Phys. Lett. B* **2025**, *866*, 139511.
373. Lobo, I.P.; Pfeifer, C.; Morais, P.H.; et al. Phenomenological signatures of two-body decays in deformed relativity. *J. High Energy Phys.* **2022**, *09*, 003.
374. Morais, P.H.; Lobo, I.P.; Pfeifer, C.; et al. Modified particle lifetimes as a signature of deformed relativity. *Phys. Lett. B* **2024**, *848*, 138380.
375. Staicova, D. Impact of cosmology on Lorentz Invariance Violation constraints from GRB time-delays. *Class. Quantum Gravity* **2023**, *40*, 195012.
376. Amelino-Camelia, G.; Mandanici, G.; Procaccini, A.; et al. Phenomenology of Doubly Special Relativity. *Int. J. Mod. Phys. A* **2005**, *20*, 6007–6037.
377. Stecker, F.W.; Scully, S.T. Searching for new physics with ultrahigh energy cosmic rays. *New J. Phys.* **2009**, *11*, 085003.
378. Torri, M.D.C.; Bertini, S.; Giammarchi, M.; et al. Lorentz Invariance Violation effects on UHECR propagation: A geometrized approach. *J. High Energy Astrophys.* **2018**, *18*, 5–14.
379. Pierre Auger Collaboration. Measurement of the Depth of Maximum of Extensive Air Showers above 10^{18}eV. *Phys. Rev. Lett.* **2010**, *104*, 091101.
380. Pierre Auger Collaboration. Interpretation of the depths of maximum of extensive air showers measured by the Pierre Auger Observatory. *J. Cosmol. Astropart. Phys.* **2013**, *2*, 026.
381. Pierre Auger Collaboration. Depth of maximum of air-shower profiles at the Pierre Auger Observatory. I. Measurements at

energies above $10^{17.8}$ eV. *Phys. Rev. D* **2014**, *90*, 122005.
382. Pierre Auger Collaboration. Depth of maximum of air-shower profiles at the Pierre Auger Observatory. II. Composition implications. *Phys. Rev. D* **2014**, *90*, 122006.
383. Pierre Auger Collaboration. Evidence for a mixed mass composition at the 'ankle' in the cosmic-ray spectrum. *Phys. Lett. B* **2016**, *762*, 288–295.
384. Pierre Auger Collaboration. Inferences on mass composition and tests of hadronic interactions from 0.3 to 100 EeV using the water-Cherenkov detectors of the Pierre Auger Observatory. *Phys. Rev. D* **2017**, *96*, 122003.
385. Telescope Array Collaboration. The Cosmic-Ray Composition between 2 PeV and 2 EeV Observed with the TALE Detector in Monocular Mode. *Astrophys. J.* **2021**, *909*, 178.
386. Alves Batista, R.; Biteau, J.; Bustamante, M.; et al. Open Questions in Cosmic-Ray Research at Ultrahigh Energies. *Front. Astron. Space Sci.* **2019**, *6*, 23.
387. Coleman, A.; Eser, J.; Mayotte, E.; et al. Ultra high energy cosmic rays The intersection of the Cosmic and Energy Frontiers. *Astropart. Phys.* **2023**, *147*, 102794.
388. Christian, J. Testing quantum gravity via cosmogenic neutrino oscillations. *Phys. Rev. D* **2005**, *71*, 024012.
389. Galaverni, M.; Sigl, G. Lorentz Violation for Photons and Ultrahigh-Energy Cosmic Rays. *Phys. Rev. Lett.* **2008**, *100*, 021102.
390. Cowsik, R.; Madziwa-Nussinov, T.; Nussinov, S.; et al. Testing violations of Lorentz invariance with cosmic rays. *Phys. Rev. D* **2012**, *86*, 045024.
391. Maccione, L.; Taylor, A.M.; Mattingly, D.M.; et al. Planck-scale Lorentz violation constrained by Ultra-High-Energy Cosmic Rays. *J. Cosmol. Astropart. Phys.* **2009**, *4*, 022.
392. Bietenholz, W. Cosmic rays and the search for a Lorentz Invariance Violation. *Phys. Rep.* **2011**, *505*, 145–185.
393. Hossenfelder, S. The Soccer-Ball Problem. *SIGMA* **2014**, *10*, 074.
394. Amelino-Camelia, G. Planck-Scale Soccer-Ball Problem: A Case of Mistaken Identity. *Entropy* **2017**, *19*, 400.
395. Amelino-Camelia, G.; Astuti, V.; Palmisano, M.; et al. Multi-particle systems in quantum spacetime and a novel challenge for center-of-mass motion. *Int. J. Mod. Phys. D* **2021**, *30*, 2150046.
396. Martínez-Huerta, H.; Pérez-Lorenzana, A. Restrictions from Lorentz invariance violation on cosmic ray propagation. *Phys. Rev. D* **2017**, *95*, 063001.
397. Alfaro, J.; Palma, G. Loop quantum gravity and ultrahigh energy cosmic rays. *Phys. Rev. D* **2003**, *67*, 083003.
398. Altschul, B. Limits on neutron Lorentz violation from the stability of primary cosmic ray protons. *Phys. Rev. D* **2008**, *78*, 085018.
399. Klinkhamer, F.R. Potential sensitivities to Lorentz violation from nonbirefringent modified Maxwell theory of Auger, HESS, and CTA. *Phys. Rev. D* **2010**, *82*, 105024.
400. Díaz, J.S.; Klinkhamer, F.R. Parton-model calculation of a nonstandard decay process in isotropic modified Maxwell theory. *Phys. Rev. D* **2015**, *92*, 025007.
401. Klinkhamer, F.R. Lorentz-violating neutral-pion decays in isotropic modified Maxwell theory. *Mod. Phys. Lett. A* **2018**, *33*, 1850104.
402. Levy, C.; Sol, H.; Bolmont, J. Separating source-intrinsic and Lorentz invariance violation induced delays in the very high-energy emission of blazar flares. *Astron. Astrophys.* **2024**, *689*, A136.
403. Piran, T. The physics of gamma-ray bursts. *Rev. Mod. Phys.* **2004**, *76*, 1143–1210.
404. Gehrels, N.; Ramirez-Ruiz, E.; Fox, D.B. Gamma-Ray Bursts in the Swift Era. *Annu. Rev. Astron. Astrophys.* **2009**, *47*, 567–617.
405. Berger, E. Short-Duration Gamma-Ray Bursts. *Annu. Rev. Astron. Astrophys.* **2014**, *52*, 43–105.
406. Kumar, P.; Zhang, B. The physics of gamma-ray bursts & relativistic jets. *Phys. Rep.* **2015**, *561*, 1–109.
407. Dai, Z.; Daigne, F.; Mészáros, P. The Theory of Gamma-Ray Bursts. *Space Sci. Rev.* **2017**, *212*, 409–427.
408. Pe'er, A. Gamma-Ray Bursts: What Do We Know Today That We Did Not Know 10 Years Ago? *Galaxies* **2024**, *13*, 2.
409. Paczynski, B. Gamma-ray bursters at cosmological distances. *Astrophys. J. Lett.* **1986**, *308*, L43–L46.
410. Goodman, J. Are gamma-ray bursts optically thick? *Astrophys. J. Lett.* **1986**, *308*, L47.
411. Rees, M.J.; Meszaros, P. Relativistic fireballs - Energy conversion and time-scales. *Mon. Not. R. Astron. Soc.* **1992**, *258*, 41.
412. Meszaros, P.; Laguna, P.; Rees, M.J. Gasdynamics of Relativistically Expanding Gamma-Ray Burst Sources: Kinematics, Energetics, Magnetic Fields, and Efficiency. *Astrophys. J.* **1993**, *415*, 181.
413. Sari, R.; Piran, T.; Narayan, R. Spectra and Light Curves of Gamma-Ray Burst Afterglows. *Astrophys. J. Lett.* **1998**, *497*, L17–L20.
414. Zhang, B.; Mészáros, P. Gamma-Ray Bursts: progress, problems & prospects. *Int. J. Mod. Phys. A* **2004**, *19*, 2385–2472.
415. Gao, H.; Lei, W.H.; Zou, Y.C.; et al. A complete reference of the analytical synchrotron external shock models of gamma-ray bursts. *New Astron. Rev.* **2013**, *57*, 141–190.
416. Srinivasaragavan, G.P.; Dainotti, M.G.; Fraija, N.; et al. On the Investigation of the Closure Relations for Gamma-Ray Bursts Observed by Swift in the Post-plateau Phase and the GRB Fundamental Plane. *Astrophys. J.* **2020**, *903*, 18.

417. IceCube Collaboration. Extending the Search for Muon Neutrinos Coincident with Gamma-Ray Bursts in IceCube Data. *Astrophys. J.* **2017**, *843*, 112.
418. AMON and ANTARES Collaboration. A Search for Cosmic Neutrino and Gamma-Ray Emitting Transients in 7.3 yr of ANTARES and Fermi LAT Data. *Astrophys. J.* **2019**, *886*, 98.
419. ANTARES Collaboration. ANTARES upper limits on the multi-TeV neutrino emission from the GRBs detected by IACTs. *J. Cosmol. Astropart. Phys.* **2021**, *3*, 092.
420. IceCube Collaboration.; Fermi Gamma-ray Burst Monitor. Searches for Neutrinos from Gamma-Ray Bursts Using the IceCube Neutrino Observatory. *Astrophys. J.* **2022**, *939*, 116.
421. IceCube Collaboration. Limits on Neutrino Emission from GRB 221009A from MeV to PeV Using the IceCube Neutrino Observatory. *Astrophys. J. Lett.* **2023**, *946*, L26.
422. Pitik, T.; Tamborra, I.; Petropoulou, M. Neutrino signal dependence on gamma-ray burst emission mechanism. *J. Cosmol. Astropart. Phys.* **2021**, *5*, 034.
423. Ulrich, M.H.; Maraschi, L.; Urry, C.M. Variability of Active Galactic Nuclei. *Annu. Rev. Astron. Astrophys.* **1997**, *35*, 445–502.
424. Dermer, C.D.; Giebels, B. Active galactic nuclei at gamma-ray energies. *Comptes Rendus Phys.* **2016**, *17*, 594–616
425. Romero, G.E.; Boettcher, M.; Markoff, S.; et al. Relativistic Jets in Active Galactic Nuclei and Microquasars. *Space Sci. Rev.* **2017**, *207*, 5–61.
426. Padovani, P.; Alexander, D.M.; Assef, R.J.; et al. Active galactic nuclei: what's in a name? *Astron. Astrophys. Rev.* **2017**, *25*, 2.
427. Blandford, R.; Meier, D.; Readhead, A. Relativistic Jets from Active Galactic Nuclei. *Annu. Rev. Astron. Astrophys.* **2019**, *57*, 467–509.
428. Urry, C.M.; Padovani, P. Unified Schemes for Radio-Loud Active Galactic Nuclei. *Publ. Astron. Soc. Pac.* **1995**, *107*, 803.
429. HEGRA Collaboration. Measurement of the flux, spectrum, and variability of TeV γ-rays from Mkn 501 during a state of high activity. *Astron. Astrophys.* **1997**, *327*, L5–L8.
430. MAGIC Collaboration. Variable Very High Energy γ-Ray Emission from Markarian 501. *The Astrophysical Journal* **2007**, *669*, 862–883.
431. NuSTAR Team; MAGIC Collaboration; VERITAS Collaboration; et al. First NuSTAR Observations of Mrk 501 within a Radio to TeV Multi-Instrument Campaign. *Astrophys. J.* **2015**, *812*, 65.
432. HAWC Collaboration. Daily Monitoring of TeV Gamma-Ray Emission from Mrk 421, Mrk 501, and the Crab Nebula with HAWC. *Astrophys. J.* **2017**, *841*, 100.
433. MAGIC Collaboration; FACT Collaboration; VERITAS Collaboration. Extreme HBL behavior of Markarian 501 during 2012. *Astron. Astrophys.* **2018**, *620*, A181.
434. Bhatta, G. Blazar Mrk 501 shows rhythmic oscillations in its γ-ray emission. *Mon. Not. R. Astron. Soc.* **2019**, *487*, 3990–3997.
435. MAGIC Collaboration. Study of the variable broadband emission of Markarian 501 during the most extreme Swift X-ray activity. *Astron. Astrophys.* **2020**, *637*, A86.
436. H.E.S.S. Collaboration. An Exceptional Very High Energy Gamma-Ray Flare of PKS 2155-304. *Astrophys. J. Lett.* **2007**, *664*, L71–L74.
437. H.E.S.S. Collaboration. VHE γ-ray emission of PKS 2155-304: spectral and temporal variability. *Astron. Astrophys.* **2010**, *520*, A83.
438. Gaidos, J.A.; Akerlof, C.W.; Biller, S.; et al. Extremely rapid bursts of TeV photons from the active galaxy Markarian 421. *Nature* **1996**, *383*, 319–320.
439. VERITAS Collaboration. Rapid TeV Gamma-Ray Flaring of BL Lacertae. *Astrophys. J.* **2013**, *762*, 92.
440. Lin, C.; Fan, J.H.; Xiao, H.B. The intrinsic γ-ray emissions of Fermi blazars. *Res. Astron. Astrophys.* **2017**, *17*, 066.
441. Wagner, S.J.; Witzel, A. Intraday Variability In Quasars and BL Lac Objects. *Annu. Rev. Astron. Astrophys.* **1995**, *33*, 163–198.
442. Ghisellini, G.; Tavecchio, F.; Bodo, G.; et al. TeV variability in blazars: how fast can it be? *Mon. Not. R. Astron. Soc.* **2009**, *393*, L16–L20.
443. Nieppola, E.; Hovatta, T.; Tornikoski, M.; et al. Long-Term Variability of Radio-Bright BL Lacertae Objects. *Astron. J.* **2009**, *137*, 5022–5036.
444. Foschini, L.; Ghisellini, G.; Tavecchio, F.; et al. Search for the shortest variability at gamma rays in flat-spectrum radio quasars. *Astron. Astrophys.* **2011**, *530*, A77.
445. Sandrinelli, A.; Covino, S.; Dotti, M.; et al. Quasi-periodicities at Year-like Timescales in Blazars. *Astron. J.* **2016**, *151*, 54.
446. Rajput, B.; Stalin, C.S.; Rakshit, S. Long term γ-ray variability of blazars. *Astron. Astrophys.* **2020**, *634*, A80.
447. Begelman, M.C.; Fabian, A.C.; Rees, M.J. Implications of very rapid TeV variability in blazars. *Mon. Not. R. Astron. Soc.* **2008**, *384*, L19–L23.
448. Rieger, F.M.; Aharonian, F.A. Variable VHE gamma-ray emission from non-blazar AGNs. *Astron. Astrophys.* **2008**, *479*, L5–L8.
449. Giannios, D.; Uzdensky, D.A.; Begelman, M.C. Fast TeV variability in blazars: jets in a jet. *Mon. Not. R. Astron. Soc.*

2009, *395*, L29–L33.
450. Levinson, A.; Rieger, F. Variable TeV Emission as a Manifestation of Jet Formation in M87? *Astrophys. J.* **2011**, *730*, 123.
451. Barkov, M.V.; Aharonian, F.A.; Bogovalov, S.V.; et al. Rapid TeV Variability in Blazars as a Result of Jet-Star Interaction. *Astrophys. J.* **2012**, *749*, 119.
452. Bhatta, G.; Dhital, N. The Nature of γ-Ray Variability in Blazars. *Astrophys. J.* **2020**, *891*, 120.
453. Sobacchi, E.; Piran, T.; Comisso, L. Ultrafast Variability in AGN Jets: Intermittency and Lighthouse Effect. *Astrophys. J. Lett.* **2023**, *946*, L51.
454. Śmiałkowski, A.; Bednarek, W. Gamma ray flares from active region within inhomogeneous AGN jet. *J. High Energy Astrophys.* **2025**, *45*, 456–462.
455. IceCube Collaboration. Evidence for neutrino emission from the nearby active galaxy NGC 1068. *Science* **2022**, *378*, 538–543.
456. IceCube Collaboration. The IceCube Collaboration—Contributions to the 39th International Cosmic Ray Conference (ICRC2025). *arXiv* **2025**, arXiv:astro-ph.HE/2507.08666.
457. VERITAS Collaboration; H.E.S.S. Collaboration. Multiwavelength Observations of the Blazar PKS 0735+178 in Spatial and Temporal Coincidence with an Astrophysical Neutrino Candidate IceCube-211208A. *Astrophys. J.* **2023**, *954*, 70.
458. Sahakyan, N.; Giommi, P.; Padovani, P.; et al. A multimessenger study of the blazar PKS 0735+178: a new major neutrino source candidate. *Mon. Not. R. Astron. Soc.* **2023**, *519*, 1396–1408.
459. Carmona, J.M.; Cortés, J.L.; Pereira, L.; et al. Bounds on Relativistic Deformed Kinematics from the Physics of the Universe Transparency. *Symmetry* **2020**, *12*, 1298.
460. Ho, C.M.; Minic, D.; Ng, Y.J. Quantum Gravity and Dark Matter. *Int. J. Mod. Phys. D* **2011**, *20*, 2887–2893.
461. Ho, C.M.; Minic, D.; Ng, Y.J. Dark matter, infinite statistics, and quantum gravity. *Phys. Rev. D* **2012**, *85*, 104033.
462. Smolin, L. MOND as a regime of quantum gravity. *Phys. Rev. D* **2017**, *96*, 083523.
463. Bertone, G.; Hooper, D.; Silk, J. Particle dark matter: evidence, candidates and constraints. *Phys. Rep.* **2005**, *405*, 279–390.
464. Duffy, L.D.; van Bibber, K. Axions as dark matter particles. *New J. Phys.* **2009**, *11*, 105008.
465. Bertone, G. *Particle Dark Matter*; Cambridge University Press: Cambridge, UK, 2010.
466. Peccei, R.D.; Quinn, H.R. CP conservation in the presence of pseudoparticles. *Phys. Rev. Lett.* **1977**, *38*, 1440–1443.
467. Peccei, R.D.; Quinn, H.R. Constraints imposed by CP conservation in the presence of pseudoparticles. *Phys. Rev. D* **1977**, *16*, 1791–1797.
468. Weinberg, S. A new light boson? *Phys. Rev. Lett.* **1978**, *40*, 223–226.
469. Wilczek, F. Problem of strong P and T invariance in the presence of instantons. *Phys. Rev. Lett.* **1978**, *40*, 279–282.
470. Zanderighi, G. *Fine-Tuning in the Physical Universe*; Cambridge University Press: Cambridge, UK, 2020; pp. 307–344.
471. Arvanitaki, A.; Dimopoulos, S.; Dubovsky, S.; et al. String axiverse. *Phys. Rev. D* **2010**, *81*, 123530.
472. Raffelt, G.; Stodolsky, L. Mixing of the photon with low-mass particles. *Phys. Rev. D* **1988**, *37*, 1237–1249.
473. Hochmuth, K.A.; Sigl, G. Effects of axion-photon mixing on gamma-ray spectra from magnetized astrophysical sources. *Phys. Rev. D* **2007**, *76*, 123011.
474. De Angelis, A.; Mansutti, O.; Roncadelli, M. Axion-like particles, cosmic magnetic fields and gamma-ray astrophysics. *Phys. Lett. B* **2008**, *659*, 847–855.
475. Simet, M.; Hooper, D.; Serpico, P.D. Milky Way as a kiloparsec-scale axionscope. *Phys. Rev. D* **2008**, *77*, 063001.
476. De Angelis, A.; Galanti, G.; Roncadelli, M. Relevance of axionlike particles for very-high-energy astrophysics. *Phys. Rev. D* **2011**, *84*, 105030.
477. De Angelis, A.; Galanti, G.; Roncadelli, M. Transparency of the Universe to gamma-rays. *Mon. Not. R. Astron. Soc.* **2013**, *432*, 3245–3249.
478. De Angelis, A.; Galanti, G.; Roncadelli, M. Erratum: Relevance of axionlike particles for very-high-energy astrophysics [Phys. Rev. D 84, 105030 (2011)]. *Phys. Rev. D* **2013**, *87*, 109903.
479. Horns, D.; Jacholkowska, A. Gamma rays as probes of the Universe. *Comptes Rendus Phys.* **2016**, *17*, 632–648.
480. Batković, I.; De Angelis, A.; Doro, M.; et al. Axion-Like Particle Searches with IACTs. *Universe* **2021**, *7*, 185.
481. Choi, K.; Im, S.H.; Shin, C.S. Recent Progress in the Physics of Axions and Axion-Like Particles. *Annu. Rev. Nucl. Part. Sci.* **2021**, *71*, 225–252.
482. Galanti, G.; Roncadelli, M. Axion-like Particles Implications for High-Energy Astrophysics. *Universe* **2022**, *8*, 253.
483. Zlosnik, T.G.; Ferreira, P.G.; Starkman, G.D. Modifying gravity with the aether: An alternative to dark matter. *Phys. Rev. D* **2007**, *75*, 044017.
484. Zlosnik, T.G.; Ferreira, P.G.; Starkman, G.D. Growth of structure in theories with a dynamical preferred frame. *Phys. Rev. D* **2008**, *77*, 084010.
485. Złośnik, T.; Urban, F.; Marzola, L.; et al. Spacetime and dark matter from spontaneous breaking of Lorentz symmetry. *Class. Quantum Gravity* **2018**, *35*, 235003.
486. Jacobson, T.; Mattingly, D. Gravity with a dynamical preferred frame. *Phys. Rev. D* **2001**, *64*, 024028.
487. Foster, B.Z.; Jacobson, T. Post-Newtonian parameters and constraints on Einstein-aether theory. *Phys. Rev. D* **2006**,

73, 064015.
488. Eling, C.; Jacobson, T.; Mattingly, D. Einstein-Æther Theory. In *Deserfest: A Celebration of the Life and Works of Stanley Deser*; World Scientific: Singapore, 2006; p. 163.
489. Jacobson, T.; Mattingly, D. Einstein-aether waves. *Phys. Rev. D* **2004**, *70*, 024003.
490. Townsend, P.K. Aether, dark energy and string compactifications. *Philos. Trans. R. Soc. Lond. Ser. A* **2022**, *380*, 20210185.
491. Mukohyama, S. Dark matter as integration constant in Hořava-Lifshitz gravity. *Phys. Rev. D* **2009**, *80*, 064005.
492. Blas, D.; Ivanov, M.M.; Sibiryakov, S. Testing Lorentz invariance of dark matter. *J. Cosmol. Astropart. Phys.* **2012**, *10*, 057.
493. Bassani, P.M.; Magueijo, J.; Mukohyama, S. Violations of energy conservation in Horava-Lifshitz gravity: a new ingredient in the dark matter puzzle. *J. Cosmol. Astropart. Phys.* **2025**, *7*, 032.
494. Saridakis, E.N. Hořava-Lifshitz dark energy. *Eur. Phys. J. C* **2010**, *67*, 229–235.
495. Wang, X.; Loeb, A. Ultrahigh energy cosmic rays from nonrelativistic quasar outflows. *Phys. Rev. D* **2017**, *95*, 063007.
496. Chamseddine, A.H.; Mukhanov, V. Mimetic dark matter. *J. High Energy Phys.* **2013**, *11*, 135.